

Aus dem Institut für Transfusionsmedizin  
der Medizinischen Fakultät Charité – Universitätsmedizin Berlin

DISSERTATION

**“Biocompatibility of Biopolymer Submicron Particles”**

zur Erlangung des akademischen Grades  
Doctor rerum medicinalium (Dr. rer. medic.)

vorgelegt der Medizinischen Fakultät  
Charité – Universitätsmedizin Berlin

von

**Nittiya Suwannasom**

aus Maha Sarakham

Datum der Promotion: .....13.12.2019.....

## Table of Contents

Abstract (English) .....	3
Abstract (Deutsch) .....	4
1. Introduction .....	5
2. Methodology .....	7
2.1. Study 1 .....	7
2.1.1 HSA particle (HSA-MPs) Fabrication using CCD-technique .....	7
2.1.2 Haemoglobin particle (Odex-HbMPs) Fabrication using One Pot-technique .....	7
2.1.3 Riboflavin-HSA particle (RF-HSA-MPs) Fabrication using CCD-technique and Characterization .....	7
2.1.4. Hemocompatibility of HSA-MPs, RF-HSA MPs, and Odex-HbMPs .....	8
2.2. Study 2 .....	9
2.2.1. Blood collection, preparation and leukocyte staining .....	9
2.2.2. Phagocytosis of bacteria at different temperatures .....	10
2.2.3 Internalization of CD33 during phagocytosis .....	10
2.2.4 Statistical analysis .....	10
3. Results and discussion .....	12
3.1 Study 1 .....	12
3.2 Study 2 .....	19
4. Bibliography .....	24
Declaration of own contribution to the submitted publications .....	26
Print copies of the selected publications .....	28
Curriculum vitae .....	62
Complete list of publications .....	64
Acknowledgments .....	65

## Abstract (English)

Recently, we employed the Co-precipitation Crosslinking Dissolution technique (CCD-technique) to fabricate biopolymer particles and to load them with riboflavin (RF). Moreover, we modified the CCD-technique by combining co-precipitation and cross-linking into one preparation step using a cross-linker, periodate-oxidized dextran (Odex). HSA and bovine haemoglobin (Hb) were used to demonstrate this technique. The haemocompatibility of these submicron particles is important for their application as intravenously administered drug carriers. *In vitro* haemocompatibility assays including haemolysis test, platelet activation test, and phagocytosis test in human blood were studied. Our results showed that, both RF-HSA-MPs and Odex-HbMPs exhibited the percentage of hemolysis in the low range of 1% - 7%. Microparticle-platelet interaction did not activate the platelets and did not augment the platelet response to antagonists. The PMN phagocytes exposed to microparticles showed no phagocytic activity. These results suggested that our RF-HSA- MPs by CCD-technique and Odex-HbMPs by One-Pot formulation revealed a good hemocompatibility. Furthermore, the RF-HSA-MPs by CCD-technique were characterized showing a narrow size distribution in the range of 0.9 to 1  $\mu\text{m}$ , uniform peanut-like morphology, and a zeta-potential of  $-15\text{ mV}$ . *In vitro* release studies represented biphasic release profiles of RF in a phosphate buffered saline (PBS) pH 7.4 and a cell culture medium (RPMI) 1640 medium over a prolonged period (study 1).

Moreover, to assess phagocytic activity, cell surface marker, CD33 is used to identify monocytes. Here, we also investigated the CD33 expression of monocytes in human blood samples processed at different temperatures and in dependence on their phagocytic activity in the presence of opsonized *Escherichia coli*. The samples were then stained by fluorescently labelled anti-human CD14 and anti-human CD33 antibodies to specify the monocyte population and to evaluate CD33 expression, respectively and evaluated by flow cytometry and confocal laser scanning microscopy. We found that the percentage of CD33-positive monocytes as well as their relative fluorescence intensity was up-regulated when the blood samples were kept at 37 °C or first pre-chilled at 0 °C with subsequent warming up to 37 °C, in comparison to samples kept constantly at 0 °C was significantly lower. After exposure to *E. coli* the CD33 relative fluorescence intensity of the monocytes activated at 37°C was 3 to 4 times higher than that of those cells kept inactive at 0 °C. Furthermore, microscopic analysis showed internalization of CD33 due to its expression on the surface and the engulfment of *E. coli* (study 2).

## Abstract (Deutsch)

Für die Herstellung von Biopolymerpartikeln und deren Beladung mit Riboflavin (RF) wurde die Co-precipitations-Crosslinking-Dissolution-Technik (CCD-Technik) verwendet. Diese Technik wurde zu einem Einschnittverfahren modifiziert, indem als Crosslinker Periodat oxidiertes Dextran (Odex) verwendet wurde. Submikropartikel bestehend aus Humanserumalbumin (HSA-MP) und Rinderhämoglobin (HbMP) wurden hergestellt, um die Methode zu demonstrieren. Die Hämokompatibilität dieser Partikel ist für deren intravenöse Anwendung als Drug Carrier erforderlich. Die *In vitro* Hämokompatibilität der Partikel wurde mittels Hämolysetest, Plättchenaktivitätstests sowie des Phagozytostest in Humanblut untersucht. Unsere Ergebnisse zeigen, dass sowohl RF-HSA-MPs als auch Odex-HbMPs eine Hämolyserate von 1 -7% aufweisen. Die Plättchen wurden durch die Mikropartikel weder aktiviert noch wurde ihre Antwort auf Agonisten beeinflusst. PMN Phagozyten zeigten bei Inkubation mit den Mikropartikeln keine Phagozytose. Diese Ergebnisse lassen den Schluss zu, dass die mittels CCD-Technik sowie der Einschnittformulierung hergestellten RF-HSA-MPs bzw. die Odex-HbMPs hämokompatibel sind. Die RF-HSA-MPs wurden zusätzlich hinsichtlich ihrer Größe und Form sowie ihres Zetapotentials untersucht. Sie weisen eine erdnussartige Form, eine enge Größenverteilung im Bereich von 0,9 und 1,0 µm sowie ein Zetapotential von -15 mV auf. Die Freisetzung von RF zeigt ein biphasisches Profil sowohl in Phosphatpuffer (pH 7,4) als auch in Zellkulturmedium RPMI 1640 über einen Zeitraum von mehr als 3 Tage (Studie 1).

Um die Phagozytoseaktivität zu charakterisieren wurde der Oberflächenmarker CD33 für Monozyten verwendet. Dazu wurde die CD33 Expression auf humanen Monozyten in Blutproben, die bei verschiedenen Temperaturen prozessiert wurden sowie in Abhängigkeit von der Phagozytose der Monozyten in Gegenwart opsonierter *Escherichia coli* untersucht. Die CD33 Expression der Monozyten wurde nach deren Markierung mit CD14 und CD33 Antikörpern mittels Durchflusszytometer und Konfokalem Laserscanningmikroskop untersucht. Der prozentuale Anteil von CD33-positiven Monozyten sowie ihrer relative Fluoreszenzintensität waren hochreguliert, wenn die Blutproben bei 37°C gehalten oder erst auf 0°C abgekühlt und danach wieder auf 37°C erwärmt wurden im Vergleich zu den Proben, die konstant bei 0°C gehalten wurden. Nach Inkubation mit *E. coli* war die CD33 relative Fluoreszenzintensität der bei 37°C aktivierten Monozyten 3 bis 4 mal höher als bei den Zellen, die bei 0°C gehalten wurden. Die mikroskopischen Untersuchungen zeigten die Internalisierung von CD33 infolge ihrer Expression auf der Monozytenoberfläche und dem Einschluss der *E. coli* (Studie 2).

## 1. Introduction

Co-precipitation of biopolymers is an approach to its immobilization for the improvement of stability, solubility, and biological activity through biopolymer capture by carbonate microspheres in the process of their formation. Consequently, these insoluble biopolymer-carbonate hybrid particles are intermolecularly cross-linked to form the particles using glutaraldehyde (GA). Finally, the carbonate templates are dissolved to obtain biopolymer particles. These processes are called CCD-technique allowing the three basic steps namely Co-precipitation–Cross-linking–Dissolution technique to fabricate biopolymer particles from common chemical reaction (1,2). CCD-technique has gained increasing attraction due to the easy preparation by simply mixing of inexpensive starting materials under mild reaction conditions, the high capacity of drug loading into porous carbonate microparticles, and easily decomposition of the carbonate template at neutral pH by EDTA.

Lately, a new formulation of protein submicron particles called “One-Pot formulation” was described (3,4). This fabrication is based on the CCD-technique using Odex as a cross-linker. The One-Pot technique, co-precipitation and cross-linking were combined in one step for the reason that a cross-linker, oxidized-dextran (Odex), is co-precipitated together with proteins into carbonate template. The submicron particles from both CCD-technique and One-Pot technique showed the uniform peanut-like shape with a relatively high protein entrapment efficiency and a narrow distribution between 700 and 1000 nm and negative zeta-potential. These carbonate particles can be easily loaded with bioactive compounds (e.g. enzyme, haemoglobin, albumin) during their formation (5–8). The particle size and shape can be controlled by adjusting the experimental conditions (e.g. pH, choice of salt and/or salt concentration, temperature, rate of mixing the solutions).

For biomedical and pharmaceutical applications, those particles enter the human body and contact with tissues and cells directly, thus it is necessary for understanding and exploring their biocompatibility. Haemolysis, platelet activation, and phagocytosis properties are commonly used to evaluate haematological toxicity of particles.

Phagocytosis by Phagotest™ kit is very useful for the investigation of the immunogenicity of particles that are developed as diagnostic tools or as drug carriers, showing a possible uptake of these particles. For the diagnostic output, it is important to distinguish whether

there are differences between the phagocytic activity of granulocytes and monocytes. Since the number of monocytes in the peripheral blood is orders of magnitude lower than the number of granulocytes (9), the identification of their population only by their scattering signals in flow cytometry is not accurate enough and needs verification by immunostaining with specific antibodies to gate out debris. CD33, cell surface markers, is used to identify monocytes in phagocytic activity.

CD33 belongs to the sialic acid-binding immunoglobulin-like lectins (Siglecs, Siglec-3) family that is that is expressed as a glycosylated 67 kDa type I transmembrane. CD33 is expressed at high level on monocytes and macrophages, but at low level on mature granulocytes (10,11). Besides, CD33 is an accepted surface marker to identify monocytes (12). However, despite the crucial role of CD33, little is known of its function in myeloid cells, except that it may acts as an inhibitory molecule on the innate immune cells to mediate the cell–cell interaction and to inhibit normal functions through a reducing effect on tyrosine kinase-driven signaling (13,14).

It is well established that several factors such as purification methods, storage and incubation temperature, or specimen age and anticoagulants, and phagocytosis affect the antigen expression levels of certain cell surface proteins of leukocytes. To date, only a few research reports give information on sample handling for the investigation of CD33 expression. The influence of temperature and phagocytosis on up- or down-regulation of CD33 expression should be clearly understood to support existing or future diagnostic and therapeutic approaches.

For our investigations, we fabricated RF-HSA-MPs immobilizing riboflavin (RF) using the CCD-technique and formulated Odex-HbMPs loading bovine haemoglobin (Hb) using One-Pot technique. We investigated the haemocompatibility of these submicron particles, which is important for their application as intravenously administered drug carriers. Furthermore, RF-HSA-MPs was characterized in terms of size, morphology, drug encapsulation and drug release (study 1). Additionally, we investigated the effect of temperature as well as the presence of phagocytosis activating agents, *E. coli*, on the expression level of monocytes (study 2).

## **2. Methodology**

### **2.1. Study 1**

#### **2.1.1 HSA particle (HSA-MPs) Fabrication using CCD-technique**

The HSA-MPs were fabricated using a modification of a previously described CCD-technique (6,7). Briefly, 20 mL of 0.5 M  $\text{MnCl}_2$  solution containing 10 mg/mL HSA were mixed in a beaker for 1 min. Then 20 mL of 0.25 M  $\text{Na}_2\text{CO}_3$  were added rapidly under vigorous stirring at room temperature (RT). The obtained hybrid particles were separated by centrifugation and washed twice with 0.9% NaCl solution. The particles were incubated in a GA solution (final concentration 0.1%) at RT for 1 h. After centrifugation, 0.08 M glycine and 0.625 mg/mL  $\text{NaBH}_4$  were added to quench the remaining unbound aldehyde groups of GA in the particles. Subsequently, the  $\text{MnCO}_3$  template was removed by treatment with EDTA solution (0.25 M, pH 7.4) at RT for 30 min. Finally, the resulting particles were centrifuged, washed 3 times and resuspended in Ampuwa<sup>®</sup> for further use.

#### **2.1.2 Haemoglobin particle (Odex-HbMPs) Fabrication using One Pot-technique**

The Odex-HbMPs were fabricated by a modified protocol based on the CCD technique using 40T- and 70T-Odex as crosslinking. Briefly, equal volumes of solution 1 consisting of 0.25 M of  $\text{MnCl}_2$  and 50 mg/mL of Hb were rapidly mixed with solution 2 containing 0.25 M of  $\text{Na}_2\text{CO}_3$  and 40mg/mL of Odex in a beaker under vigorous stirring at RT for 30 s. Then, 5 mg/mL of HSA was added to the suspension and incubated for 5 min under stirring to allow the HSA to absorb on the surface of particles. The resulting suspension particles were dissolved in 0.25 M EDTA/0.05 M glycine for 30 min and reduced by 0.4 mg/mL of  $\text{NaBH}_4$ . Finally, the obtained Odex-cross-linked Hb particles (Odex-HbMP) were washed three times with PBS by centrifugation and suspended in sterile 0.9% NaCl. Odex cross-linked albumin particles (Odex-APs) as a control, were prepared following the same protocol using HSA particles.

#### **2.1.3 Riboflavin-HSA particle (RF-HSA-MPs) Fabrication using CCD-technique and Characterization**

The RF-HSA-MPs were fabricated following the method from section 2.1.1 using 10 mM RF in  $\text{MnCl}_2$  solution. The fabrication scheme of the submicron particles is shown Fig. 1.

HSA-MPs, as a control, were prepared following the same protocol using HSA particles with 4 mL DMSO without RF.

The amount of compound (RF/HSA/Hb) entrapped in the particles was determined as the difference between the total compound amount added and the free non-entrapped compound amount in the supernatants after co-precipitation and after each washing step. The RF concentration was determined spectroscopically measuring the absorbance of the supernatants at 445 nm with a microplate reader. The protein concentration was determined by Coomassie Plus (Bradford) Assay Kit (Thermo Fisher Scientific, IL, U.S.A.) and absorbance measurement at 595 nm. The Hb concentration in the Odex-HbMP was determined by alkaline haematin detergent (AHD)-575 method. The optical density of haematin was measured at 575 nm.

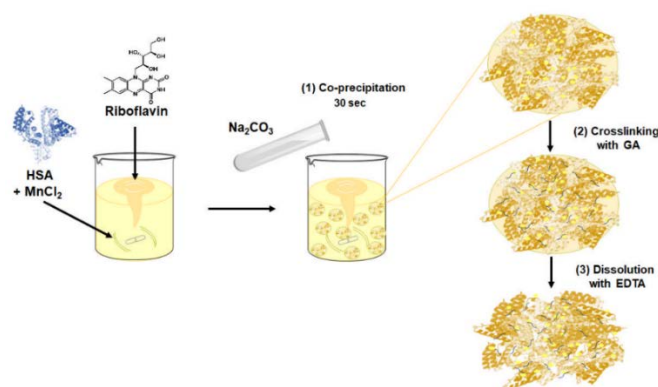


**Figure 1.** Scheme of the fabrication procedure of the submicron HSA particles containing RF (modified CCD-technique).

Measurement of the size, and zeta potential of microparticle prepared using PBS pH 7.4 were made on a Zetasizer Nano ZS instrument at 25 °C. Furthermore, the morphology of microparticles was investigated by atomic force microscopy (AFM) in tapping mode using a Nanoscope III Multimode AFM. The Nanoscope software was applied to record and analyze the obtained images. Moreover, the microparticle images were obtained by a confocal microscope equipped and the obtained images were subjected to the size analysis using the ImageJ software. Additionally, the particles were visualized using an Axio Observer.

#### 2.1.4. Hemocompatibility of HSA-MPs, RF-HSA MPs, and Odex-HbMPs

*In vitro* haemolytic activity was determined on the haemoglobin released by damaged erythrocytes. Blood sample stabilized by lithium heparin was washed with PBS by centrifugation in to separate red blood cells (RBCs). The washed RBCs were diluted with PBS and further mixed with microparticles, double distilled water as the positive (PC) or

PBS as a negative (NC) control. After incubation and centrifugation, the supernatants were collected and analysed by a microplate reader at 545 nm. The haemolysis ratio was calculated as the following Equation 1:

$$HR\% = (A_{test} - A_{NC}) / (A_{PC} - A_{NC}) \times 100\%, \quad (1)$$

where  $A_{test}$  is the absorbance of the tested sample,  $A_{NC}$  – the absorbance of the negative control in PBS and  $A_{PC}$  – the absorbance of the positive control in distilled water.

The influence of the microparticles on human platelets was investigated in platelet-rich plasma (PRP) samples. Whole human blood with sodium heparin anticoagulant was centrifuged to collect the PRP fraction. Then the microparticles were added to the PRP, carefully mixed and incubated in a water bath. PRP incubated with PBS were used as a control. To induce activation and aggregation of the platelets, the pre-incubated PRP samples were treated with arachidonic acid or epinephrine (Mölab, Langenfeld, Germany). Finally, the platelets were stained with anti-CD41a and anti-CD62p (p-selectin) antibodies and analyzed by flow cytometry.

The investigation of the phagocytic function of blood leukocytes with microparticles was evaluated *in vitro* in human whole blood using the commercial Phagotest kit. Manufacturer's instructions were partially modified (as described in (15)). The phagocytosing cell fractions were quantified by flow cytometry.

## 2.2. Study 2

### 2.2.1. Blood collection, preparation and leukocyte staining

Venous blood from healthy volunteers (written consent) was collected in two lithium heparin tubes at the same time: one tube was immediately transferred to an ice bath (0 °C), and the other was taken into a water bath and kept at 37 °C. Fig 2. shows an experimental design. The samples were handled in three different ways. Whole blood was aliquoted into 50 µL samples in three separate tubes. One tube was maintained always on ice. A second tube was chilled for 10 min at 0 °C and then transferred to a water bath for 10 min at 37 °C. The third tube was placed immediately and maintained in the water bath at 37 °C. After 10 min, all samples were placed in the ice-bath, and washed with ice-cold PBS. The cells were re-suspended and then incubated with anti-CD14 and anti-CD33 antibody

using concentrations suggested by the manufacturer for 30 min at 0 °C in darkness. After erythrocyte lysis, the cells were washed twice and analyzed by flow cytometry.

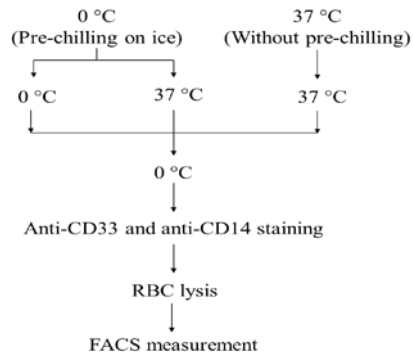


**Figure 2.** Schematic experimental design. Two sets of three tubes with whole blood from the test subject were handled as followed: two 50 µL aliquots of whole blood from ice bath (0 °C) cooler were either maintained always on ice or after pre-chilling warmed up to 37 °C. One 50 µL aliquot of whole blood from water bath (37 °C) was always prepared throughout at 37 °C.

### 2.2.2. Phagocytosis of bacteria at different temperatures

Opsionized *E. coli* ( $1-2 \times 10^9$  bacteria per mL, Phagoburst kit™) was used to examine the engulfment of bacteria. The samples were handled in the same way as in the temperature experiments, but were added 10 µL of non-labeled opsonized *E. coli*.

Phagotest of FITC-labeled opsonized *E. coli* was used to confirm healthy phagocytic activity of monocytes.

### 2.2.3 Internalization of CD33 during phagocytosis

To examine the internalization of CD33, 50 µL of blood were mixed with anti-CD14 and anti-CD33 antibody for 30 min at 0 °C in darkness. Then 10 µL opsonized *E. coli* was added and incubated at 37 °C or an ice bath for negative controls for 10 min.

After 10 min, the samples were cooled to 0 °C and washed with ice cold PBS. After erythrocyte lysis, cells were washed and analyzed by flow cytometry and confocal microscope.

### 2.2.4 Statistical analysis

Analyses and graphs were performed using GraphPad Prism 6 software (GraphPad, San Diego, CA). p-value of < 0.05, and is presented as \* (p < 0.05), \*\* (p < 0.05), or \*\*\*\* (p < 0.0001).

**Table 1:** List of all substances, antibodies, and test kits.

Substances	Abbreviation	Dilution/Dose	Company
Riboflavin	RF	50 mM	Sigma-Aldrich
Glutaraldehyde	GA	0.1%	Sigma-Aldrich
Manganese chloride tetrahydrate	MnCl <sub>2</sub> ·4H <sub>2</sub> O	0.5 M	Sigma-Aldrich

Sodium carbonate	Na <sub>2</sub> CO <sub>3</sub>	0.25 M	Sigma-Aldrich
Glycine	C <sub>2</sub> H <sub>5</sub> NO <sub>2</sub>	10%	Sigma-Aldrich
Sodium borohydride	NaBH <sub>4</sub>	10 mg/mL	Sigma-Aldrich
10x Phosphate buffered saline pH 7.4	PBS	1x	Fisher Scientific
20% Human albumin solution	HSA		Grifols Deutschland GmbH
Sodium hydroxide	NaOH	0.1 M	Carl Roth
Dimethyl sulfoxide	DMSO	100%	Carl Roth
Ampuwa® (aqua ad injectable)			Fresenius Kabi
Sodium chloride	NaCl	0.9%	Fresenius Kabi
Ethylenediaminetetraacetic acid	EDTA	0.5 M	Fluka
<b>Antibodies</b>			
PerCP/Cy5.5 anti-human CD33 antibody (clone WM53)	Anti-CD33	1:25	BioLegend
Alexa Fluor® 488 anti-human CD14 antibody (Clone M5E2)	Anti-CD14	1:25	BD Pharmingen
APC mouse anti-human CD41a	Anti-CD41a	1:20	Exbio
Alexa Fluor® 488 anti-human CD62P (P-Selectin) Antibody	Anti-CD62p	1:20	BioLegend
<b>Test kits</b>			
Phagotest™ kit		1:2	Glycotope-biotechnology
Phagoburst™ kit		1:2	Glycotope-biotechnology

**Table 2:** List of equipment/facility

<b>Equipment/facility</b>	<b>Company</b>
Hematocrit centrifuge	Mikro 22R, Hettich GmbH & CoKG, Tuttlingen, Germany
Confocal laser scanning microscopy	CLSM ZeissLSM 510 meta, Zeiss MicroImaging GmbH, Jena, Germany
Atomic force microscopy	Digital Instrument Inc., Santa Barbara, CA, USA
Axio Observer	Zeiss, Göttingen, Germany
Flow cytometry	FACS-Canto II, Becton and Dickinson, Franklin Lakes City, NJ, USA.
Magnetic Stirrer	Bibby Scientific CB161, Bibby Sterilin Ltd., Stone, Staffordshire, UK.
UV-vis-spectrophotometer	Hitachi U2800, Hitachi High-Technologies Corporation, Kreefeld, Germany
Zetasizer nano instrument	Malvern Instruments Ltd., Malvern, UK
Nanoscope III Multimode AFM	Digital Instrument Inc., Santa Barbara, CA, USA
Microplate reader	PowerWave340, BioTek Instruments GmbH, Bad Friedrichshall, Germany
ABX Micros 60 hematology analyzer	Horiba Europe GmbH, Berlin, Germany

### 3. Results and discussion

#### 3.1 Study 1

##### 3.1.1 Haemocompatibility of HSA-MPs, RF-HSA MPs, and Odex-HbMPs

Both HSA-MPs and RF-HSA MPs exhibited the percentage of hemolysis in the low range of 4% - 7% and in a dose-dependent manner as shown in Fig. 3. Therefore, the MPs did not cause strong hemolytic effects. However, according to criterion listed in the ASTM E2524-08 standard, more than 5% hemolysis indicates damage to RBCs caused by the test materials. This critical value is reached at particle concentration of 1% for both HSA-MPs and RF-HSA-MPs.

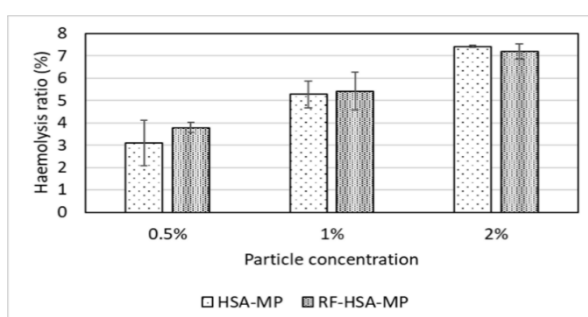


**Figure 3.** Hemolytic activity induced by HSA-MPs and RF-HSA-MPs for 3 h at 37 °C, concentration ranging from 0.5, 1, and 2%. Water and PBS served as positive (100%) and negative (0%) control, respectively. Data are presented as the mean percentage  $\pm$  SD (n = 3).

The haemolytic ratio of the RBCs incubated with different Odex-crosslinked particles is demonstrated in Table 3. It can be seen that the haemolysis ratio for the samples with Odex-APs and Odex-HbMPs was between 1% and 2% and so far they obviously do not damage the RBCs.

**Table 3.** The haemolytic ratio of the Odex-crosslinked particles

Test sample	Haemolysis ratio (%)
40T-APs	1.14 $\pm$ 0.36
70T-APs	1.03 $\pm$ 0.16
40T-HbMPs	1.67 $\pm$ 0.58
70T-HbMPs	1.77 $\pm$ 0.52
PBS	0 $\pm$ 0.00
Water	100 $\pm$ 0.00

Data are presented as mean  $\pm$  SD (n = 3).

Particle interaction with RBCs depends on the particle physicochemical properties such as size, surface charge and surface area. Negatively charged particles interact less with the negative charged cell surface than positively charged particles. Micron-sized particles are likely to produce a lower level of hemolysis than smaller particles (16–18). The increase in surface-to-volume ratio with the decrease in size of particles results in enlarged surface contact area and provides the chance for a cell membrane damage to

take place. This could explain the dose-dependent increase of hemolysis observed with the microparticles.

The measurement of the CD42b/CD62p co-expression in platelet samples treated with HSA-MPs and RF-HSA MPs revealed that there was no effect on the CD62p expression in CD42b positive cells. This is comparable to the control sample. Together with agonist, particles did not induce different behavior in the activation of the platelets in comparison with the samples treated with agonists only. Therefore, both HSA-MPs and RF-HSA-MPs did not activate the platelets and did not augment the platelet response to antagonists as shown in Fig. 4A.

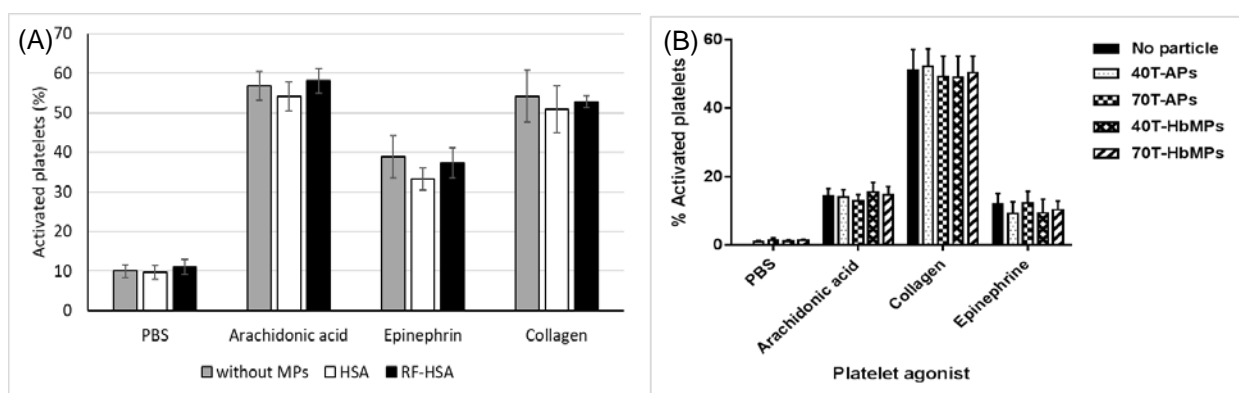


**Figure 4.** Platelet activation assay. FACS analysis of HSA-MPs or RF-HSA-MPs (A), and Odex-APs or Odex-HbMPs on platelet activation measured by determination of CD62p/CD42 co-expression. The presence of particles did not influence on platelet activation. The agonists (arachidonic acid, epinephrine, and collagen) induced platelet activation independent from the presence of particles.

The Odex-APs or Odex-HbMPs did not cause activation of the platelets as compared to the control sample which was incubated with PBS. Additionally, platelet activation induced by agonists including arachidonic acid, collagen and epinephrine of pre-incubated PRP with particles was comparable to the control samples. It can be concluded that Odex-APs or Odex-HbMPs do not influence the function of platelets and therefore no negative side effects on the haemostasis are expected as show in Fig. 4B.

Representative results of the phagocytic activity of the HSA-MPs and RF-HSA-MPs was analyzed are shown in Fig. 5. The fluorescence signal from both kind of particles can be detected in the PE-A channel of the flow cytometer and the FITC-labelled *E. coli* (used as a standard positive control for phagocytosis) can be detected in the FITC-A channel. The three main populations of white blood cells: granulocytes, monocytes and lymphocytes were gated on a SSC/FSC dot plots (dot-plot Fig. 5A). The histograms in Fig. 5B and C

represent the distribution of the fluorescence intensity within the population of HSA-MPs and RF-HSA-MPs in the PE-channel. The higher fluorescence emission of the RF-HSA-MPs is clearly visible by the shift of their histogram by one order of magnitude to higher fluorescence intensities. The analysis of the fluorescence distribution in the granulocyte and monocyte populations of the samples incubated at 37°C with FITC-*E. coli* (Fig. 5D and G) shows a strong right shift in the FITC channel due to the engulfment of the fluorescent bacteria. This is not the case in the samples incubated with both kind of particles (Fig. 5E-I). The particles do not induce phagocytosis and therefore their immunogenicity is low.

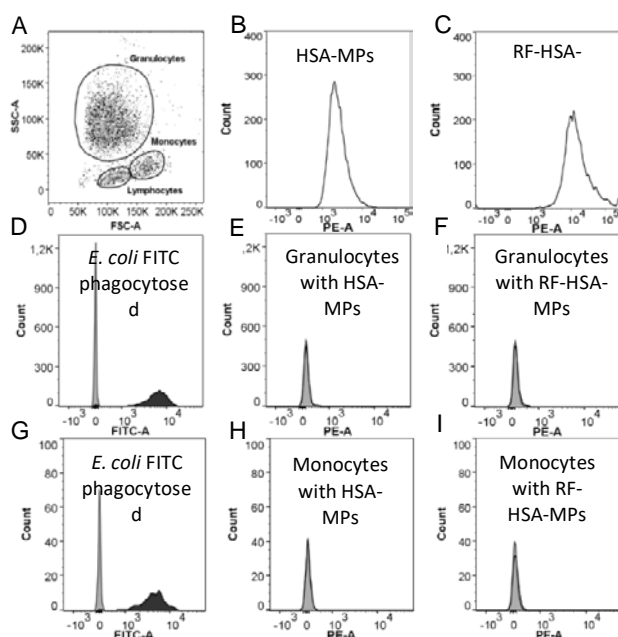


**Figure 5.** Phagocytosis assay. (A) Three groups of white blood cells are identified based on their FSC/SSC: granulocytes, monocytes and lymphocytes. Histograms represent fluorescence intensity of (B) HSA-MPs and (C) RF-HSA-MPs in the PE-A channel. Phagocytosis of FITC-labeled opsonized *E. coli* in granulocytes (D) and monocytes (G) (grey area: negative controls incubated at 0 °C; black area: granulocytes and monocytes with phagocytosed FITC-*E. coli*). Representative histograms of fluorescence intensity of monocytes and granulocytes after interaction with (E, H) HSA-MPs and (F, I) RF-HSA-MPs (grey area: negative controls incubated at 0 °C; black line, granulocytes and monocytes incubated at 37 °C MP). Data are representative of n = 3 independent phagocytosis assays showing the same trends.

Indirect phagocytic assay was employed to investigate Odex-crosslinking particles. The summarized results in dependency on the pre-incubation time are shown in Figure 6. The number of granulocytes and monocytes phagocytosing FITC-*E. coli* was not significantly different for Odex-crosslinked particles and PBS (negative control) over all pre-incubation times. In contrast, the positive control, *E. coli*, demonstrated a gradually decrease in the percentage of the cells engulfing FITC-*E. coli* in a time-dependent manner, due to the previously performed phagocytosis of non-fluorescing *E. coli*.

Avoiding clearance by phagocytosis is very important in drug delivery systems using microparticles and in many cases requires complicated and expensive surface modification of the drug carriers (19). Therefore, our microparticles are highly promising for applications as drug delivery systems.

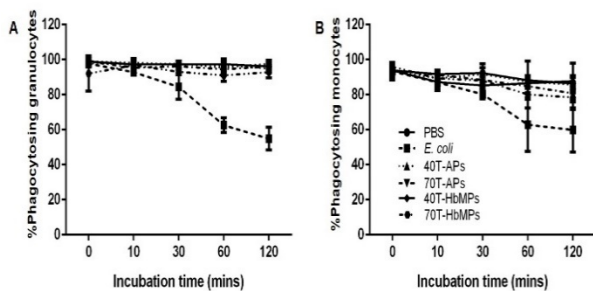


**Figure 6.** Percentage of phagocytic activity of (A) granulocyte and (B) monocyte on Odex-APs and Odex-HbMPs compared with PBS (negative control) and *E. coli* (positive control). On one hand, the fluorescence signal of detective FITC-*E. coli* decreased grammatically across incubation periods in positive control. On the other hand, leukocyte preincubated with PBS as well as Odex-APs and Odex-HbMPs showed a strong detective FITC-*E. coli* and there was no change over the incubation times. Data are presented as mean  $\pm$  SD (n = 3)

### 3.1.2. Fabrication and Characterization of RF-HSA-MPs

The immobilization of compounds through compound capture in the process of their formation (co-precipitation) is effective for the protein entrapment for carbonate particles (20,21). The encapsulation efficiency was attributed to the electrostatic attraction between negatively charged proteins and more positively charged  $\text{MnCO}_3$  as well as to the stronger affinity of  $\text{Mn}^{2+}$  to HSA (22).

Nevertheless, the immobilization of low molecular weight compounds into polymeric systems is still a great challenge. Here we used RF as a model to investigate the potential of the CCD-technique to deliver carrier systems for low molecular weight drugs with poor water solubility. The weakly water-soluble RF was incorporated together with HSA via the CCD technique. RF was added during the first step of the particle preparation, the co-precipitation, together with HSA. It has been shown previously that RF interacts with albumin through adsorption on tryptophan residues via hydrophobic interactions (23,24), which was expected to support the RF entrapment into the HSA-MPs.

The co-precipitation was performed at the previously optimized concentration of  $\text{MnCl}_2$  and  $\text{Na}_2\text{CO}_3$  for the entrapment of HSA (0.125 M). The average amounts of entrapped HSA and RF under these preparation conditions were  $2.9 \pm 0.8$  mg and  $2.5 \pm 0.5$  mg/mL particles, respectively. Accordingly, in a particle suspension with a volume concentration of 10%, the RF concentration will be roughly 290  $\mu\text{g/mL}$  which is more than 4 times higher than the solubility of RF in water at 20°C (70  $\mu\text{g/mL}$ , GESTIS – materials data base).

On CLSM images the HSA-MPs and RF-HSA-MPs exhibited a size between 0.9 and 1.1  $\mu\text{m}$  with an average long diameter of 1  $\mu\text{m}$ . These values correlated well with the DLS measurements by Zetasizer Nano which delivered values of  $1.04 \pm 0.15$   $\mu\text{m}$ . No

significant differences were found between HSA-MPs and RF-HSA-MPs. Under the conditions chosen for this study, a rapid mixing of all compound at RT, the size of the particles was highly reproducible.

Compatible with AFM as shown in Fig. 7, the shape of both kind of particles was peanut-like. Here the long diameter measured for both kinds of particles varied between 780 and 890 nm without significant differences between them. The thickness of the particles determined from the height profiles was  $400 \pm 45$  nm, which corresponds to the half of the long diameter. The incorporation of RF does not seem to interfere with the geometry of the particles.

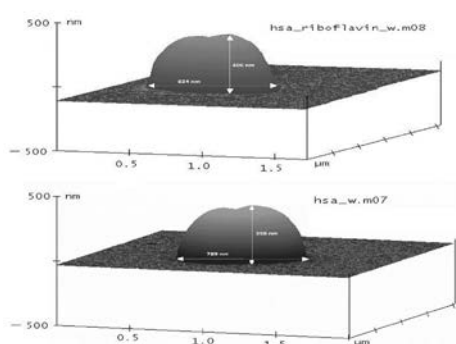


**Figure 7.** AFM images of RF-HSA-MPs (top) and HSA-MPs (bottom) in three dimensional (3D)-mode. The size of the particles was determined from the height profiles in horizontal and vertical direction. The values included in the images are representative examples.

The main factors, which determine the size of the  $\text{MnCO}_3$  particles are the concentrations of manganese and carbonate ions, the flow rate of the solutions during mixing and the temperature. Variation of these parameters in a suitable way is needed for controlling size and shape of the particles in co-precipitation reactions (25). In this study,  $\text{MnCO}_3$  was synthesized by a co-precipitation method using  $\text{MnCl}_2$  and  $\text{Na}_2\text{CO}_3$  as manganese and carbonate source, respectively. The precipitation is completed very fast at RT with high salt concentration, and with EDTA dissolution at neutral pH. These conditions are suitable for the preparation of protein particles avoiding denaturation and preserving the function of the proteins.

In addition, the zeta-potential of microparticles is important parameter for the stability of a particle suspension, in particular for the behavior of the particles in biological fluids. Therefore, the measurements of the zeta-potential were conducted in PBS (pH 7.4, conductivity 17 mS/cm). Both kind of particles exhibited zeta potential of approximately -15 mV, which is a relatively high value at the high ionic strength of PBS. In water the zeta-potential was around -39 mV, which contributes to the high colloidal stability and absence of aggregation of the particles in biologically relevant media.

Due to a weak autofluorescence of the GA cross-linking, microparticles could be detected in the fluorescence channels of the confocal microscope. However, the RF-HSA-MPs showed significantly stronger fluorescence due to the entrapped-RF (Fig. 8B1-2). More clearly the difference of the fluorescent emission is demonstrated in the 3D color surface map of representative a single HSA-MP and RF-HSA-MP (Fig. 8(A3) and 8(B3), respectively). The higher value of the intrinsic fluorescence of the RF-HSA-MP confirms the successful entrapment of the drug into the particles. Additionally, the intrinsic fluorescence is very useful for tracking these particles upon their interactions with cells without need of additional labeling.

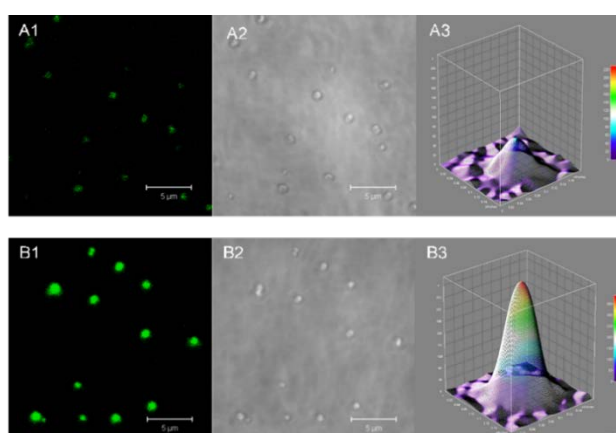


**Figure 8.** Analysis of intrinsic fluorescence in MPs. Confocal micrograph of HSA-MPs in (A1) fluorescence mode and (A2) transmission mode, respectively and B1 and B2, confocal micrograph of RF-HSA-MPs in fluorescence mode and transmission mode, respectively. Fluorescence emission intensity in 3D color map surface images of (A3) HSA-MPs and (B3) RF-HSA-MPs at excitation wavelength of 480 nm and emission wavelength of 535 nm.

### 3.1.2. *In Vitro* Release of RF from the RF-HSA-MPs

The drug release from RF-HSA-MPs was studied using a dialysis technique against release media shown in Fig. 9A. The decrease of the RF concentration remaining in the particle suspensions was followed for 80 hours. The drug release profiles in both investigated media is bi-phasic with an initial burst release of approximately 7% in PBS and 12% in RPMI from the initial RF concentration during the first 2 to 3 hours. Thereafter, the release rate decreases and a sustained release was observed until the end of the experiments. After 80 hours the drug release will remain 30% and 45% of the initial loading in PBS and in RPMI, respectively.

The RF release in RPMI 1640 medium containing various amino acids and 10% calf serum albumin is significantly faster, probably due to the adsorption of the released RF by these compounds, which results in a clearance of the free RF from the solution. Consequently, the concentration of the freely dissolved RF in the RPMI will remain lower than in PBS leading to a faster release. A similar release behavior was shown for a

hydrophobic anti-cancer drug from a micelle system. The release was accelerated in buffers containing albumin (26) due to the binding of the drug to hydrophobic regions of albumin.

The release profiles were fitted using the model of Pappas (Equation 2), which is suitable to describe bi-phasic controlled release of entrapped drugs from particles. The values calculated for  $K_1$  are larger than  $K_2$  by more than one magnitude for both PBS and RPMI. This indicates that the release is dominated by the diffusion mechanism. In RPMI the predomination by the Fickian diffusion is much stronger due to the greater RF concentration gradient between RF in the RF-HSA-MPs and the bulk RPMI-phase as shown in Fig. 9B.

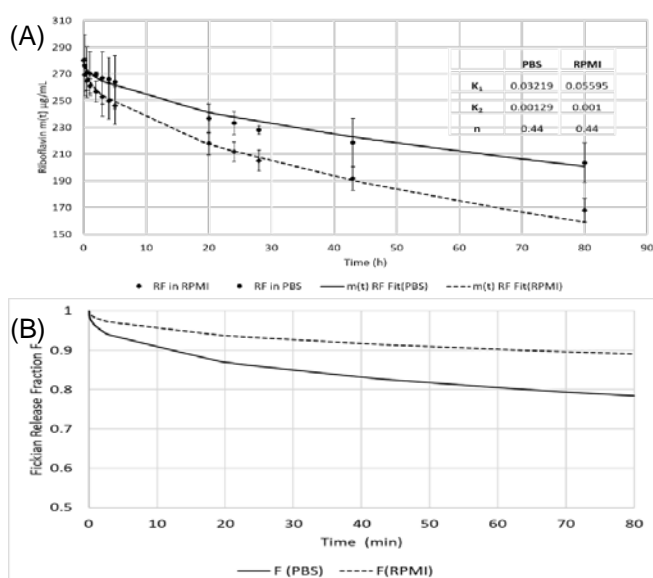


**Figure 9.** (A) Release profiles of RF in PBS pH 7.4 (●) and RPMI 1640 medium (◆) at RT calculated for the remaining RF concentration entrapped in the RF-HSA-MPs. The RF concentrations were fitted using the Pappas equation  $m(t)/m(\infty) = k_1t^n + k_2t^{2n}$ . Values are expressed as mean  $\pm$  SD ( $n = 3$ ). (B) Fickian release fraction (F) of RF-HSA-MPs in PBS and in RPMI. The release of RF in RPMI is much stronger predominated by the Fickian diffusion, due to the greater RF concentration gradient between RF in the RF-HSA-MPs and the bulk RPMI-phase.

To sum up, we demonstrated that the encapsulation of biopolymers can be performed by capturing into the growing  $MnCO_3$  particles using CCD-technique and One-Pot formulation. These microparticles exhibited a very good haemocompatibility. The HSA-MPs and RF-HSA-MPs produced by CCD-technique showed negatively charged with a narrow size distribution with diameters less than 1  $\mu m$ . The release behavior of RF exhibited prolonged-release formulation. These finding suggested that RF-HSA-MPs represent a compelling strategy for a long-term drug delivery. Taken together, the CCD-technique and One-Pot formulation is applicable to various biopolymers despite their molecular weight. This work provides basic information for the production and application of HSA-based micro-particles as a drug carrier system.

## **3.2 Study 2**

The monocyte, granulocyte and lymphocyte populations could be clearly distinguished on the basis of their SSC/FSC dot plots using flow cytometry. The monocytes are then defined by sequential gating on all CD14-positive leukocytes in light scatter plots. More than ninety percent of the CD-33 positive were CD14-positive cells. The CD33 labeling was highly specific for the monocytes (Fig. 10A).

### **3.2.1 Temperature-dependent influence in CD33 expression**

The CD33 expression on monocytes was examined under temperature treatment. Monocytes maintained at 0 °C at all stages of preparation were defined as the reference levels of expression of CD33.

Monocytes that were pre-chilled and subsequently warmed up and those maintained at 37 °C throughout their preparation showed a significantly higher RFI of CD33 compared to the reference cells maintained at 0 °C. There was slightly lower, but not significantly different expression level, for cells cooled at 0 °C and subsequently warmed to 37 °C than those cells maintained at 37 °C at all stages of preparation. The effect of incubation temperature on CD33 expression on monocytes is shown in Fig. 10B.

Our results have shown that the RFI of CD33-positive monocytes which had been first cooled and then re-warmed was up-regulated compared with those held throughout at 0 °C, but not significantly different from those handled throughout at 37 °C. To our knowledge, the effect of temperature on the expression levels of CD33 had not been evaluated yet. The molecular mechanism underlying up-regulation are still unclear. One possibility is that the rapid increase in surface presentation of CD33 on stimulated monocytes may be caused by a translocation of intracellular pool to the cell surface (27).

### **3.2.2 Changes in CD33 expression due to phagocytosis of *E. coli***

Phagocytosis of *E. coli* induced a significant increase in monocyte expression of CD33 of cells maintained at 37 °C, or cooled to 0 °C and subsequently warmed to 37 °C in comparison with the reference population of cells held at 0 °C which did not phagocytose *E. coli* (Fig. 10C). The ability of monocytes to perform phagocytosis was tested for each donor in parallel applying the standard procedure of FITC-labeled *E. coli* as recommended in the Phagotest™ kit instructions.

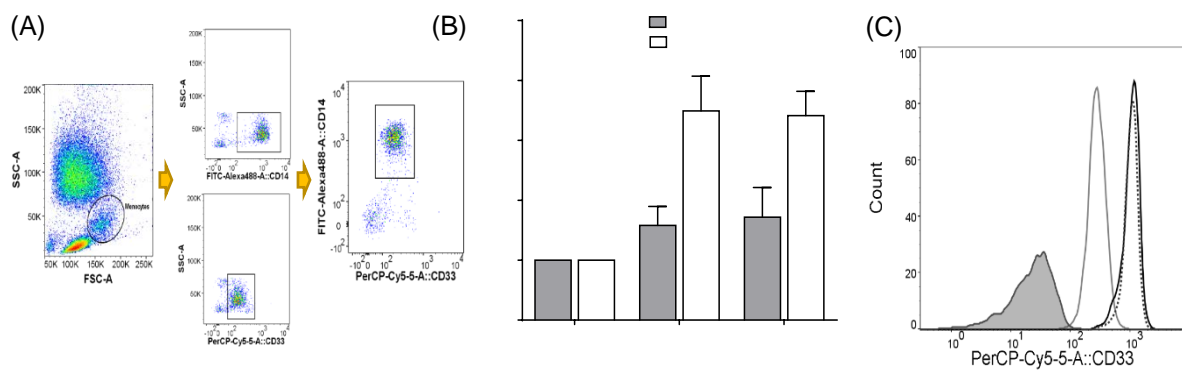


Figure 10. (A) Gating of the cells, CD14 and CD33 labeled cells. Three groups of cells were identified based on their FSC/SSC. By incubating these cells with Alexa Fluor® 488 anti-CD14 and PerCP/Cy5.5-anti-CD33, monocytes can be identified and MFI was interpreted as positive for CD33 expression from the sample held at 0 °C. (B) Effect of incubation temperature and phagocytosis on CD33 expression on monocytes. The bar graphs show the percentage of RFI of CD33 expression (n = 6). Three populations of monocytes were assessed for expression, cells chilled at 0 °C, those warmed from 0 °C to 37 °C, cells held throughout at 37 °C without stimulation (solid bar) or with *E. coli* stimulation (open bar). Each bar represents the mean  $\pm$  SD, and asterisks indicate the significance of differences (\*P < 0.1; \*\*\*\*P < 0.0001). (C) FACS analysis of CD33 fluorescence intensity (gray area, background; gray line, monocytes chilled at 0 °C; black line, monocytes chilled at 0 °C, warmed up from 0 °C to 37 °C; dash line, monocytes held through-out at 37 °C).

The results clearly show that together with temperature, phagocytosis has an augmented effect on the expression of CD33. Monocytes held permanently at 37 °C and incubated with *E. coli* up-regulate the expression of CD33 during phagocytosis in contrast to cells chilled throughout at 0 °C. An additional large increment of CD33 expression occurs when the cells interact with *E. coli*. The effect of phagocytosis on CD33 expression on monocytes is shown Fig. 10B.

It has been reported that the stimulation of LPS results in increased surface expression of CD11b, and CD35 on monocytes, suggesting that these rapid changes may be caused by the inflammatory response (28). In our study, an increase in CD33 expression upon *E. coli* stimulation was found. Therefore, up-regulation in CD33 may be involved in the inflammatory response, which has been shown to follow the initial systemic pro-inflammatory reaction. CD33 has a high expression on monocyte surface as well as in an internal compartment after stimulation of formylated peptides (fMLP), a bacterial-derived peptide. This could affect the expression of CD33 on the cell surface in response to an inflammatory stimulus (27). It is also found that the high antigen induction on the cell surface upon *E. coli* activation may imply the preformed intracellular pool of surface antigen which was rapidly translocated to the surface upon activation of these cells (27). However, how LPS-elicited cell signaling regulates CD33 surface expression is not clear.

The results presented here are in contradiction with previous studies which have published that down-regulation of CD33 expression was observed when monocytes were activated by LPS (27,29). However, LPS is only one component of the gram-negative bacterial cell wall. Our work was performed with opsonized *E. coli* which present a cellular pathogen. The immune system activation and subsequent responses to LPS and *E. coli* may therefore differ. Another observation, in our experiments, CD33 expression increases considerably within a very short time after contact with bacteria. This is in disagreement with the previously reported results, where the incubation time of LPS was up to 2h (27,29). It appears that a longer time period is required to change the CD33 expression profiles by LPS. Based on the raising level of CD33 expression after exposure to *E. coli*, revealed significantly altered expression levels in monocytes might be a key element for diagnosis of septic shock. However, the outcomes should be further verified by higher number of blood samples from healthy donors and sepsis patients.

### **3.2.3 Internalization of CD33 during phagocytosis**

The influence of phagocytosis was further investigated comparing the CD33 staining in samples where the antibody was applied after stopping the phagocytosis of *E. coli* (shock-cooling at 0 °C) with the staining of samples where the antibody was added before phagocytosis activation (warming up to 37 °C). In parallel to the quantitative determination of CD33 expressing monocytes by flow cytometry, we studied also the distribution of fluorescence in the cells by CLSM. Interestingly, by performing double staining, we found that in monocytes the CD14 co-localized with CD33. It can be seen that the monocytes stained after stopping the phagocytosis exhibit a relatively weak fluorescence signal with a distribution mainly on the cell surface shown fig. 10A. In contrast, the samples stained before adding *E. coli*, the fluorescence signal was significantly higher and fluorescence was observed by microscopy not only on the surface but also inside the cells as shown in Fig. 11B.

The flow cytometry measurements of the blood samples activated for phagocytosis with *E. coli* showed a slightly enhanced fluorescence signal in the PerCP-Cy5.5 channel of the granulocyte population. Fluorescence from CD33-positive granulocytes could only be detected when anti-CD33 was added before performing phagocytosis in contrast to the samples where the staining was performed after stopping phagocytosis (Fig. 12B).

Since this population was also clearly negative for staining with anti-CD33 without *E. coli* stimulation, a certain non-specific binding of the PerCP-Cy5.5-stained CD33 antibody on the opsonized *E. coli* was assumed. To confirm this, we incubated the opsonized unlabeled *E. coli* used for the activation of phagocytosis with the PerCP-Cy5.5-anti-CD33 and measured the fluorescence signal of the bacteria in the PerCP-Cy5.5 channel with the same settings as for the cells (Fig. 12A). The obtained fluorescence signal was similar to the signal measured in the PerCP-Cy5.5 for granulocytes stained before phagocytosis confirming that this signals is due to the engulfed bacteria with some antibody bound on them. In contrast, the fluorescence signal of the monocyte population is at least one order of magnitude higher in the same sample (Fig. 12C).

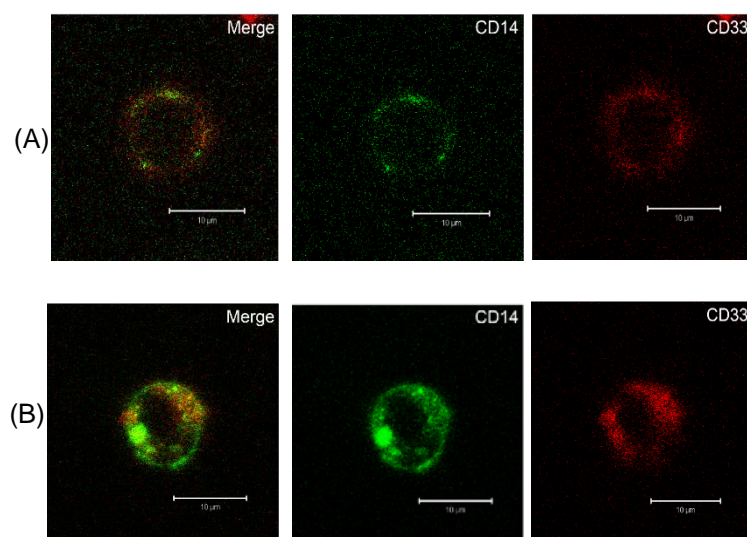


**Figure 11.** CLSM images of monocytes stained with PerCP/Cy5.5 anti-CD33 (fluorescence mode and overlay micrographs). (A) The cells were stained at 0 °C with PerCP/Cy5.5 anti-CD33 after performing phagocytosis of non-labeled *E. coli*. (B) The cells were first incubated with both Alexa Fluor® 488 anti- CD14 and PerCP/Cy5.5 anti-CD33 for 30 min at 37 °C and then with non-labeled *E. coli* at 37 °C, which allowed to internalize antibody-bound CD14 and CD33. The monocytes phagocytosed *E. coli*, which results in intracellular fluorescence. Co-localization of CD14 and CD33 staining was detected in yellow.

It has been shown that the engagement of both surface CD33 antigen and anti-CD33 antibody, induces receptor-mediated endocytosis (30), resulting in CD33 internalization of the antigen/antibody complex into the cells (31). This process may reduce the CD33 presented on the cell surface, but it is continuously re-expressed (32). The mechanism of action indicated that the presence of ITIM in the intracellular domain of CD33 is critical for the antibody-mediated CD33 internalization (30,33). Intracellular trafficking of CD33 shows that it undergoes endocytosis *via* clathrin-mediated uptake and further traffics to endosomes and processes in lysosomes (33). Moreover, phosphorylation-dependent ubiquitylation of CD33 decreased the cell surface expression and increased the rate of CD33 internalization (34). As a Siglec family member, CD33 has lectin-like recognition molecules which is one of the pattern-recognition receptors (PRRs) (35). These receptors

recognize pathogen-associated molecular patterns (PAMPs) from microbial pathogens in the first step of phagocytic process. An immune response is then triggered when PAMPs are recognized. There are some studies mentioned that the treatment of monocytes with anti-CD33 antibodies induced the production of pro-inflammatory cytokines (IL-1 $\beta$ , IL-8 and TNF- $\alpha$ ) (29) including recruited the tyrosine phosphatase SHP-1 and SHP-2 (14,36) and resulted in down-regulated CD64-induced calcium influx (14,37). Taken together, our findings may imply that CD33 could play an associate or even a crucial role in phagocytosis of microbial pathogens.

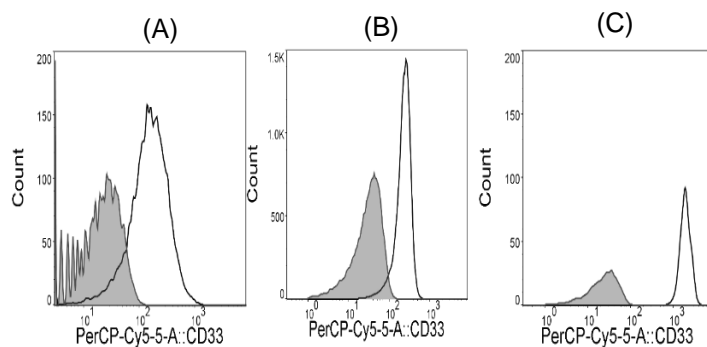


**Figure 12.** Flow cytometry histograms. (A) Opsonized *E. coli* (grey area) and opsonized *E. coli* incubated with PerCP-Cy5.5-anti-CD33 at 37 °C (black line). (B) Granulocytes and (C) monocytes in samples stained with PerCP-Cy5.5-anti-CD33 after performing phagocytosis (grey area), and samples incubated with PerCP-Cy5.5-anti-CD33 before stimulation with non-labeled *E. coli* at 37 °C (black line). The y-axis value varies depending on the number of cell count.

In conclusion, this study shows that the expression of CD33 on monocytes is influenced by various stimuli such as temperature as well as pathogen. Therefore, excessive processing temperatures and the presence of *E. coli* should be taking into account when analyzing leukocyte surface antigens. Further studies are required to elucidate the particular mechanisms of CD33 expression and its impact to the immune system.

## 4. Bibliography

1. Xiong Y, Georgieva R, Steffen A, Smuda K, Bäuml H. Structure and properties of hybrid biopolymer particles fabricated by co-precipitation cross-linking dissolution procedure. *J Colloid Interface Sci.* 2018;514:156–64.
2. Bäuml H, Xiong Y, Liu ZZ, Patzak A, Georgieva R. Novel hemoglobin particles—promising new-generation hemoglobin-based oxygen carriers. *Artif Organs.* 2014;38(8):708–14.
3. Kloypan C, Prapan A, Suwannasom N, Kaewprayoon W, Steffen A, Xiong Y, Baisaeng N, Georgieva R, Bäuml H. Improved oxygen storage capacity of haemoglobin submicron particles by One-Pot formulation. *Artif Cells, Blood Substitutes, Biotechnol.* 2018;46(sup3):S964–72.
4. Kloypan C, Suwannasom N, Chaiwaree S, Prapan A, Smuda K, Baisaeng N, Pruß A, Georgieva R, Bäuml H. In-vitro haemocompatibility of dextran-protein submicron particles. *Artif Cells, Nanomedicine Biotechnol.* 2019;47(1).
5. Bäuml H, Georgieva R. Micro-particles, blood-substitute and method for forming same. 12741 P-EP, 2007.
6. Bäuml H, Georgieva R. Coupled enzyme reactions in multicompartement microparticles. *Biomacromolecules.* 2010;11(6):1480–7.
7. Xiong Y, Steffen A, Andreas K, Müller S, Sternberg N, Georgieva R, Bäuml H. Hemoglobin-based oxygen carrier microparticles: Synthesis, properties, and in vitro and in vivo investigations. *Biomacromolecules.* 2012;13(10):3292–300.
8. Xiong Y, Liu ZZ, Georgieva R, Smuda K, Steffen A, Sendeski M, Voigt A, Patzak A, Bäuml H. Nonvasoconstrictive hemoglobin particles as oxygen carriers. *ACS Nano.* 2013;7(9):7454–61.
9. Sucić M, Kolevska T, Kopjar B, Kosanovic M, Drobnjak M, Zalud I, Marusic M.. Accuracy of routine flow-cytometric bitmap selection for three leukocyte populations. *Cytometry.* 1989;10(4):442–7.
10. Freeman SD, Kelm S, Barber EK, Crocker PR. Characterization of CD33 as a new member of the sialoadhesin family of cellular interaction molecules. *Blood.* 1995;85(8):2005–12.
11. Andrew RG, Torok-Storb B, Bernstein ID. Myeloid-associated differentiation antigens on stem cells and their progeny identified by monoclonal antibodies. *Blood.* 1983;62(1):124–32.
12. Terstappen LWMM, Hollander Z, Meiners H, Loken MR. Quantitative comparison lineages of mature of myeloid peripheral antigens on five lineages of mature peripheral blood cells. *J Leukoc Biol.* 1990;48:138–48.
13. Crocker PR, Redelinguys P. Siglecs as positive and negative regulators of the immune system. *Biochem Soc Trans.* 2008;36(6):1467–71.
14. Paul SP, Taylor LS, Stansbury EK, McVicar DW. Myeloid specific human CD33 is an inhibitory receptor with differential ITIM function in recruiting the phosphatases SHP-1 and SHP-2. *Blood.* 2000;96(2):483–90.
15. Suwannasom N, Smuda K, Kloypan C, Kaewprayoon W, Baisaeng N, Prapan A, Chaiwaree S, Georgieva R, Bäuml H. Albumin submicron particles with entrapped riboflavin — fabrication and characterization. *Nanomaterials.* 2019;9(3):482.
16. Choi J, Reipa V, Hitchins VM, Goering PL, Malinauskas RA. Physicochemical characterization and in vitro hemolysis evaluation of silver nanoparticles. *Toxicol Sci.* 2011;123(1):133–43.
17. Zook JM, MacCuspie RI, Locascio LE, Halter MD, Elliott JT. Stable nanoparticle aggregates/agglomerates of different sizes and the effect of their size on hemolytic cytotoxicity. *Nanotoxicology.* 2011;5(4):517–30.
18. Mayer A, Vadon M, Rinner B, Novak A, Wintersteiger R, Fröhlich E. The role of nanoparticle size in hemocompatibility. *Toxicology.* 2009;258(2–3):139–47.
19. Evora C, Soriano I, Rogers RA, Shakesheff KM, Hanes J, Langer R. Relating the phagocytosis of microparticles by alveolar macrophages to surface chemistry: the effect of

- 1,2-dipalmitoylphosphatidylcholine. *J Control Release*. 1998;51(2–3):143–52.
20. Petrov AI, Volodkin D V, Sukhorukov GB. Protein calcium-carbonate coprecipitation: a tool for protein encapsulation. *Biotechnol Prog*. 2005;21:918–25.
  21. Vantsyan MA, Kochetkov AA, Marchenko IV, Kiryukhin YI, Nabatov BV, Artemov VV, Bukreeva, TV. Nanostructured calcium carbonate particles as fluorophore carriers. *Crystallogr Reports*. 2015;60(6):951–8.
  22. Fanali G, Cao Y, Ascenzi P, Fasano M. Mn(II) binding to human serum albumin: A <sup>1</sup>H-NMR relaxometric study. *J Inorg Biochem* . 2012;117:198–203.
  23. Zhao H, Ge M, Zhang Z, Wang W, Wu G. Spectroscopic studies on the interaction between riboflavin and albumins. *Spectrochim Acta Part A Mol Biomol Spectrosc*. 2006;65(3):811–7.
  24. Memarpoor-Yazdi M, Mahaki H. Probing the interaction of human serum albumin with vitamin B2 (riboflavin) and L-Arginine (L-Arg) using multi-spectroscopic, molecular modeling and zeta potential techniques. *J Lumin*. 2013;136:150–9.
  25. Pourmortazavi SM, Rahimi-Nasrabadi M, Davoudi-Dehaghani AA, Javidan A, Zahedi MM, Hajimirsadeghi SS. Statistical optimization of experimental parameters for synthesis of manganese carbonate and manganese oxide nanoparticles. *Mater Res Bull*. 2012;47(4):1045–50.
  26. Liu J, Zeng F, Allen C. Influence of serum protein on polycarbonate-based copolymer micelles as a delivery system for a hydrophobic anti-cancer agent. *J Control Release*. 2005;103(2):481–97.
  27. Siddiqui SS, Springer SA, Verhagen A, Sundaramurthy V, Alisson-Silva F, Jiang W, GhoshP, Varki A. The Alzheimer's disease-protective CD33 splice variant mediates adaptive loss of function via diversion to an intracellular pool. *J Biol Chem*. 2017;292(37):15312–20.
  28. Furebring M, Håkansson L, Venge P, Sjölin J. Differential expression of the C5a receptor and complement receptors 1 and 3 after LPS stimulation of neutrophils and monocytes. *Scand J Immunol*. 2004;60(5):494–9.
  29. Lajaunias F, Dayer J-M, Chizzolini C. Constitutive repressor activity of CD33 on human monocytes requires sialic acid recognition and phosphoinositide 3-kinase-mediated intracellular signaling. *Eur J Immunol*. 2005;35(1):243–51.
  30. Walter RB, Raden BW, Zeng R, Häusermann P, Bernstein ID, Cooper JA. ITIM-dependent endocytosis of CD33-related Siglecs: role of intracellular domain, tyrosine phosphorylation, and the tyrosine phosphatases, Shp1 and Shp2. *J Leukoc Biol*. 2008;83(1):200–11.
  31. Audran R, Drenou B, Wittke F, Gaudin A, Lesimple T, Toujas L. Internalization of human macrophage surface antigens induced by monoclonal antibodies. *J Immunol Methods*. 1995;188(1):147–54.
  32. Van Der Velden VHJ, Te Marvelde JG, Hoogeveen PG, Bernstein ID, Houtsmuller AB, Berger MS, van Dongen JJM. Targeting of the CD33-calicheamicin immunoconjugate Mylotarg (CMA-676) in acute myeloid leukemia: in vivo and in vitro saturation and internalization by leukemic and normal myeloid cells. *Blood*. 2001;97(10):3197–204.
  33. Walter RB, Raden BW, Kamikura DM, Cooper JA, Bernstein ID, Dc W, Walter RB, Raden BW, Kamikura DM, CoopeJA, Bernstein ID. Influence of CD33 expression levels and ITIM-dependent internalization on gemtuzumab ozogamicin-induced cytotoxicity. *neoplasia*. 2012;105(3):1295–302.
  34. Walter RB, Häusermann P, Raden BW, Teckchandani AM, Kamikura DM, Bernstein ID, Cooper JA. Phosphorylated ITIMs enable ubiquitylation of an inhibitory cell surface receptor. *Traffic*. 2008;9(2):267–79.
  35. Vasta GR. Roles of galectins in infection. *Nat Rev Microbiol*. 2009;7(6):424–38.
  36. Taylor VC, Buckley CD, Douglas M, Cody AJ, Simmons DL, Freeman SD. The myeloid-specific sialic acid-binding receptor, CD33, associates with the protein-tyrosine phosphatases , SHP-1 and SHP-2. *J Biol Chem*. 1999;274(17):11505–12.
  37. Ulyanova T, Blasioli J, Woodford-Thomas TA, Thomas ML. The sialoadhesin CD33 is a myeloid-specific inhibitory receptor. *Eur J Immunol*. 1999;29(11):3440–9.

## **Declaration of own contribution to the submitted publications**

„Ich, Nittiya Suwannasom, versichere an Eides statt durch meine eigenhändige Unterschrift, dass ich die vorgelegte Dissertation mit dem Thema: Biocompatibility of Biopolymer Submicron Particles selbstständig und ohne nicht offengelegte Hilfe Dritter verfasst und keine anderen als die angegebenen Quellen und Hilfsmittel genutzt habe.

Alle Stellen, die wörtlich oder dem Sinne nach auf Publikationen oder Vorträgen anderer Autoren beruhen, sind als solche in korrekter Zitierung kenntlich gemacht. Die Abschnitte zu Methodik (insbesondere praktische Arbeiten, Laborbestimmungen, statistische Aufarbeitung) und Resultaten (insbesondere Abbildungen, Graphiken und Tabellen werden von mir verantwortet.

Meine Anteile an etwaigen Publikationen zu dieser Dissertation entsprechen denen, die in der untenstehenden gemeinsamen Erklärung mit dem/der Betreuer/in, angegeben sind. Für sämtliche im Rahmen der Dissertation entstandenen Publikationen wurden die Richtlinien des ICMJE (International Committee of Medical Journal Editors; [www.icmje.org](http://www.icmje.org)) zur Autorenschaft eingehalten. Ich erkläre ferner, dass mir die Satzung der Charité – Universitätsmedizin Berlin zur Sicherung Guter Wissenschaftlicher Praxis bekannt ist und ich mich zur Einhaltung dieser Satzung verpflichte.

Die Bedeutung dieser eidesstattlichen Versicherung und die strafrechtlichen Folgen einer unwahren eidesstattlichen Versicherung (§156,161 des Strafgesetzbuches) sind mir bekannt und bewusst.“

Datum

\_\_\_\_\_  
Unterschrift

## **Anteilserklärung an den erfolgten Publikationen**

Nittiya Suwannasom hatte folgenden Anteil an den folgenden Publikationen:

Publikation 1: Suwannasom N, Smuda K, Kloypan C, Kaewprayoon W, Baisaeng N, Prapan A, Chaiwaree S, Georgieva R, Bäuml H. Albumin submicron particles with entrapped riboflavin – fabrication and characterization. Nanomaterials. 2019.

IF: 3.504 (2017/2018)

Beitrag im Einzelnen: 80%. Performed experiments including particle fabrication, Particle characterization, Release study, Haemocompatibility assay, analyzed and interpreted the data together with the coauthors, performed statistical analysis, wrote the manuscript.

Publikation 2: Kloypan C, Suwannasom N, Chaiwaree S, Prapan A, Smuda K, Baisaeng N, Pruß A, Georgieva R, Bäuml H. *In-vitro* haemocompatibility of dextran-protein submicron particles. *Artif Cells, Nanomedicine, Biotechnol.* 2019.

IF: 3.026 (2017/2018)

Beitrag im Einzelnen: 20%. Partly performed experiments including collected the data and analyzed the results.

Publikation 3: Kloypan C, Prapan A, Suwannasom N, Kaewprayoon W, Steffen A, Xiong Y, Baisaeng N,

Georgieva R, Bäuml H. Improved Oxygen Storage Capacity of Haemoglobin Submicron Particles by One-Pot Formulation. *Artif Cells, Blood Substitutes, Biotechnol.* 2018.

IF: 3.026 (2017/2018)

Beitrag im Einzelnen: 5%. Partly performed experiments including collected the data and analyzed the results.

---

Unterschrift, Datum und Stempel des betreuenden Hochschullehrers/der betreuenden Hochschullehrerin

---

Unterschrift des Doktoranden/der Doktorandin



Article

# Albumin Submicron Particles with Entrapped Riboflavin—Fabrication and Characterization

Nittiya Suwannasom <sup>1,2</sup>, Kathrin Smuda <sup>1</sup>, Chiraphat Kloypan <sup>1,3</sup>, Waraporn Kaewprayoon <sup>1,4</sup>, Nuttakorn Baisaeng <sup>5</sup>, Ausanai Prapan <sup>1,6</sup>, Saranya Chaiwaree <sup>1,4</sup>, Radostina Georgieva <sup>1,7</sup> and Hans Bäumlér <sup>1,\*</sup>

<sup>1</sup> Institute of Transfusion Medicine, Charité-Universitätsmedizin Berlin, 10117 Berlin, Germany; Nittiya.Suwannasom@charite.de (N.S.); Kathrin.smuda@charite.de (K.S.); chiraphat.kloypan@charite.de (C.K.); Waraporn.Kaewprayoon@charite.de (W.K.); Ausanai.Prapan@charite.de (A.P.); Saranya.Chaiwaree@charite.de (S.C.); radostina.georgieva@charite.de (R.G.)

<sup>2</sup> School of Medical Sciences, University of Phayao, Phayao 56000, Thailand

<sup>3</sup> School of Allied Health Sciences, University of Phayao, Phayao 56000, Thailand

<sup>4</sup> Faculty of Pharmacy, Payap University, Chiang Mai 50000, Thailand

<sup>5</sup> School of Pharmaceutical Sciences, University of Phayao, Phayao 56000, Thailand; patchateeya@yahoo.com

<sup>6</sup> Faculty of Allied Health Sciences, Naresuan University, Phitsanulok 65000, Thailand

<sup>7</sup> Department of Medical Physics, Biophysics and Radiology, Medical Faculty, Trakia University, 6000 Stara Zagora, Bulgaria

\* Correspondence: hans.baeumlér@charite.de; Tel.: +49-30-450525131

Received: 14 February 2019; Accepted: 19 March 2019; Published: 25 March 2019



**Abstract:** Although riboflavin (RF) belongs to the water-soluble vitamins of group B, its solubility is low. Therefore, the application of micro-formulations may help to overcome this limiting factor for the delivery of RF. In this study we immobilized RF in newly developed albumin submicron particles prepared using the Co-precipitation Crosslinking Dissolution technique (CCD-technique) of manganese chloride and sodium carbonate in the presence of human serum albumin (HSA) and RF. The resulting RF containing HSA particles (RF-HSA-MPs) showed a narrow size distribution in the range of 0.9 to 1  $\mu\text{m}$ , uniform peanut-like morphology, and a zeta-potential of  $-15\text{ mV}$ . In vitro release studies represented biphasic release profiles of RF in a phosphate buffered saline (PBS) pH 7.4 and a cell culture medium (RPMI) 1640 medium over a prolonged period. Hemolysis, platelet activation, and phagocytosis assays revealed a good hemocompatibility of RF-HSA-MPs.

**Keywords:** riboflavin; immobilization; biopolymer; CCD-technique

## 1. Introduction

Riboflavin (RF), also known as vitamin B<sub>2</sub>, is a partially water-soluble vitamin that belongs to the group of flavoenzymes which catalyze oxidation-reduction reactions [1]. It is intrinsically fluorescent and has been used as modern drug [2]. It has been reported that RF has in vivo anti-metastatic properties in melanoma [3]. Several studies have shown that RF may also have antioxidant and anti-inflammatory effects [4,5]. Protective properties against cancer were shown in connection with co-enzyme Q<sub>10</sub>, RF, and niacin in tamoxifen-treated postmenopausal breast cancer patients [6]. RF has also been useful in photodynamic therapy (PDT). Because of its photosensitizing characteristics, it has a wide range of biological actions, such as inducing apoptosis in leukemia [7] and reducing the progression of prostate cancer cells [8], renal cancer cells [4], and melanoma [3]. Moreover, irradiated RF has been used to inactivate pathogens in blood transfusions [9] and it has the stabilized the corneal collagen crosslinking in keratoconus treatment [10].

RF is required in many oxidation-reduction reactions, and therefore RF deficiency may affect many systems [1]. RF is considered to be one of the most common vitamins with a deficiency in people of developing countries, particularly the countries where rice is their staple food. Consequently, a long-term use of RF supplement is required. Although it belongs to the water-soluble vitamins of group B, its solubility is about  $2.65 \times 10^{-5} \text{ mol/L}^{-1}$  [11]. Therefore, micro-formulations based on hydrophobic interactions between RF and human serum albumin (HSA) may apply to overcome this limiting factor and to increase the therapeutic efficiency of the RF photosensitizer in cancer therapy [12,13].

The immobilization of compounds is a promising strategy for the improvement of stability, solubility, and biological activity through compound capture by carbonate microspheres in the process of their formation (Co-precipitation). The Co-precipitation Crosslinking Dissolution technique (CCD-technique) resulted in the fabrication of biopolymer particles using the precipitation of  $\text{MnCl}_2$  and  $\text{Na}_2\text{CO}_3$  in the presence of a biopolymer solutions [14,15]. In the case of proteins, we used glutaraldehyde to crosslink the proteins in the  $\text{MnCO}_3$  template. The concentration was very low (<0.1%) and the final particles did not contain free aldehyde groups. Therefore, no toxic effects could be found [15]. The uniform peanut-like submicron particles were produced with a relatively high protein entrapment efficiency and a narrow distribution of around 700 nm. These carbonate particles could be easily loaded with bioactive compounds (e.g., enzyme) during their preparation [16–19]. The particle size and shape could be altered by adjusting the experimental conditions such as pH, choice of salt and/or salt concentration, temperature, and rate of mixing the solutions. This technique becomes increasingly interesting due to the high drug-loading capacity of the carbonate particles, the ease of preparation by simply mixing two starting solutions under mild conditions, and the complete dissolution of the carbonate template using EDTA at a neutral pH.

Micro- and nanoparticles made of human serum albumin (HSA) are an attractive alternative to synthetic polymers for use in the field of medicine and drug delivery due to their high binding capacity to both hydrophobic and hydrophilic drugs. Albumin nanoparticles showed the benefits of biocompatibility, biodegradability, non-toxic and non-immunogenic properties, thus avoiding inflammatory responses [20]. The HSA-based nanoparticles have been employed to deliver a variety of drugs such as brucine [21] and paclitaxel [22]. Various methods have been developed for the preparation of albumin particles such as desolvation/coacervation [23], emulsification [24], thermal gelation [25], nano spray drying [26], and self-assembly techniques [27] as well as co-precipitation which is used in our studies presented here.

For our investigations, RF served as model substance to demonstrate that more or less hydrophobic small molecules can be loaded into protein submicron particles using the CCD-technique. Additionally, the release of RF *in vitro* was studied in a phosphate buffered saline (PBS) and a cell culture medium (RPMI). Finally, we investigated the hemocompatibility of the RF containing HSA particles (RF-HSA-MPs), which is important for their application as intra-venously administered drug carriers.

## 2. Materials and Methods

### 2.1. Materials

Riboflavin (RF, >98% purity), glutaraldehyde (GA), fluorescein isothiocyanate (FITC), manganese chloride tetra-hydrate ( $\text{MnCl}_2 \cdot 4\text{H}_2\text{O}$ ), sodium carbonate ( $\text{Na}_2\text{CO}_3$ ), phosphate buffered saline (PBS) pH 7.4, glycine, and sodium borohydride ( $\text{NaBH}_4$ ) were purchased from Sigma-Aldrich (Munich, Germany). Ethylene diamine tetra-acetic acid (EDTA) was purchased from Fluka (Buchs, Switzerland). Ampuwa<sup>®</sup> (aqua ad injectable) and sterile 0.9% NaCl solution was purchased from Fresenius Kabi Deutschland GmbH (Bad Homburg, Germany). NaOH and DMSO were purchased from Carl Roth GmbH, Karlsruhe, Germany. Human serum albumin solution 20% was purchased from Grifols

Deutschland GmbH (Frankfurt a.M., Germany). A Phagotest™ kit was purchased from Glycotope Biotechnology GmbH, Berlin, Germany.

## 2.2. Fabrication and Characterization of RF-HSA-MPs

### 2.2.1. Fabrication of RF-HSA-MPs Particles

As RF is slightly soluble in water, a stock solution of 50 mM RF was prepared by dissolving it in 100% DMSO. The RF stock solution was protected from light by aluminum foil to prevent photo-degradation.

The RF-HSA-MPs were fabricated using a modified protocol based on the previously described CCD-technique [17,18]. Briefly, 20 mL of  $MnCl_2$  solution containing 10 mM RF and 10 mg/mL HSA were mixed in a 100 mL beaker for 1 min. Then 20 mL of  $Na_2CO_3$  were added rapidly under vigorous stirring (Bibby Scientific CB161 Magnetic Stirrer, level 3) for 30 s at room temperature (final concentrations of RF and HSA were 5 mM ( $\approx 1.9$  mg/mL) and 80  $\mu M$  (5 mg/mL), respectively). The final concentration of  $MnCl_2/Na_2CO_3$  varied from 0.0625 to 0.25 M with a constant RF solution and HSA concentration. The hybrid particles obtained were separated by centrifugation at  $3000\times g$  for 3 min and washed twice with a 0.9% NaCl solution. The particles were suspended in a GA solution (final concentration 0.1%) and incubated at room temperature for 1 h, followed by centrifugation at  $3000\times g$  for 3 min. The remaining unbound aldehyde groups of GA in the particles were quenched using 0.08 M glycine and 0.625 mg/mL  $NaBH_4$ , and the  $MnCO_3$  template was subsequently removed by treatment with EDTA solution (0.25 M, pH 7.4) at room temperature for 30 min. Finally, the resulting particles were centrifuged, washed until the washing solution became colorless, and resuspended in Ampuwa® for further use. The fabrication scheme of the submicron particles is shown in Figure 1.

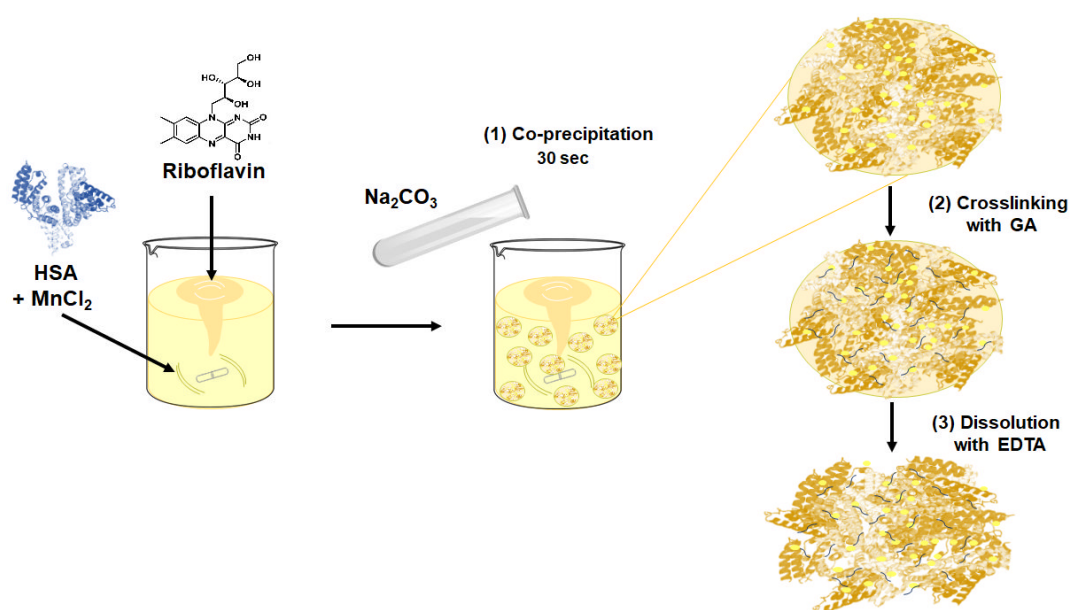


**Figure 1.** Scheme of the fabrication procedure for the submicron human serum albumin (HSA) particles containing riboflavin (RF), i.e., modified Co-precipitation Crosslinking Dissolution technique (CCD-technique).

HSA particles with 4 mL DMSO without RF (HSA-MPs) were prepared following the same procedures and used as a control.

The amount of RF or HSA entrapped in the particles was determined as the difference between the total RF ( $RF_t$ ) or HSA ( $P_t$ ) amount added and the free non-entrapped RF ( $RF_f$ ) or HSA ( $P_f$ ) amount in the supernatants after co-precipitation and after each washing step. The RF concentration was determined spectroscopically measuring the absorbance of the supernatants at 445 nm with a microplate reader (PowerWave 340, BioTek Instruments GmbH, Bad Friedrichshall, Germany). The protein concentration was determined using a Coomassie Plus (Bradford) Assay Kit (Thermo Fisher Scientific, Waltham, IL, USA) with an absorbance measurement at 595 nm.

### 2.2.2. Size, Zeta-Potential and Morphology of the HSA-MPs and RF-HSA-MPs

The size, polydispersity index, and zeta potential of the obtained particles were measured using a Zetasizer Nano ZS instrument (Malvern Instruments Ltd., Malvern, UK) at 25 °C. The particles were dispersed in PBS pH 7.4 and taken in a clear disposable zeta cell for zeta-potential measurement and in a plastic disposable cuvette for particle size measurement. Additionally, the particles were imaged using a confocal microscope (CLSM ZeissLSM 510 meta, Zeiss MicroImaging GmbH, Jena, Germany) and the size was assessed from the obtained images using the ImageJ-1 software (NIH, Bethesda, MD, USA).

The morphology of HSA-MPs and RF-HSA-MPs was investigated using an atomic force microscopy (AFM) in tapping mode and a Nanoscope III Multimode AFM (Digital Instrument Inc., Santa Barbara, CA, USA). The samples were prepared on a freshly cleaved mica substrate pretreated with polyethylene imine (Mw 25 kDa, 1 mM for 20 min) by applying a drop of diluted particle suspension. The substrate was then rinsed with deionized water and dried under a gentle stream of nitrogen. The scans of the particles were first performed in the dry state, followed by the addition of a drop of deionized water and a scan in the wet state. For the scans in air (dry state) micro-lithographed tips on silicon nitride ( $Si_3N_4$ ) cantilevers with a spring constant of 42 N/m and a resonance frequency of 300 kHz (Olympus Corporation, Tokyo, Japan) were used. Cantilevers with a spring constant of 3 N/m and a resonance frequency of 75 kHz (Budget Sensors, Innovative Solutions Bulgaria Ltd., Sofia, Bulgaria) were used for the measurements in the wet state. The Nanoscope software was used to record and analyze the obtained images.

### 2.2.3. Intrinsic Fluorescence of the HSA-MPs and RF-HSA-MPs

The HSA-MPs and the RF-HSA-MPs were observed using a confocal laser scanning microscope (CLSM; ZeissLSM 510 meta, Zeiss MicroImaging GmbH, Jena, Germany) equipped with a 100× oil immersion objective (a numerical aperture of 1.3). Images of the samples were prepared in transmission and fluorescence mode with fluorescence excitation at 488 nm and a 505 nm long pass emission filter. The same settings were used for the imaging of the particles prepared with and without RF. Additionally, the particles were mounted on a glass slide using DakoCytomation fluorescent mounting medium and visualized using an Axio Observer (Zeiss, Göttingen, Germany). The fluorescence intensity was recorded at an excitation wavelength of 480 nm and an emission wavelength of 535 nm. A Zeiss filter cube no. 9 was used for fluorescence microscopy (EX 450–490, BS 510, EM LP 515).

The distribution of the fluorescence intensity inside the populations of the HSA-MPs and RF-HSA-MPs was analyzed using a flow cytometry (FACS-Canto II, Becton and Dickinson, Franklin Lakes City, NJ, USA) after diluting the samples with PBS at a ratio of 1:40 [28]. The performance of the flow cytometer was checked regularly using Cytometer Setup and Tracking Beads (BD Biosciences, Franklin Lakes, NJ, USA) to ensure the accuracy and precision of the measurements. A total of 10,000 events of particles were recorded from each sample. Subsequently, the fluorescence of the particles was determined in the PE-A channel as the relative median fluorescence intensity (RFI). The data were analyzed using the FlowJo v10 software (Tree Star, Ashland, OR, USA).

### 2.3. In Vitro Release of RF from the RF-HSA-MPs

For the release studies, 2.5 mL of 16% (*v/v*) RF-HSA-MPs suspension were transferred into a dialysis membrane sleeve (Cellu Sep T3, MWCO 12,000–14,000, Creative BioMart, Shirley, NY, USA) and sealed at both ends after adding 1 mL release media (0.1 M PBS pH 7.4 or RPMI 1640 medium supplemented with 10% fetal bovine serum (FBS) and 1% PenStrep to mimic the biological environment). The dialyzer was then introduced into a 25 mL glass cylinder containing 9 mL of release media (0.1 M PBS pH 7.4 or RPMI 1640 medium), which was stirred continuously at 100 rpm using a magnetic stir bar at room temperature. The samples were removed from any light because of the light sensitivity of RF. The RF-release was assessed intermittently by sampling (400  $\mu$ L) the contents of the outer media and replacing this with an equal volume of fresh PBS pH 7.4 or RPMI 1640 medium immediately after sampling, correspondingly. The amount of released RF was measured at a wavelength of 445 nm using an UV-vis spectrophotometer (Hitachi U2800, Hitachi High-Technologies Corporation, Kreefeld, Germany).

The release profiles of RF in PBS pH 7.4 and in RPMI 1640 medium were displayed as time dependency for the remaining RF concentration in the RF-HSA-MPs and fitted with the release model of Pappas [29], Equation (1) was used:

$$m(t)/m(\infty) = k_1 t^n + k_2 t^{2n} \quad (1)$$

where  $m(t)/m(\infty)$  is the cumulative drug release,  $t$  is the release time (in hours), the first term of the right side is the Fickian contribution (F), the second term is the Case-II relaxational contribution (R) that reflects the structural and geometric characteristics of the MPs, and  $n$  is a diffusional exponent that is characteristic for the controlled release of the loaded drug [30,31].

### 2.4. Hemocompatibility of HSA-MPs and RF-HSA MPs

Freshly withdrawn venous blood was collected from healthy volunteers and anticoagulated using lithium heparin (368494, BD Vacutainers) or into sodium citrate (366575, BD Vacutainer). The blood samples were collected at the Charité—Universitätsmedizin Berlin (# EA1/137/14) and all donors provided written informed consent. The blood samples were mixed gently (but thoroughly) to ensure adequate mixing with the anticoagulant immediately after blood collection. All samples were processed within 2 h of blood collection.

#### 2.4.1. Hemolysis Test

The hemolytic activity was determined on the release of hemoglobin from damaged erythrocytes *in vitro*. Human heparinized blood was washed with PBS by centrifugation at  $3000 \times g$  for 5 min to isolate the red blood cells (RBCs). The RBCs were further washed until a colorless pellet was obtained and then diluted to achieve a cell suspension with a volume concentration of 2% in PBS. Then, 0.5 mL of the 0.5%, 1%, and 2% diluted RBCs suspension was mixed with 0.5 mL of 2% HSA-MPs, RF-HSA-MPs, double distilled water as the positive (PC) or PBS as a negative (NC) control. After incubation at 37 °C for 3 h and centrifugation at  $3000 \times g$  for 5 min, the supernatants were transferred carefully to a 96-well plate and the absorbance was measured using a microplate reader at 545 nm. The degree of hemolysis was calculated as the hemolytic ratio (HR) using Equation (2):

$$\text{HR}\% = (A_{\text{test}} - A_{\text{NC}}) / (A_{\text{PC}} - A_{\text{NC}}) \times 100\% \quad (2)$$

where  $A_{\text{test}}$  is the absorbance of the tested sample,  $A_{\text{NC}}$  is the absorbance of the negative control in PBS and  $A_{\text{PC}}$  is the absorbance of the positive control in distilled water.

#### 2.4.2. Phagocytosis Test

The interaction of the HSA-MPs and RF-HSA-MPs with the blood leukocytes was evaluated *in vitro* in human whole blood using a commercial Phagotest kit (Glycotope-Biotechnology GmbH, Heidelberg, Germany). Manufacturer's instructions were partially modified: all reactions were performed with half of the volume (50  $\mu\text{L}$  instead of 100  $\mu\text{L}$ ), lysing solution was changed to ammonium chloride lysing solution (155 mM  $\text{NH}_4\text{Cl}$ , 12 mM  $\text{NaHCO}_3$ , 0.1 mM EDTA), and DNA was not stained. To put it briefly, 10  $\mu\text{L}$  of  $2 \times 10^{11}$  per mL, RF-HSA-MPs, HSA-MPs, were added into 50  $\mu\text{L}$  heparinized whole blood and carefully mixed. For the negative control 10  $\mu\text{L}$  of PBS were added to 50  $\mu\text{L}$  blood and for the positive control (functional test of the granulocytes and monocytes in the blood) 10  $\mu\text{L}$  of  $2 \times 10^{11}$  FITC-labeled opsonized *E. coli* (positive control) were applied. The samples were incubated at 37 °C for 30 min (PBS and FITC-labeled opsonized *E. coli* were incubated for 10 min). The control samples remained on ice. At the end of the incubation period, all samples were placed in the ice-bath. A quenching solution was added and washed with ice-cold PBS. The erythrocytes were lysed with ammonium chloride solution for 15 min. The cells were washed twice and re-suspended in ice-cold PBS. The percentage of granulocytes and monocytes exhibiting phagocytosis was determined using a flow cytometer (BD FACS Canto II, Franklin Lakes, NJ, USA).

#### 2.4.3. Platelet Activation Test

The effect of the HSA-MPs and RF-HSA-MPs on the function of the blood platelets was tested in a platelet-rich plasma (PRP). The PRP was isolated from human whole blood anticoagulated with sodium citrate by centrifugation at  $150 \times g$  for 15 min and used immediately. Then the HSA-MPs and RF-HSA-MPs were added to the PRP at a final ratio of 5 particles per 1 platelet, carefully mixed and incubated in a water bath at 37 °C for 30 min. A negative control was prepared adding the same volume of PBS instead of particle suspension. To induce activation and aggregation of the platelets, the pre-incubated PRP samples were treated with 0.5 mg/mL of arachidonic acid or 0.018 mg/mL of epinephrine (Mölab, Langenfeld, Germany) at 37 °C for 30 min. An ABX Micros 60 hematology analyzer (Horiba Europe GmbH) was used to detect the platelet number in the samples before and after incubation. Finally, the platelets were stained with APC-mouse anti-human CD41a and Alexa Fluor® 488-mouse anti-human CD62p (p-selectin), kept in the dark for 20 min, and fixed with 500  $\mu\text{L}$  of a fixative solution (0.5% paraformaldehyde in PBS) to each test tube to stop the reactions. The expression of the platelet activation marker CD62P and the constitutively present platelet marker CD42b were analyzed using a flow cytometry (BD FACS Canto II).

### 3. Results and Discussion

#### 3.1. Fabrication and Characterization of RF-HSA-MPs

##### 3.1.1. HSA and RF Content, Size, Zeta-Potential and Morphology

In previous studies by our group, it has been shown that the co-precipitation technique is much more effective for the protein entrapment than the absorption onto the carbonate particles [32,33]. Moreover, it was found that the entrapment of proteins using the  $\text{MnCO}_3$  template was higher than that of the  $\text{CaCO}_3$  template [14,15]. The encapsulation efficiency was attributed to the electrostatic attraction between negatively charged proteins and more positively charged  $\text{MnCO}_3$  as well as to the stronger affinity of  $\text{Mn}^{2+}$  to proteins and in particular to HSA [34].

However, the addition of low molecular weight compounds into polymeric particles and capsules still remains a challenge. In our study we used RF as a model to investigate the potential of the CCD-technique to deliver carrier systems for low molecular weight drugs with poor water solubility. The weak water-soluble RF was added together with HSA via the CCD-technique as shown in Figure 1. To achieve this RF was already added during the first step of the particle preparation, the co-precipitation, together with HSA. It had been previously shown that RF interacts with albumin through adsorption on the tryptophan residues via hydrophobic interactions [12,13], which was expected to support the RF entrapment into the HSA-MPs.

The co-precipitation was performed at the previously optimized concentration of  $\text{MnCl}_2$  and  $\text{Na}_2\text{CO}_3$  for the entrapment of HSA (0.125 M). The average amounts of entrapped HSA and RF particles under these preparation conditions were  $2.9 \pm 0.8$  mg and  $2.5 \pm 0.5$  mg per mL, respectively. This means that in a particle suspension with a volume concentration of 10%, the RF concentration will be roughly 290  $\mu\text{g}/\text{mL}$  which is over four times higher than the solubility of RF in water at 20 °C (70  $\mu\text{g}/\text{mL}$ , GESTIS—materials database).

On CLSM images the HSA-MPs and RF-HSA-MPs exhibited a size between 0.9 and 1.1  $\mu\text{m}$  with an average long diameter of 1  $\mu\text{m}$ . These values correlated well with the measurements using the dynamic light scattering (Zetasizer Nano ZS, Malvern Instruments Ltd., Malvern, UK) which delivered values of  $1.04 \pm 0.15$   $\mu\text{m}$ . There were no significant differences found between HSA-MPs and RF-HSA-MPs. Under the conditions chosen for this study, which were a rapid mixing of all compound at room temperature, the size of the particles was highly reproducible.

The main factors that determine the size of the  $\text{MnCO}_3$  particles were the concentrations of manganese and carbonate ions, the flow rate of the solutions during mixing, and the temperature. Particular variations of these parameters are needed for controlling size and shape of the particles in co-precipitation reactions [35]. The mixing of  $\text{MnSO}_4$  and  $\text{NH}_4\text{HCO}_3$  has been widely employed to prepare manganese carbonate particles and used as scarified templates for the assembly of polyelectrolyte multilayers via layer-by-layer (LBL) self-assembly technique. Micron  $\text{MnCO}_3$  crystals with different size distributions varying from 1 to 10  $\mu\text{m}$  have been synthesized at low concentration ratios of  $\text{MnSO}_4/\text{NH}_4\text{HCO}_3$  with long precipitation times and additional solvents at high temperature [36–40]. Subsequently, the manganese carbonate core was dissolved in HCl at low pH. In this study,  $\text{MnCO}_3$  was synthesized by a co-precipitation method using  $\text{MnCl}_2$  and  $\text{Na}_2\text{CO}_3$  as the manganese and carbonate source, respectively. The precipitation was completed very fast, at room temperature with high salt concentration, and the dissolution was completed with EDTA at neutral pH. These conditions are suitable for the preparation of protein particles avoiding denaturation and preserving the function of the proteins.

The morphology of HSA-MPs and RF-HSA-MPs was analyzed using an AFM as shown in Figure 2. The shape of both kinds of particles was peanut-like. The long diameter measured for both kinds of particles varied between 780 and 890 nm without significant differences between them. The thickness of the particles was determined from the height profiles were  $400 \pm 45$  nm, which corresponds to half of the long diameter. The addition of RF did not seem to interfere with the geometry of the particles.

The RF-HSA-MPs und HSA-MPs were further investigated with respect to their electrokinetic potential (zeta-potential). This parameter is important for the stability of a particle suspension, in particular for the behavior of the particles in biological fluids. Therefore, three measurements of the zeta-potential were conducted in PBS pH 7.4 (conductivity 17 mS/cm). Both HSA-MPs and RF-HSA-MPs exhibited zeta-potential of approximately  $-15$  mV, which is a relatively high value at the high ionic strength of PBS. In water (conductivity 14  $\mu\text{S}/\text{cm}$ ) the zeta-potential was approximately  $-39$  mV, which contributed to the high colloidal stability and absence of aggregation of the particles in a biologically relevant media.

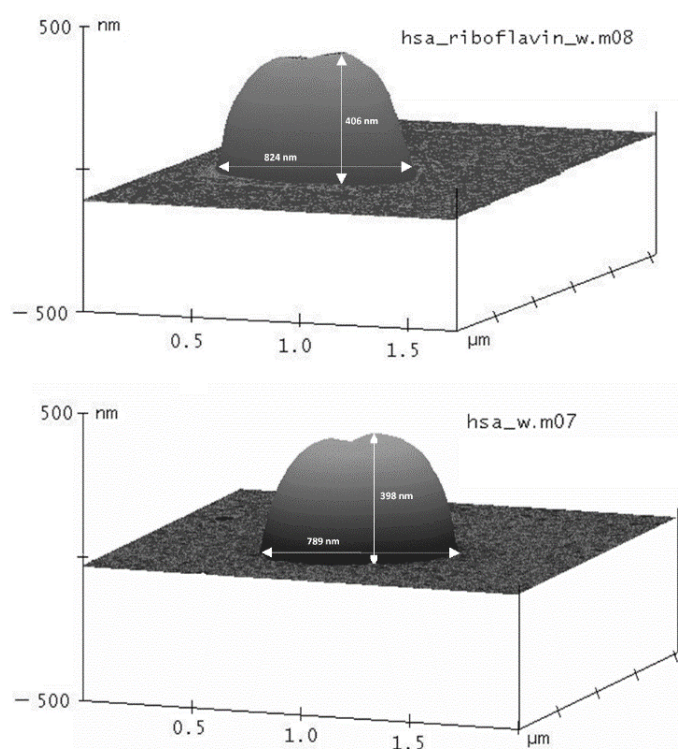


**Figure 2.** AFM images of RF containing HSA particles (RF-HSA-MPs) (**top**) and HSA particles with 4 mL DMSO without RF (HSA-MPs) (**bottom**) in three dimensional (3D)-mode. The size of the particles was determined from the height profiles in horizontal and vertical directions. The values included in the images are representative examples.

### 3.1.2. Intrinsic Fluorescence of the HSA-MPs and RF-HSA-MPs

Both HSA-MPs and RF-HSA-MPs could be detected in the fluorescence channels of the confocal microscope. A weak autofluorescence due to the GA crosslinking was observed in the HSA-MPs as seen in Figure 3(A1,A2), whereas the RF-HSA-MPs showed significantly stronger fluorescence due to the entrapped RF as seen in Figure 3(B1,B2).

More clearly the difference of the fluorescent emission is demonstrated in the 3D color surface map representing a single HSA-MP and RF-HSA-MP in Figure 3(A3,B3), respectively.

The higher value of the intrinsic fluorescence of the RF-HSA-MP confirms the successful entrapment of the drug into the particles. Additionally, the intrinsic fluorescence is very useful for tracking these particles when they interact with cells without the need for additional labeling.

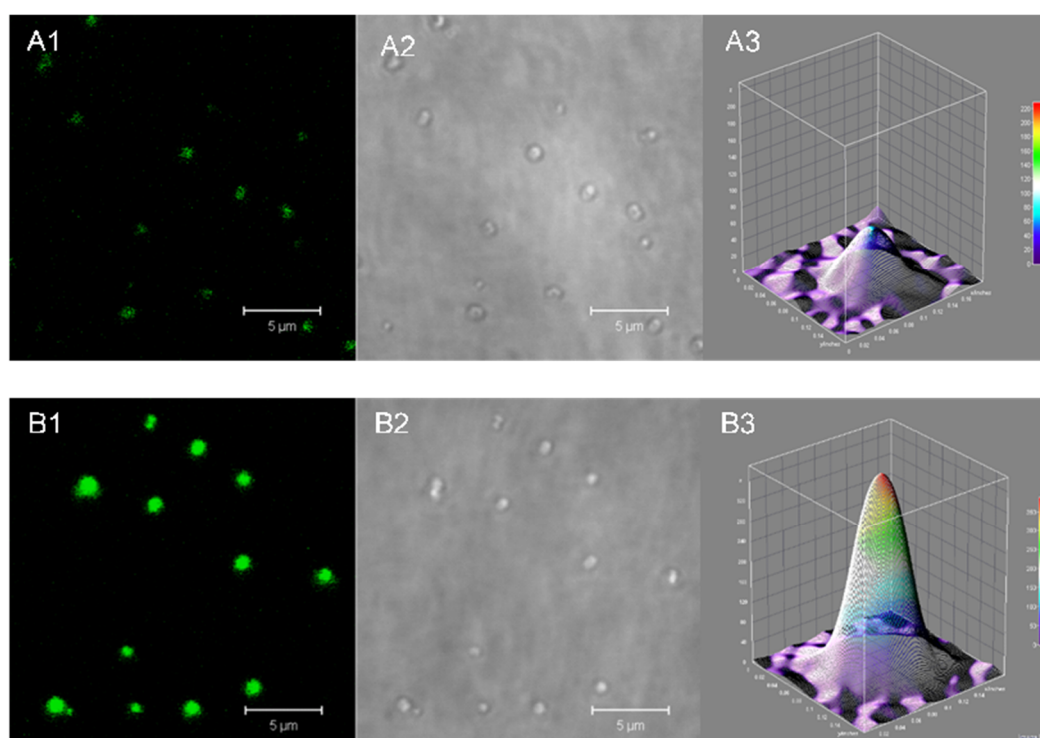


**Figure 3.** Analysis of intrinsic fluorescence in HSA-MPs and RF-HSA-MPs. Confocal micrograph of HSA-MPs in (A1) fluorescence mode and (A2) transmission mode, respectively and confocal micrograph of RF-HSA-MPs in fluorescence mode (B1) and transmission mode (B2), respectively. Fluorescence emission intensity in 3D color map surface images of (A3) HSA-MPs and (B3) RF-HSA-MPs at an excitation wavelength of 480 nm and an emission wavelength of 535 nm.

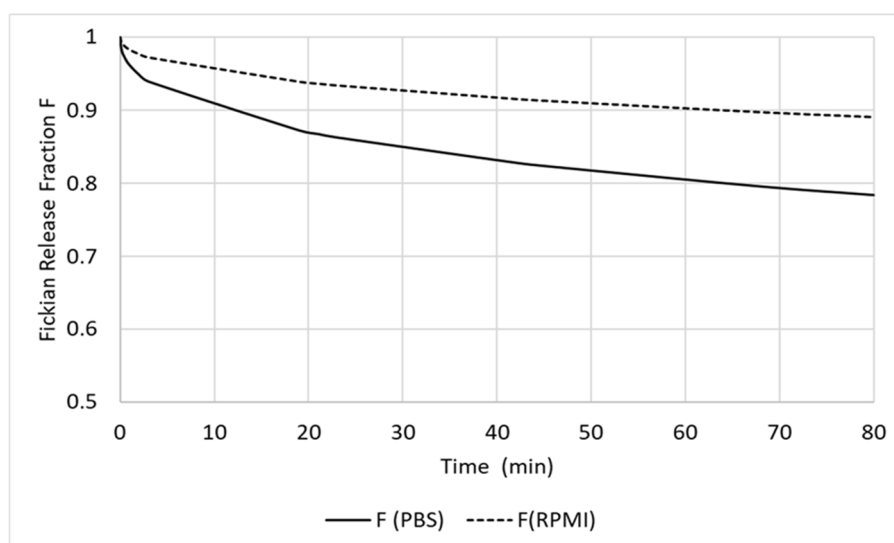
### 3.2. In Vitro Release of RF from the RF-HSA-MPs

The investigation of the drug release was performed using a dialysis-bag diffusion method against PBS pH 7.4 as well as RPMI 1640 medium. The cut-off of the dialysis bag allowed the free diffusion of released RF through the semi-permeable membrane from the solution inside the dialysis bag to the outside following the concentration gradient. The results of the in vitro release of RF from RF-HSA-MPs are shown in Figure 4a. The decrease of the RF concentration remaining in the particle suspensions was followed for 80 h. It can be seen that the drug release profiles, in both investigated media, are bi-phasic with an initial burst release of approximately 7% in PBS and 12% in RPMI from the initial RF concentration during the first 2 to 3 h. Thereafter, the release rate decreased and a sustained release was observed until the end of the experiments. After 80 h the drug release remained 30% and 45% of the initial loading in PBS and in RPMI, respectively.

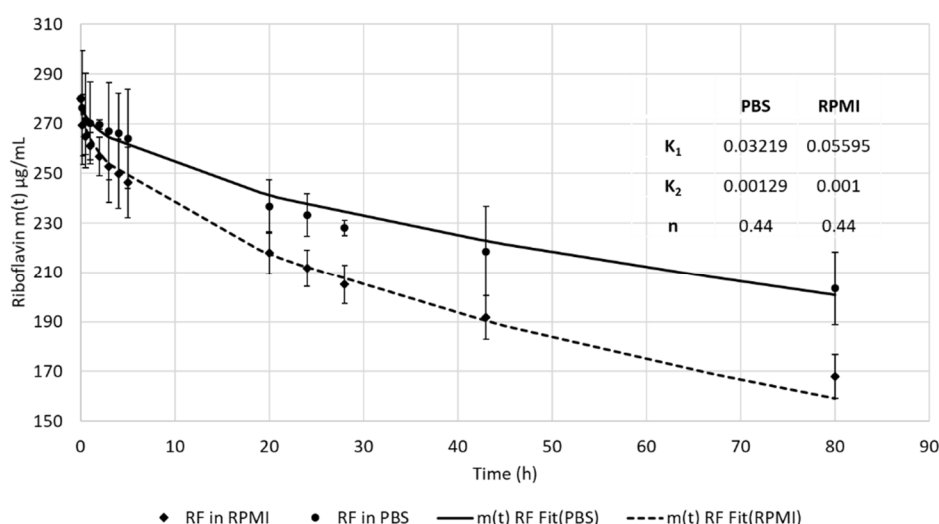
The release in the RPMI 1640 medium which contained varying amino acids and 10% calf serum albumin was significantly faster, probably due to the adsorption of the released RF by these compounds, which resulted in a clearance of the free RF from the solution. Consequently, the concentration of the freely dissolved RF remained lower in the RPMI as compared with the concentration of the freely dissolved RF in the PBS, which led to a faster release. A similar release behavior was shown for a hydrophobic anti-cancer drug from a micelle system. The release was accelerated in buffers containing albumin [41] due to the binding of the drug to the hydrophobic regions of albumin.

The release profiles were fitted using the model of Pappas Equation (2), which is suitable to describe bi-phasic controlled release of entrapped drugs from particles. The values calculated for  $K_1$  are larger than those calculated for  $K_2$  by more than one magnitude for both PBS and RPMI. This indicates that the release is dominated by the diffusion mechanism. In RPMI the domination by the

Fickian diffusion is much stronger due to the greater RF concentration gradient between RF in the RF-HSA-MPs and the bulk RPMI-phase.



(a)



(b)

**Figure 4.** (a) Release profiles of RF in the phosphate buffered saline (PBS) pH 7.4 (●) and in the cell culture medium (RPMI) 1640 medium (◆) at room temperature calculated for the remaining RF concentration entrapped in the RF-HSA-MPs. The RF concentrations were fitted using the Pappas equation  $m(t)/m(\infty) = k_1 t^n + k_2 t^{2n}$ . Values are expressed as mean  $\pm$  SD ( $n = 3$ ). (b) Fickian release fraction (F) of RF-HSA-MPs in PBS and in RPMI. The release of RF in RPMI is much stronger in the domination by the Fickian diffusion, due to the greater RF concentration gradient between RF in the RF-HSA-MPs and the bulk RPMI-phase.

### 3.3. Hemocompatibility of RF-HSA MPs

#### 3.3.1. Hemolysis Test

Hemolysis tests were performed to assess the impact of HSA-MPs and RF-HSA-MPs on the membrane stability of human erythrocytes. The HSA-MPs and RF-HSA-MPs showed low hemolytic activity with the percentage of hemolysis in the range of 4–7% and in a dose-dependent manner as

shown in Figure 5. Therefore, the HSA-MPs and RF-HSA-MPs did not cause strong hemolytic effects. However, according to criterion listed in the ASTM E2524-08 standard, more than 5% hemolysis indicates damage to RBCs caused by the test materials. This critical value was reached at particle concentration of 1% for both HSA-MPs and RF-HSA-MPs.

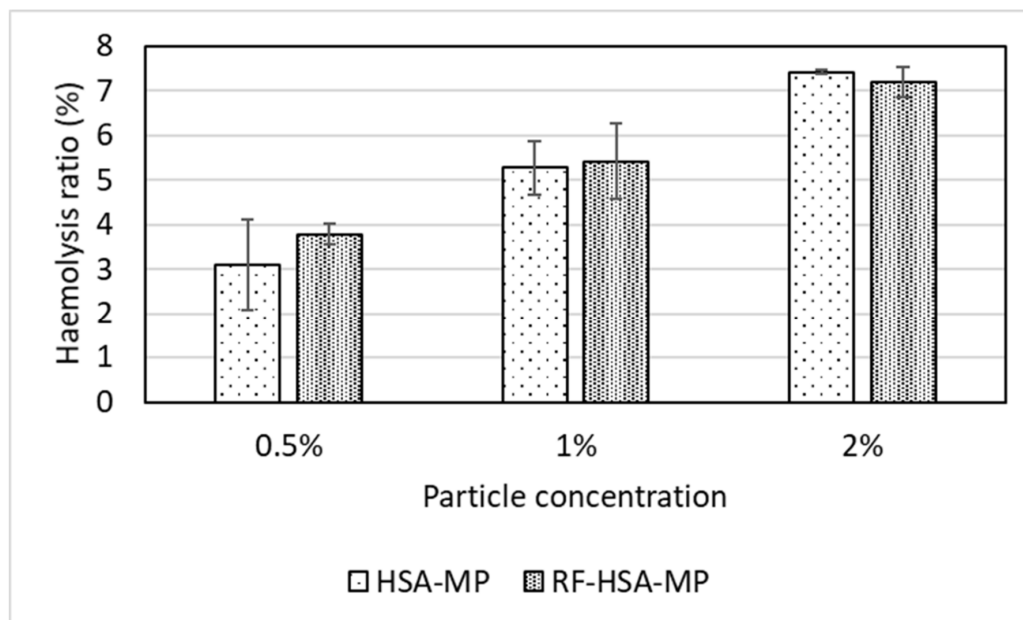


**Figure 5.** Hemolytic activity induced by HSA-MPs and RF-HSA-MPs for 3 h at 37 °C, concentration ranging from 0.5%, 1%, and 2%. Water and PBS served as positive (100%) and negative (0%) control, respectively. Data are presented as the mean percentage  $\pm$  SD (n = 3).

In general, size, surface charge, and surface area are key parameters that affect the hemolytic potential of particles. Negatively charged particles interact less with the negative charged cell surface than positively charged particles. Micron-sized particles are more likely to produce a lower level of hemolysis than smaller particles [42–44]. The increase in surface-to-volume ratio with the decrease in size of particles results in enlarged surface contact area and provides the chance for damage to take place to a cell membrane. This could explain the dose-dependent increase of hemolysis observed with the HSA-MPs and RF-HSA-MPs.

### 3.3.2. Phagocytosis Test

The ability of the HSA-MPs and RF-HSA-MPs to induce phagocytic activity of granulocytes and monocytes in whole blood was analyzed using a standard phagocytosis kit. Representative results of these tests are shown in Figure 6. The fluorescence signal from HSA-MPs and RF-HSA-MPs was detected in the PE-A channel of the flow cytometer, and the FITC-labelled *E. coli* (used as a standard positive control for phagocytosis) was detected in the FITC-A channel. The three main populations of white blood cells were identified based on their forward scatter (FSC) and side scatter (SSC): granulocytes, monocytes, and lymphocytes (dot-plot Figure 6A). The histograms in Figure 6B,C represent the distribution of the fluorescence intensity within the population of HSA-MPs and RF-HSA-MPs in the PE-A-channel. The higher fluorescence emission of the RF-HSA-MPs is clearly visible in the shift of their histogram by one order of magnitude to higher fluorescence intensities. The analysis of the fluorescence distribution in the granulocyte and monocyte populations of the samples incubated at 37 °C with FITC-*E. coli* (Figure 6D,G) shows a strong right shift in the FITC channel due to the engulfment of the fluorescent bacteria. This was not the case in the samples incubated with HSA-MPs and RF-HSA-MPs (Figure 6E,I). The particles did not induce phagocytosis, and therefore their immunogenicity is low. Avoiding clearance by phagocytosis is very important in

drug delivery systems using micro-particles and in many cases requires complicated and expensive surface modification of the drug carriers [45]. Therefore, our HSA-MPs and RF-HSA-MPs are very promising for use in applications for drug delivery systems.

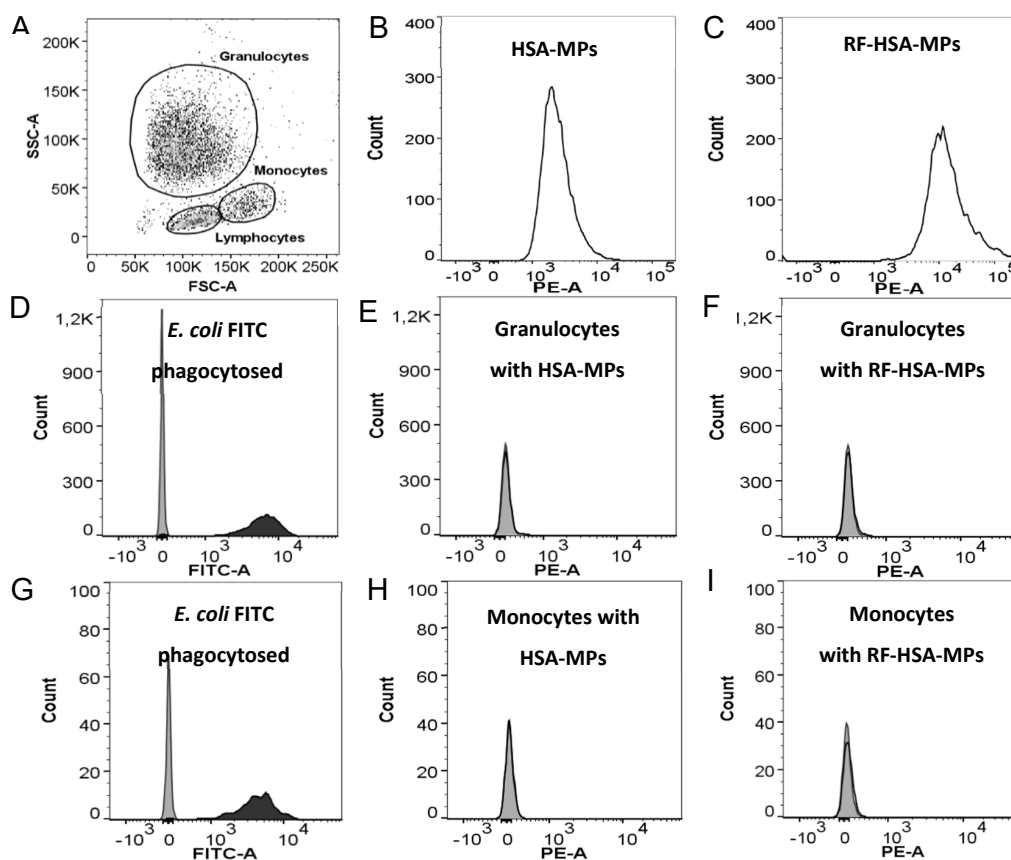
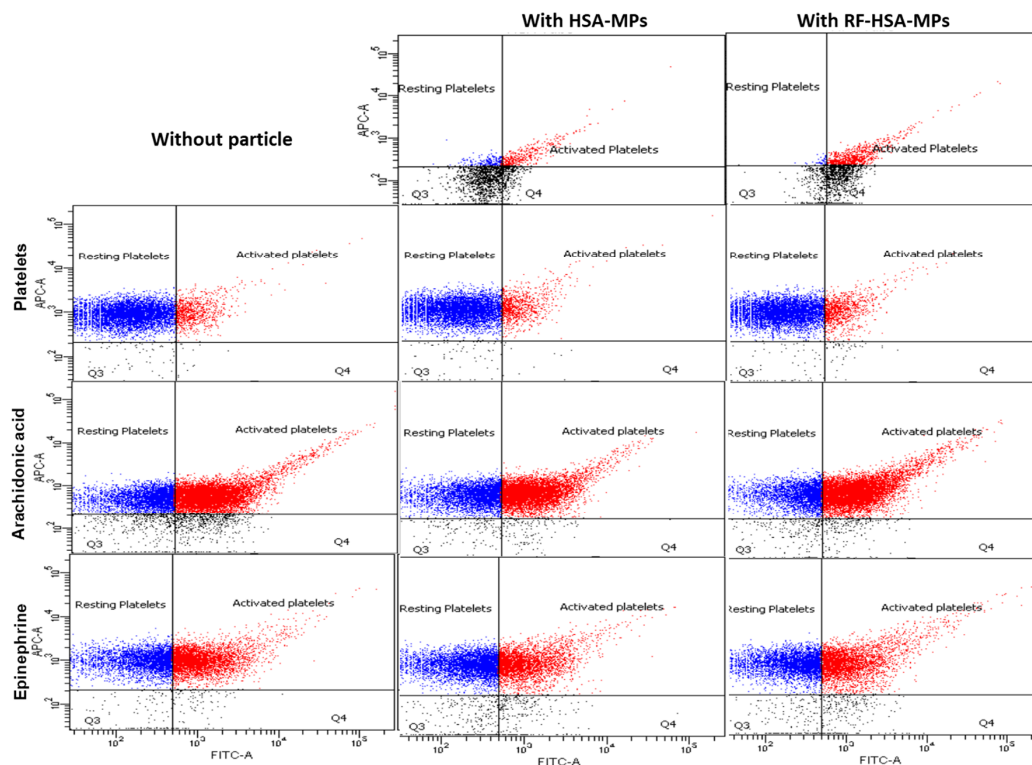


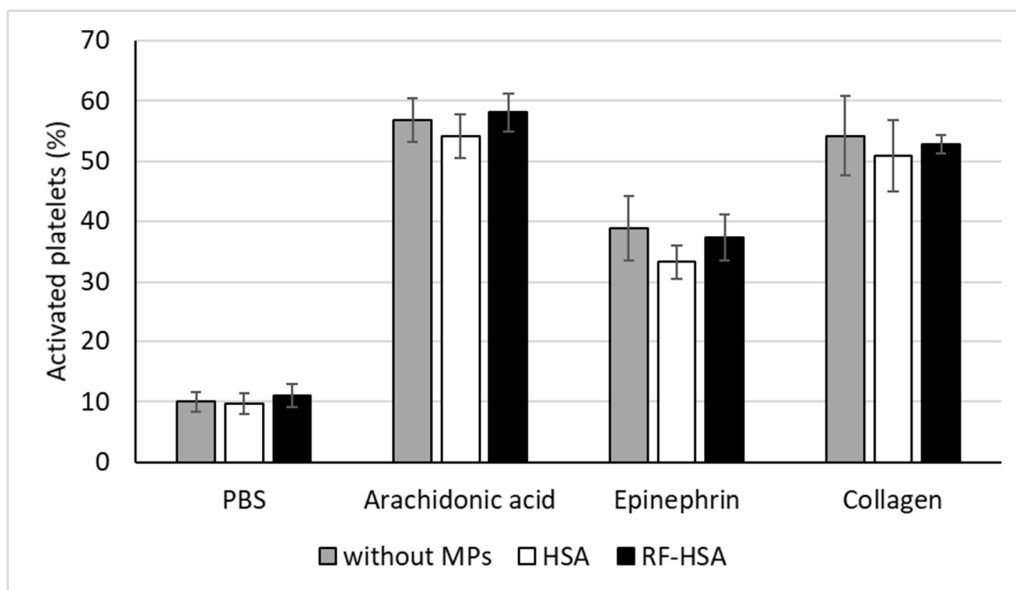
**Figure 6.** Phagocytosis assay showing (A) three groups of white blood cells identified by their forward scatter (FSC) and side scatter (SSC): granulocytes, monocytes, and lymphocytes. Histograms representing fluorescence intensity of (B) HSA-MPs and (C) RF-HSA-MPs in the PE-A channel. Phagocytosis of FITC-labeled opsonized *E. coli* in granulocytes (D) and monocytes (G) (grey area: negative controls incubated at 0 °C; black area: granulocytes and monocytes with phagocytosed FITC *E. coli*). Representative histograms of fluorescence intensity of monocytes and granulocytes after interacting with (E,H) HSA-MPs and (F,I) RF-HSA-MPs (grey area: negative controls incubated at 0 °C; black line: granulocytes and monocytes incubated at 37 °C MPs; k stands for kilo). Data are representative of n = 3 independent phagocytosis assays showing the same trends.

### 3.3.3. Platelet Activation Test

Further, platelet activation was determined by evaluating expression of CD62p (P-selectin) and CD42b platelet surface markers. Non-treated PRP (negative control) showed nearly 10% platelet activation (expression of CD62p) caused by sample handling and preparation. Incubation with agonists (arachidonic acid, epinephrine, and collagen) caused an increased expression of CD62p in the platelets confirming their functionality. The measurement of the CD42b/CD62p co-expression in platelet samples treated with the HSA-MPs or RF-HSA-MPs revealed that there was no effect on the CD62p expression in CD42b positive cells. This is comparable to the control sample. Together with agonist, HSA-MPs or RF-HSA-MPs did not induce a different behavior in the activation of the platelets in comparison with the samples treated with agonists only. Therefore, both HSA-MPs and RF-HSA-MPs did not activate the platelets and did not augment the platelet response to antagonists. Representative dot plots are shown in Figure 7B and summarized results of the platelet activation test are shown in Figure 7B.



(A)



(B)

**Figure 7.** Platelet activation assay showing (A) representative dot plots in APC-A/FITC-A channel for HSA-MPs and RF-HSA-MPs (upper row); CD42b (APC-A)/CD62P (FITC-A) dot plots gated for platelets at rest and after stimulation with HSA-MPs and RF-HSA-MPs (second row); CD42b (APC-A)/CD62P (FITC-A) dot plots gated for platelets after stimulation with arachidonic acid, arachidonic acid and HSA-MPs, arachidonic acid and RF-HSA-MPs (third row); CD42b (APC-A)/CD62P (FITC-A) dot plots gated for platelets after stimulation with epinephrine, epinephrine and HSA-MPs, epinephrine and RF-HSA-MPs (lower row); (B) FACS analysis of MPs platelet activation measured by the determination of CD62p/CD42 co-expression. The presence of particles did not have an influence on platelet activation. The agonists (arachidonic acid, epinephrine, and collagen) induced platelet activation independent from the presence of particles. Data are representative of n = 4 independent platelet activations showing the same trends and are presented as mean ± SD (n = 4).

#### 4. Conclusions

In conclusion, we demonstrated that the encapsulation of a drug with a low molecular weight and low water-soluble macromolecule, RF, can be performed by capturing the growing  $\text{MnCO}_3$  particles together with HSA. The negatively charged particles can be produced with a narrow size distribution and diameters less than 1  $\mu\text{m}$ . The release of RF from the particles exhibits bi-phasic profile with a dominating Fickian diffusion mechanism. These findings suggest that RF-HSA-MPs represent a compelling strategy for a long-term drug delivery system, and that the CCD-technique of incorporation is applicable to various biomolecules with different molecular weights. Taken together, with the investigation of the release of RF and the hemocompatibility, this work provides basic information for the production and application of HSA-based micro-particles as a drug carrier system.

**Author Contributions:** N.S. experiments, data analysis, and writing; K.S. experiments and data analysis; C.K., W.K., and N.B. data analysis; A.P. and S.C. performed part of the measurements; R.G. conceptualization, design of experiments, performing specific experiments, interpretation and discussion of results, revision of manuscript; H.B. conceptualization, advised all research, design of experiments, evaluation and discussion of results, revision of manuscript, and provided research funding.

**Funding:** This work was supported by the European Research Council (grant number PIRSES-GA-2013-612673). N.S. and C.K. hold an academic development scholarship from the University of Phayao, A.P. from Naresuan University, and W.K. and S.C. from Payap University.

**Acknowledgments:** The authors acknowledge the technical support for AFM measurements by Anne Heilig, at the Max-Planck-Institute of Colloids and Interfaces, Golm-Potsdam, Germany.

**Conflicts of Interest:** The authors declare no conflict of interest.

#### References

1. Powers, H.J. Riboflavin (vitamin B-2) and health. *Am. J. Clin. Nutr.* **2003**, *77*, 1352–1360. [[CrossRef](#)] [[PubMed](#)]
2. O'Neill, G.J.; Egan, T.; Jacquier, J.C.; O'Sullivan, M.; O'Riordan, E.D. Kinetics of immobilisation and release of tryptophan, riboflavin and peptides from whey protein microbeads. *Food Chem.* **2015**, *180*, 150–155. [[CrossRef](#)]
3. Machado, D.; Shishido, S.M.; Queiroz, K.C.S.; Oliveira, D.N.; Faria, A.L.C.; Catharino, R.R.; Spek, C.A.; Ferreira, C.V. Irradiated riboflavin diminishes the aggressiveness of melanoma in vitro and in vivo. *PLoS ONE* **2013**, *8*, e54269. [[CrossRef](#)]
4. Chaves Neto, A.H.; Pelizzaro-Rocha, K.J.; Fernandes, M.N.; Ferreira-Halder, C.V. Antitumor activity of irradiated riboflavin on human renal carcinoma cell line 786-O. *Tumor Biol.* **2015**, *36*, 595–604. [[CrossRef](#)]
5. Mazur-Bialy, A.I.; Kolaczowska, E.; Plytycz, B. Modulation of zymosan-induced peritonitis by riboflavin co-injection, pre-injection or post-injection in male Swiss mice. *Life Sci.* **2012**, *91*, 1351–1357. [[CrossRef](#)] [[PubMed](#)]
6. Powers, H.J. Current knowledge concerning optimum nutritional status of riboflavin, niacin and pyridoxine. *Proc. Nutr. Soc.* **1999**, *58*, 435–440. [[CrossRef](#)]
7. De Souza, A.C.S.; Kodach, L.; Gadelha, F.R.; Bos, C.L.; Cavagis, A.D.M.; Aoyama, H.; Peppelenbosch, M.P.; Ferreira, C.V. A promising action of riboflavin as a mediator of leukaemia cell death. *Apoptosis* **2006**, *11*, 1761–1771. [[CrossRef](#)] [[PubMed](#)]
8. De Souza Queiroz, K.C.; Zambuzzi, W.F.; Santos de Souza, A.C.; da Silva, R.A.; Machado, D.; Justo, G.Z.; Carvalho, H.F.; Peppelenbosch, M.P.; Ferreira, C.V. A possible anti-proliferative and anti-metastatic effect of irradiated riboflavin in solid tumours. *Cancer Lett.* **2007**, *258*, 126–134. [[CrossRef](#)]
9. Reddy, H.L.; Dayan, A.D.; Cavagnaro, J.; Gad, S.; Li, J.; Goodrich, R.P. Toxicity testing of a novel riboflavin-based technology for pathogen reduction and white blood cell inactivation. *Transfus. Med. Rev.* **2008**, *22*, 133–153. [[CrossRef](#)] [[PubMed](#)]
10. Pron, G.; Ieraci, L.; Kaulback, K. Collagen cross-linking using riboflavin and ultraviolet-a for corneal thinning disorders: An evidence-based analysis. *Ont. Health Technol. Assess. Ser.* **2011**, *11*, 1–89. [[PubMed](#)]
11. Filipowicz, A.; Wołowicz, S. Solubility and in vitro transdermal diffusion of riboflavin assisted by PAMAM dendrimers. *Int. J. Pharm.* **2011**, *408*, 152–156. [[CrossRef](#)] [[PubMed](#)]

12. Memarpour-Yazdi, M.; Mahaki, H. Probing the interaction of human serum albumin with vitamin B2 (riboflavin) and L-Arginine (L-Arg) using multi-spectroscopic, molecular modeling and zeta potential techniques. *J. Lumin.* **2013**, *136*, 150–159. [[CrossRef](#)]
13. Zhao, H.; Ge, M.; Zhang, Z.; Wang, W.; Wu, G. Spectroscopic studies on the interaction between riboflavin and albumins. *Spectrochim. Acta Part A Mol. Biomol. Spectrosc.* **2006**, *65*, 811–817. [[CrossRef](#)] [[PubMed](#)]
14. Xiong, Y.; Georgieva, R.; Steffen, A.; Smuda, K.; Bäuml, H. Structure and properties of hybrid biopolymer particles fabricated by co-precipitation cross-linking dissolution procedure. *J. Colloid Interface Sci.* **2018**, *514*, 156–164. [[CrossRef](#)] [[PubMed](#)]
15. Bäuml, H.; Xiong, Y.; Liu, Z.Z.; Patzak, A.; Georgieva, R. Novel hemoglobin particles—Promising new-generation hemoglobin-based oxygen carriers. *Artif. Organs* **2014**, *38*, 708–714. [[CrossRef](#)] [[PubMed](#)]
16. Bäuml, H.; Georgieva, R. Micro-Particles, Blood-Substitute and Method for Forming Same. Patent EP07112474.7A, 13 July 2007.
17. Bäuml, H.; Georgieva, R. Coupled enzyme reactions in multicompartiment microparticles. *Biomacromolecules* **2010**, *11*, 1480–1487. [[CrossRef](#)]
18. Xiong, Y.; Steffen, A.; Andreas, K.; Müller, S.; Sternberg, N.; Georgieva, R.; Bäuml, H. Hemoglobin-based oxygen carrier microparticles: Synthesis, properties, and in vitro and in vivo investigations. *Biomacromolecules* **2012**, *13*, 3292–3300. [[CrossRef](#)]
19. Xiong, Y.; Liu, Z.Z.; Georgieva, R.; Smuda, K.; Steffen, A.; Sendeski, M.; Voigt, A.; Patzak, A.; Bäuml, H. Nonvasoconstrictive hemoglobin particles as oxygen carriers. *ACS Nano* **2013**, *7*, 7454–7461. [[CrossRef](#)]
20. Kratz, F. Albumin as a drug carrier: Design of prodrugs, drug conjugates and nanoparticles. *J. Control. Release* **2008**, *132*, 171–183. [[CrossRef](#)]
21. Chen, Z.; Chen, J.; Wu, L.; Li, W.; Chen, J.; Cheng, H.; Pan, J.; Cai, B. Hyaluronic acid-coated bovine serum albumin nanoparticles loaded with brucine as selective nanovectors for intra-articular injection. *Int. J. Nanomed.* **2013**, *8*, 3843–3853. [[CrossRef](#)]
22. Lee, J.Y.; Bae, K.H.; Kim, J.S.; Nam, Y.S.; Park, T.G. Intracellular delivery of paclitaxel using oil-free, shell cross-linked HSA-multi-armed PEG nanocapsules. *Biomaterials* **2011**, *32*, 8635–8644. [[CrossRef](#)]
23. Von Storp, B.; Engel, A.; Boeker, A.; Ploeger, M.; Langer, K. Albumin nanoparticles with predictable size by desolvation procedure. *J. Microencapsul.* **2012**, *29*, 138–146. [[CrossRef](#)] [[PubMed](#)]
24. Mishra, V.; Mahor, S.; Rawat, A.; Gupta, P.N.; Dubey, P.; Khatri, K.; Vyas, S.P. Targeted brain delivery of AZT via transferrin anchored pegylated albumin nanoparticles. *J. Drug Target.* **2006**, *14*, 45–53. [[CrossRef](#)] [[PubMed](#)]
25. Qi, J.; Yao, P.; He, F.; Yu, C.; Huang, C. Nanoparticles with dextran/chitosan shell and BSA/chitosan core-doxorubicin loading and delivery. *Int. J. Pharm.* **2010**, *393*, 177–185. [[CrossRef](#)] [[PubMed](#)]
26. Lee, S.H.; Heng, D.; Ng, W.K.; Chan, H.K.; Tan, R.B.H. Nano spray drying: A novel method for preparing protein nanoparticles for protein therapy. *Int. J. Pharm.* **2011**, *403*, 192–200. [[CrossRef](#)] [[PubMed](#)]
27. Xu, R.; Fisher, M.; Juliano, R.L. Targeted albumin-based nanoparticles for delivery of amphiphathic drugs. *Bioconjug. Chem.* **2011**, *22*, 870–878. [[CrossRef](#)] [[PubMed](#)]
28. Zhao, L.; Kaewprayoon, W.; Zhou, H.; Georgieva, R.; Bäuml, H. RBC aggregation in dextran solutions can be measured by flow cytometry. *Clin. Hemorheol. Microcirc.* **2017**, *65*, 93–101. [[CrossRef](#)]
29. Dvir, T.; Timko, B.P.; Kohane, D.S.; Langer, R. Nanotechnological strategies for engineering complex tissues. *Nat. Nanotechnol.* **2011**, *6*, 13–22. [[CrossRef](#)]
30. Peppas, N.A.; Sahlin, J.J. A simple equation for the description of solute release. III. Coupling of diffusion and relaxation. *Int. J. Pharm.* **1989**, *57*, 169–172. [[CrossRef](#)]
31. Ritger, P.L.; Peppas, N.A. A simple equation for description of solute release II. Fickian and anomalous release from swellable devices. *J. Control. Release* **1987**, *5*, 37–42. [[CrossRef](#)]
32. Pourmortazavi, S.M.; Rahimi-Nasrabadi, M.; Davoudi-Dehaghani, A.A.; Javidan, A.; Zahedi, M.M.; Hajimirsadeghi, S.S. Statistical optimization of experimental parameters for synthesis of manganese carbonate and manganese oxide nanoparticles. *Mater. Res. Bull.* **2012**, *47*, 1045–1050. [[CrossRef](#)]
33. Fanali, G.; Cao, Y.; Ascenzi, P.; Fasano, M. Mn(II) binding to human serum albumin: A 1H-NMR relaxometric study. *J. Inorg. Biochem.* **2012**, *117*, 198–203. [[CrossRef](#)]
34. Petrov, A.I.; Volodkin, D.V.; Sukhorukov, G.B. Protein calcium-carbonate coprecipitation: A tool for protein encapsulation. *Biotechnol. Prog.* **2005**, *21*, 918–925. [[CrossRef](#)] [[PubMed](#)]

35. Vantsyan, M.A.; Kochetkov, A.A.; Marchenko, I.V.; Kiryukhin, Y.I.; Nabatov, B.V.; Artemov, V.V.; Bukreeva, T.V. Nanostructured calcium carbonate particles as fluorophore carriers. *Crystallogr. Rep.* **2015**, *60*, 951–958. [[CrossRef](#)]
36. Lauth, V.; Maas, M.; Rezwan, K. Coacervate-directed synthesis of CaCO<sub>3</sub> microcarriers for pH-responsive delivery of biomolecules. *J. Mater. Chem. B* **2014**, *2*, 7725–7731. [[CrossRef](#)]
37. Simioni, A.R.; de Jesus, P.C.C.; Tedesco, A.C. Layer-by-layer hollow photosensitizer microcapsule design via a manganese carbonate hard template for photodynamic therapy in cells. *Photodiagn. Photodyn. Ther.* **2018**, *22*, 169–177. [[CrossRef](#)] [[PubMed](#)]
38. Tong, W.; Gao, C. Selective removal of particle cores to fabricate manganese carbonate hollow spheres and composite microcapsules. *Colloids Surf. A Physicochem. Eng. Asp.* **2007**, *295*, 233–238. [[CrossRef](#)]
39. Zhu, H.; Stein, E.W.; Lu, Z.; Lvov, Y.M.; McShane, M.J. Synthesis of size-controlled monodisperse manganese carbonate microparticles as templates for uniform polyelectrolyte microcapsule formation. *Chem. Mater.* **2005**, *17*, 2323–2328. [[CrossRef](#)]
40. Antipov, A.A.; Shchukin, D.; Fedutik, Y.; Petrov, A.I.; Sukhorukov, G.B.; Möhwald, H. Carbonate microparticles for hollow polyelectrolyte capsules fabrication. *Colloids Surf. A Physicochem. Eng. Asp.* **2003**, *224*, 175–183. [[CrossRef](#)]
41. Liu, J.; Zeng, F.; Allen, C. Influence of serum protein on polycarbonate-based copolymer micelles as a delivery system for a hydrophobic anti-cancer agent. *J. Control. Release* **2005**, *103*, 481–497. [[CrossRef](#)] [[PubMed](#)]
42. Choi, J.; Reipa, V.; Hitchins, V.M.; Goering, P.L.; Malinauskas, R.A. Physicochemical characterization and in vitro hemolysis evaluation of silver nanoparticles. *Toxicol. Sci.* **2011**, *123*, 133–143. [[CrossRef](#)] [[PubMed](#)]
43. Zook, J.M.; MacCuspie, R.I.; Locascio, L.E.; Halter, M.D.; Elliott, J.T. Stable nanoparticle aggregates/agglomerates of different sizes and the effect of their size on hemolytic cytotoxicity. *Nanotoxicology* **2011**, *5*, 517–530. [[CrossRef](#)] [[PubMed](#)]
44. Mayer, A.; Vadon, M.; Rinner, B.; Novak, A.; Wintersteiger, R.; Fröhlich, E. The role of nanoparticle size in hemocompatibility. *Toxicology* **2009**, *258*, 139–147. [[CrossRef](#)] [[PubMed](#)]
45. Evora, C.; Soriano, I.; Rogers, R.A.; Shakesheff, K.M.; Hanes, J.; Langer, R. Relating the phagocytosis of microparticles by alveolar macrophages to surface chemistry: The effect of 1,2-dipalmitoylphosphatidylcholine. *J. Control. Release* **1998**, *51*, 143–152. [[CrossRef](#)]



© 2019 by the authors. Licensee MDPI, Basel, Switzerland. This article is an open access article distributed under the terms and conditions of the Creative Commons Attribution (CC BY) license (<http://creativecommons.org/licenses/by/4.0/>).



## Improved oxygen storage capacity of haemoglobin submicron particles by one-pot formulation

Chiraphat Kloypan<sup>a,b</sup>, Ausanai Prapan<sup>a,c</sup>, Nittiya Suwannasom<sup>a,d</sup>, Saranya Chaiwaree<sup>a,e</sup>, Waraporn Kaewprayoon<sup>a,e</sup>, Axel Steffen<sup>a</sup>, Yu Xiong<sup>a</sup>, Nuttakorn Baisaeng<sup>f</sup>, Radostina Georgieva<sup>a,g</sup> and Hans Bäuml<sup>a</sup> 

<sup>a</sup>Institute of Transfusion Medicine, Charité – Universitätsmedizin Berlin, Berlin, Germany; <sup>b</sup>Division of Clinical Immunology and Transfusion Sciences, School of Allied Health Sciences, University of Phayao, Phayao, Thailand; <sup>c</sup>Department of Radiological Technology, Naresuan University, Phitsanulok, Thailand; <sup>d</sup>Division of Biochemistry and Nutrition, School of Medical Sciences, University of Phayao, Phayao, Thailand; <sup>e</sup>Department of Pharmaceutical Technology, Payap University, Chiang Mai, Thailand; <sup>f</sup>Division of Pharmaceutical Sciences, School of Pharmaceutical Sciences, University of Phayao, Phayao, Thailand; <sup>g</sup>Department of Medical Physics, Biophysics and Radiology, Trakia University, Stara Zagora, Bulgaria

### ABSTRACT

The coprecipitation–cross-linking–dissolution (CCD) technique for protein submicron particle fabrication was improved by omitting one preparation step using the macromolecular cross-linker, periodate-oxidized dextran (Odex, M.W. of 40 and 70 kDa). The coprecipitation and cross-linking of haemoglobin (Hb) were combined in one single step since the cross-linker is incorporated into the inorganic template, MnCO<sub>3</sub>, together with the protein. After removal of the MnCO<sub>3</sub> templates by EDTA, the amount of entrapped Hb was 60 to 70% of the initial amount. This technique provides deformable Hb submicron particles (HbMP) with narrow size distribution between 800 and 1000 nm, uniform morphology and negative zeta-potential. More than 40% of Hb in the particles was able to carry oxygen over a storage period of 90 days. The results suggest that our new protein submicron particle fabrication technique minimizes the fabrication time and is very efficient and cost-effective.

### ARTICLE HISTORY

Received 17 August 2018  
Revised 29 August 2018  
Accepted 29 August 2018

### KEYWORDS

Coprecipitation; cross-linker; haemoglobin; submicron particles; oxidized dextran

### Introduction

In the last decades, protein particles have been proposed for a number of biomedical applications such as drug delivery systems and haemoglobin (Hb)-based oxygen carriers [1]. Many techniques are available for the fabrication of protein nano- and microparticles including spray drying, emulsification, layer-by-layer assembly, solvent displacement and polymeric formation [2]. However, each of these techniques has serious drawbacks which impair its function and/or biocompatibility. For example, spray drying or lyophilization techniques deliver protein particles in dry powder formulation but their polydispersity is usually high [3,4] and entrapment efficiency is typically poor in protein particles prepared by solvent displacement [5]. Apart from that, tertiary and quaternary structures of proteins need to be preserved to maintain protein function that is hard to fulfil by many of these conventional methods due to exposure to high temperature, high ionic strength, non-physiological pH, organic solvents or hydrophobic interfaces.

Previously, we described a micro- and sub-microparticle fabrication method called coprecipitation–cross-linking–dissolution (CCD), which consists of three main steps. First, protein and inorganic template are precipitated together followed by a cross-linking step where glutaraldehyde (GA) was used to cross-link the proteins. Finally, EDTA was used to remove the inorganic template to obtain protein microparticles [6–8].

This technique is favourable to fabricate in mild condition and provides pure protein particles with uniform morphology and narrow size distribution. However, the cross-linking of protein with GA needs to be taken into consideration.

The GA can react with several functional groups of proteins, such as amine, thiol, phenol and imidazole, and is very effective as a protein cross-linker because the most reactive amino acid side chains are nucleophiles [9]. It, therefore, has been widely used to cross-link proteins and other biopolymers for medical applications. However, there are many reports concerning the undesired properties of GA-cross-linked biomaterials such as autofluorescence as well as its toxicity [10,11]. For that reason, “biocompatible” cross-linkers are now being investigated as alternatives for GA to reduce the risks of side effects.

Polysaccharides are natural biopolymers which have a great number of reactive groups on their molecular chains, such as hydroxyl, carboxyl and amino groups, which can make them be easily modified chemically and biochemically. They are highly safe, non-toxic, stable, biodegradable and biocompatible. Besides, polysaccharides have abundant resources in nature and low cost in their processing. There are various sources from animal (chitosan, chondroitin), plant (e.g. pectin, cellulose), alga (e.g. alginate) and microorganisms (e.g. dextran). The polysaccharide is desirably oxidized to extent sufficient to provide the aldehyde groups capable of promoting rapid cross-linking of the polymers. For that reason, there are several usages of

polysaccharide in the biomedical application as a biopolymer cross-linker; for instance, oxidized hydroxyethyl starch [12], oxidized raffinose (*O*-raffinose) [13–15] and oxidized dextran (Odex) [16,17] were used as a cross-linker for Hb conjugation.

Dextran is a glucose homopolymer, produced by the bacteria called *Leuconostoc mesenteroides*. It is consisting essentially of  $\alpha$ -1,6 linked D-glucopyranose residues with a few per cent of  $\alpha$ -1,2-,  $\alpha$ -1,3- or  $\alpha$ -1,4-linked side chains. Dextran is selected in many biomedical applications because it is slowly degraded by human enzymes compared to other polysaccharides (e.g. glycogen with  $\alpha$ -1,4 linkages) and cleaved by microbial dextranases in the gastrointestinal tract. It has been previously used as plasma expander and was investigated as a macromolecular carrier for the delivery of drugs and proteins, to increase the durability of therapeutic agents in the blood circulation and to decrease the *in vivo* immunogenicity of proteins and enzymes [18,19]. It is also an excellent candidate as a bio-cross-linker because of its chemical properties such as high water solubility, high stability, high content of hydroxyl groups, which are suitable for derivatization and can be subsequently used for chemical cross-linking of proteins [20]. Oxidation of dextran by periodate ions is a common dextran functionalizing modification reaction which yields a purified product with simple dialysis method. Glucose residue of dextran has vicinal diol which houses two oxidizable bonds. The oxidation of those bonds forms an aldehyde in C<sub>3</sub>, which is susceptible to periodate oxidation on account of the presence of the hydroxyl groups in C<sub>2</sub> and C<sub>4</sub> and subsequently leads to a double oxidation of the same residue. This leads to the opening of the glucose ring and formation of double aldehyde groups, which may react with amino groups creating Schiff's base (Maillard reaction). The dextran oxidation reaction may perform under mild conditions with high efficiency but no catalyst is needed [21]. For this reason, oxidized dextran (Odex) has recently been investigated as an "alternative biocompatible hydrophilic cross-linker" for biopolymers, that is hydrogel formation, tissue engineering and drug delivering particles [22–24]. Nevertheless, to the best of our knowledge, Odex was not used for the fabrication of micro- or nano-protein particles.

Therefore, the aim of this study was to develop a novel biopolymer microparticle fabrication method based on the CCD technique by applying Odex as a cross-linker for Hb. Here, the coprecipitation and the cross-linking steps are combined in one single step for the reason that the cross-linker, Odex, is coprecipitated together with the protein. The physiochemical properties of the resulting Odex-cross-linked Hb particles (Odex-HbMP) were investigated by several techniques including scanning electron microscopy (SEM), atomic force microscopy (AFM) and dynamic light scattering, zeta-potential measurements, spectrophotometry. Additionally, the functionality of the Hb entrapped in the Odex-HbMP as well as the stability of Odex-HbMP in a salt solution and their deformability was determined.

## Materials and methods

### Materials

Dextran (from *Leuconostoc mesenteroides*, M.W. 40, 70 kDa) was purchased from AppliChem GmbH (Darmstadt, Germany).

Human serum albumin (HSA) solution was purchased from Grifols GmbH (Frankfurt, Germany). Ethylenediaminetetraacetic acid (EDTA), potassium ferricyanide (K<sub>3</sub>[Fe(CN)<sub>6</sub>]), glycine, manganese chloride, sodium borohydride, sodium carbonate, sodium chloride, sodium dithionite, sodium hydroxide and sodium (meta) periodate were purchased from Sigma-Aldrich (Darmstadt, Germany).

### Preparation of haemoglobin

Haemoglobin was extracted from bovine red blood cells by hypotonic haemolysis as previously described [25,26]. Briefly, fresh bovine whole blood (EDTA-anticoagulated, obtained from Biophyll GmbH, Dietersburg, Germany) was centrifuged at 2500 g for 15 min at 4 °C. The resulting packed red blood cells were washed three times with 0.9% NaCl (B. Braun Melsungen AG, Melsungen, Germany). Haemolysis was performed by adding five volumes of lysing NaCl solution (100 mOsmol/kg). The solution was stirred at 4 °C overnight and then centrifuged for 3 h at 5500 g. The supernatant was filtered by means of tangential flow filtration (TFF) using the KrosFlo Research II TFF system (Spectrum Europe B.V., the Netherlands) similar to the process described earlier [23]. One 500 kDa mPES hollow fibre filter module (MiniKros Sampler, Spectrum) was used with a permeate flow rate of 30 to 25 ml/min and a transmembrane pressure (TMP) of 0.3 to 0.5 bar. The filtered Hb was stored as a stock solution at –30 °C until use.

### Synthesis and characterization of oxidized dextran (Odex)

Sodium periodate (6.6 g, 30.9 mmol) was added into 50 ml of 10% of dextran (30.9 mmol glucose subunits) in water, shielded from light, with constant stirring at room temperature. The reaction was allowed to proceed for 1 h [27]. Then, the reaction mixture containing the oxidized dextran (Odex) was transferred to a cellulose dialysis tube (MWCO of 12,000: Carl Roth GmbH, Karlsruhe, Germany) and dialyzed against water. Finally, the Odex solution was lyophilized by the freeze-drying method and the obtained dried powder was maintained at room temperature for further usage [28].

The aldehyde group content of Odex was determined using the hydroxylamine hydrochloride titration method, and non-oxidized dextran samples were used as a control [23,28]. Briefly, 0.1 g of lyophilized oxidized dextran was dissolved in 25 ml of 0.25 N hydroxylamine hydrochloride-methyl orange solution pH 4.0. The mixtures were then titrated with standardized 0.1 N NaOH solution until the red-to-yellow endpoint was achieved by the equivalent of the colour of the non-oxidized dextran titrated solution. Thereby, the number of aldehyde groups per 100 glucose subunits was calculated with the following formula:

$$\text{Aldehyde per 100 glucose subunits} = \quad (1)$$

$$N \times V \times \left( \frac{\text{MW}}{\text{wt}} \right) \times \left( \frac{100}{S} \right)$$

where  $N$  is the concentration of standardized sodium hydroxide,  $V$  is the volume of NaOH solution used in the titration,  $MW$  is the molecular weight of dextran,  $wt$  is the weight of dextran and  $S$  is the number of glucose subunits in dextran.

### Preparation of Odex-HbMP

Haemoglobin particles (HbMP) were fabricated by a modified protocol based on the CCD technique as previously described by Bäumlner et al. [6–8,29,30]. In brief, equal volumes of solution 1 consisting of 0.25 M of  $MnCl_2$  and 10 to 50 mg/mL of Hb were rapidly mixed with solution 2 containing 0.25 M of  $Na_2CO_3$  and 5 to 40 mg/mL of Odex in a beaker under vigorous stirring using a mechanical stirrer (model IKA RW 20 DZM equipped with a 35-mm-diameter rotor) at room temperature. In this step, the Hb and the cross-linker Odex were precipitated together into the inorganic  $MnCO_3$  allowing the cross-linking reaction to perform in the formulated submicron particles. After incubation for 30 s, 5 mg/mL of HSA was added to the suspension and incubated for 5 min under stirring as a result of the adsorption of HSA on the surface of particles. After HSA incubation, the resulting suspension particles were proceeded to the dissolution of the  $MnCO_3$  template by 0.25 M EDTA/0.05 M glycine for 30 min and the reduction by 0.4 mg/mL of  $NaBH_4$ . Finally, the obtained Odex-cross-linked Hb particles (Odex-HbMP) were centrifuged, washed three times (6000 g for 5 min) and suspended in sterile 0.9% NaCl.

The amount of entrapped protein was determined as the difference between the total amount of applied protein ( $P_t$ ) and the remaining amount of protein in the supernatant ( $P_f$ ) after coprecipitation and washing steps. Subsequently, the entrapment efficiency (EE%) was calculated according to the following equation:

$$EE \% = \frac{(P_t - P_f)}{P_t} \times 100\% \quad (2)$$

The Hb concentration in the Odex-HbMP was determined by alkaline haematin detergent (AHD)-575 method. The optical density of haematin was measured at 575 nm.

### Particles characterization

#### Scanning electron microscopy

For SEM imaging, samples were prepared by applying a drop of particles suspension onto glass slide followed by drying overnight. After sputtering with gold, measurements were conducted at an operation voltage of 3 keV using Gemini Leo 1550 instrument (Oberkochen, Germany) and ImageJ 1.44p software (Wayne Rasband, National Institute of Mental Health, Bethesda, MD).

#### Cryo-SEM

The Odex-HbMP suspension was frozen in a copper sandwich holder by submersion in liquid propane at  $-180^\circ C$  in a Cryoplunge (Gatan, USA) and subsequently freeze-fractured (Alto 2500 cryo preparation chamber) at  $-180^\circ C$ , freeze-etched

at  $-98^\circ C$  for 54 s and finally sputtered with platinum at  $-130^\circ C$ . After this procedure, the sample was transferred into an ultrahigh-resolution field-emission scanning electron microscopy (SEM) system (Hitachi, S-4800). The SEM micrographs were obtained at a stage temperature of  $-130^\circ C$  and an accelerating voltage of 5 kV.

#### Particle size and zeta-potential

The hydrodynamic diameter (Z-average diameter) and the zeta-potential of HbMP were measured by dynamic light scattering using a Zetasizer Nano ZS instrument (Malvern Instruments Ltd., Malvern, UK) in PBS solution.

#### Haemoglobin content in Odex-HbMP

For Hb determination, modified AHD-575 method was employed. 2% (v/v) Odex-HbMP suspension was mixed with pronase to achieve a final concentration of 0.5 mg/ml pronase (Roche Diagnostics GmbH, Mannheim, Germany). The particles were digested by pronase with the purpose to terminate the binding of Odex and Hb in order to reduce the noise scattering from of particles. The pronase-HbMP suspension was then incubated for 30 min at  $45^\circ C$ . Afterwards, AHD reagent was added at the volume ratio of 1:1 to the pronase-HbMP mixture for hemin conversion. Absorption spectra of the particles were recorded using a UV-VIS spectrophotometer at 575 nm (Hitachi U2800, Hitachi High-Technologies Corporation).

#### Determination of oxygen carrying capacity of Odex-HbMP

The Hb solution was diluted into different concentrations (0.75–6 mg/mL). 1 ml of each concentration was filled into a 2-ml glass vial containing a magnetic stirrer. After an equilibration time of 5 min, a miniaturized optical needle type oxygen sensor (oxygen microsensor NTH-PSt7, PreSens – Precision Sensing GmbH, Regensburg, Germany), which was connected to a portable oxygen meter with data logging (Microx 4, PreSens – Precision Sensing GmbH, Germany), was inserted into the stirred sample. The concentration of dissolved oxygen was recorded at the starting point. Then, 50  $\mu L$  of 10% potassium ferricyanide ( $K_3[Fe(CN)_6]$ ) dissolved in water was added, and the change in concentration of dissolved oxygen was measured and recorded every second. After reaching a stable value, the measurement was stopped. An increase of dissolved oxygen concentration after adding ferricyanide is dependent on the Hb concentration manner. The change in  $pO_2$  is determined by subtracting the  $pO_2$  from the beginning and the end of the measurement. The released oxygen was previously bound to Hb and defined as a functional Hb. A calibration curve demonstrated the ratio of Hb concentration versus  $pO_2$ . For Odex-HbMP, the particle volume concentration was measured by the haematocrit (Hettich Mikro 22R; at 20,000 g for 10 min) and then adjusted to 2%. The measurement of 2% of Odex-HbMP was performed by using the same procedure as described for standard Hb. The functional Hb in the particles compared with a determined calibration curve [31,32]. Finally, the

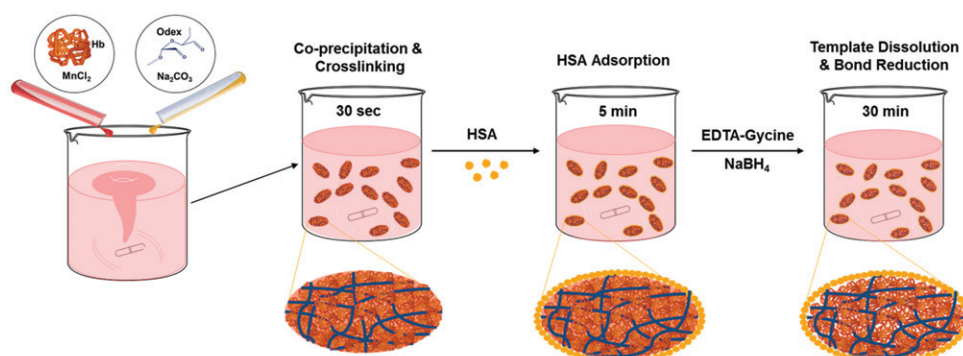


**Figure 1.** Scheme of particle preparation through the one-pot fabrication technique. Two mixtures of inorganic solutions,  $\text{MnCl}_2$  containing haemoglobin and  $\text{Na}_2\text{CO}_3$  with Odex, are mixed together. Here,  $\text{MnCO}_3$  particles are formed with entrapped biopolymers; meanwhile, the Hb is cross-linked by Odex in the particle. HSA was absorbed into particle surface. The  $\text{MnCO}_3$  template is then dissolved and the pure biopolymer particles remain in the solution.

percentage of functional Hb to total Hb was calculated using the identical sample.

### Particles deformability

Particle compression and dilation behaviour were measured by using an automatic measuring system based on an analytical centrifuge with an integrated optoelectronic sensor (LUMiFuge, LUM GmbH, Berlin, Germany). The integrated transmitted light intensity during the centrifugation at different accelerations allows quantification of the suspension stability by means of an instability index:

$$\text{Instability index } \% = \frac{\text{clarification as a function of time}}{\text{maximal possible clarification}} \quad (3)$$

where clarification is the integral of transmission along the cuvette during the centrifugation. The maximal possible clarification is obtained at the highest possible centrifugation force until no changes in the profile will be detected.

In total, 10% haematocrit of particles was placed into the cuvette. The centrifugal force was applied to particles as a cycle to observe the compression and relaxation of particles [33]. Particles were first equilibrated at the beginning with a centrifugal force of 5 g for 10 min. Then, the centrifugal force up to 2300 g was applied to compress particles for 4 h. Finally, the centrifugal force was reduced to 5 g again for 4 h to observe the relaxation of particles. The profiles are simultaneously registered along the cuvette by the STEP technology as a function of time and of the applied centrifugal force and analyzed using the software SEPIVIEW 6.

### Atomic force microscopy

Atomic force microscopy images were obtained using a Nanoscope III Multimode AFM (Digital Instrument Inc., Santa Barbara, CA) in tapping mode as described earlier [34]. Briefly, Odex-HbMP were applied into polyethyleneimine (25 kDa, 1 mM)-pretreated mica substrate. After allowing the particles to attach, the substrate was rinsed with deionized water and dried under a gentle stream of nitrogen. The particles were first scanned in the dry state, then a drop of deionized water was added, and the particles were scanned again in the wet state. The height of each particle in the dry and wet state was measured applying the Nanoscope software as the

height difference between the support and the highest point of the particle surface profile.

### Storage stability of Odex-HbMP

The storage stability of Odex-HbMP in 0.9% NaCl was determined at day 0, 30 and 90 after fabrication. The individual aliquots were kept at 4 °C. Then, the size distribution, the Hb content and the amount of functional Hb of the stored Odex-HbMP were evaluated.

### Statistical analysis

The results were presented as means  $\pm$  standard deviation (SD). The data were compared using ANOVA-like test. GraphPad Prism 6 software (GraphPad, La Jolla, CA) was employed for graphs and statistical analyses.  $p$ -Values  $< .05$  were considered statistically significant.

## Results

### Synthesis of oxidized dextran and characterization

Oxidized dextran was successfully prepared using periodate oxidation reaction. The actual number of aldehyde groups of periodate-oxidized dextran was determined by hydroxylamine hydrochloride titration method. The results showed that aldehydes amount was constant at approximately  $157 \pm 9$  and  $152 \pm 6$  aldehyde groups per 100 glucose subunits for oxidized dextran MW of 40,000 (40T) and dextran MW 70,000 (70T), respectively.

### Preparation of Odex-HbMP

Bovine Hb was selected to demonstrate this novel fabrication procedure as shown in Figure 1. At constant protein concentration of 0.5%, the concentration of 40T- and 70T-Odex during coprecipitation was optimized from 0.25, 0.5, 1.0 and 2.0%, respectively. At low concentrations of Odex, 0.25 and 0.5%, particles were not obtained. The final volume concentration of the Odex-HbMP suspension obtained with 1.0% Odex was lower than that of the Odex-HbMP suspension prepared with 2.0% Odex. Therefore, Odex concentration of 2% was considered as optimal for the fabrication of

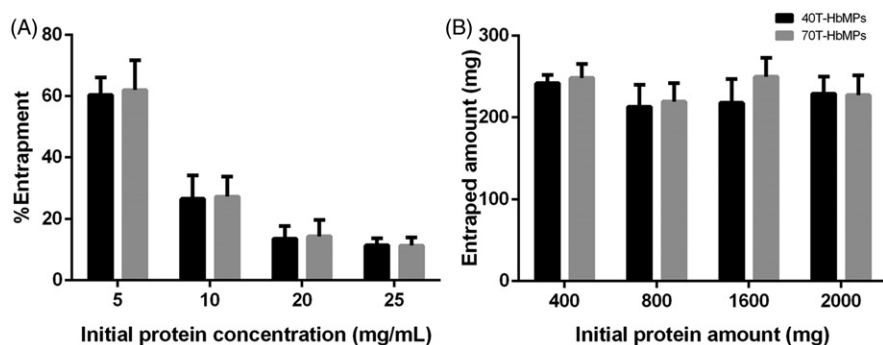


**Figure 2.** (A) Hb entrapment efficiency of  $\text{MnCO}_3$  template. (B) The absolute amount of entrapped protein by different initial Hb concentration. Hb content of Hb- $\text{MnCO}_3$  was independent of the initial protein amount and it was not able to increase by increasing the initial Hb concentration. Data are presented as mean  $\pm$  SD ( $n = 5$ ).

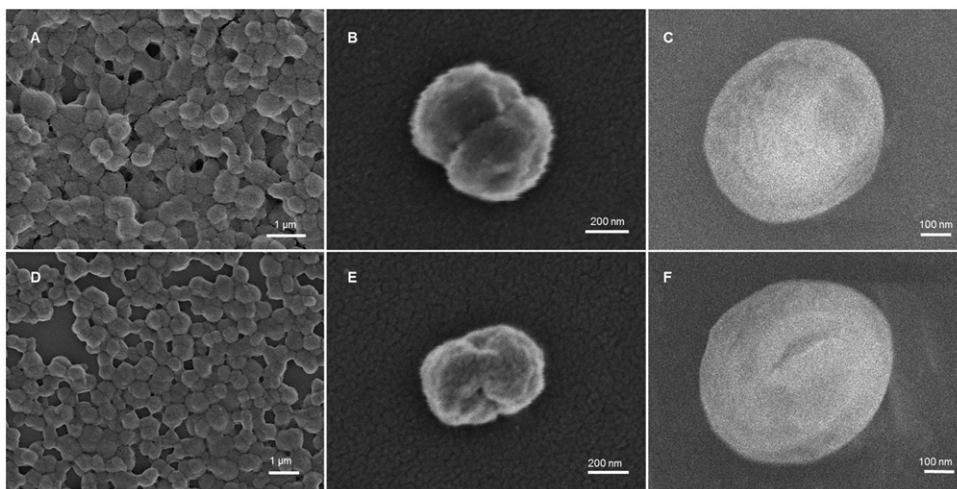


**Figure 3.** SEM images of (A,B) 40T-HbMP and (D,E) 70T-HbMP show a peanut-like shape. Cryo-SEM images of (C) 40T-HbMP and (F) 70T-HbMP show a smooth surface of the particles.

Odex-HbMP. Odex-HbMP fabricated with 40T-Odex and 70T-Odex are named 40T-HbMP and 70T-HbMP, respectively.

Figure 2 shows the Hb entrapment efficiency of our technique using different initial Hb concentrations and 2% Odex for cross-linking. It can be seen that the entrapped protein remains constant with increasing initial Hb concentration. Hence, the initial Hb concentration of 5 mg/mL the maximal entrapment capacity of the  $\text{MnCO}_3$  template is reached (Figure 2(B)). Therefore, Odex-HbMP prepared with 5 mg/mL and 2% Odex were used for all further experiments.

### Particles characterization

#### Morphology, particles size and zeta-potential

The scanning electron micrographs of the Odex-HbMP prepared from 2% Odex and 0.5% Hb in Figure 3 show clearly a peanut-like shape with shortest and longest diameter of about 700 and 1000 nm. Additionally, cryo-SEM micrographs demonstrated that their surface in aqueous environment appears smooth.

The size of the Odex-HbMP measured by dynamic light scattering was around 800–1000 nm (Figure 4(A)) which corresponds to the observations by SEM. Additionally, Odex-HbMP suspend in PBS (conductivity 18–20 mS/cm) showed a negative

zeta-potential (Figure 4(B)) of approximately  $-9$  mV. No significant differences in the physicochemical properties of Odex-HbMP cross-linked by 40T- or 70T-Odex could be found.

#### Deformability of Odex-HbMP

The deformability of the Odex-HbMP cross-linked with both 40T- and 70T-Odex was studied using an analytical centrifuge with integrated optoelectric sensor system. If the particles are exposed to the high centrifugal force at 2300  $g$ , rapidly packing is obtained which results in a constant thickness of the sediment layer. This becomes visible in the high instability index (Figure 5(A)). After exposure to a low centrifugal force at 5  $g$ , the particles are decompressed, which increases the thickness of the sediment layer and results in a decreased instability index. This phenomenon demonstrates the deformability of these particles.

To confirm the deformability of the Odex-HbMP, AFM scans in the dry and wet state were performed. Example of these scans is shown in Figure 5(B). Figure 5(C) represents the measured size of the particles at the long axis and Figure 5(D) present their thickness measured as the vertical distance between the mica support and the highest point of the height profiles. The mean thickness determined from scans of particles in the dry state of 40T- and

70T-HbMP was  $214 \pm 40$  and  $213 \pm 12$  nm and in the wet state  $308 \pm 15$  and  $321 \pm 18$  nm, respectively. It can be clearly seen that the particles are swollen in the wet state.

### Haemoglobin content and oxygen carrying capacity of Odex-HbMP

The concentration of total Hb entrapped in Odex-HbMP was 28–30 mg/mL as calculated for a suspension with a Hct of 20%. The values for 40T-HbMP and 70T-HbMP did not significantly differ from each other ( $28.8 \pm 2.2$  and  $30.4 \pm 2.1$ , respectively). The amount of functional Hb was  $11.59 \pm 0.6$  and  $12.53 \pm 0.9$  mg/mL, respectively.

The ability of oxygenation and deoxygenation of the Odex-HbMP was confirmed using UV-VIS spectrophotometric analysis as shown in Figure 6. Odex-HbMP have similar spectra and spectral changes compared to free Hb in the oxygenated and deoxygenated state.

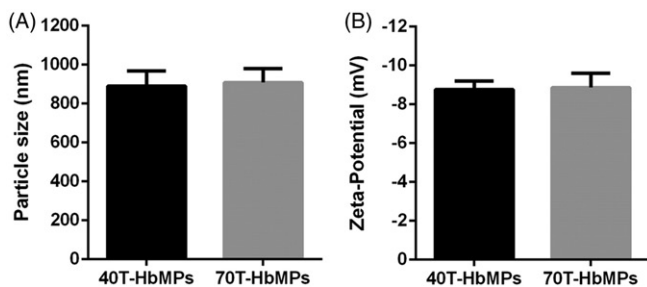


**Figure 4.** Characterization of Odex-HbMP samples. Size (A) and zeta-potential (B) measured in 10 mM PBS (conductivity 18–20 mS/cm) at room temperature by dynamic light scattering analysis. Data are presented as mean  $\pm$  SD ( $n = 5$ ).

### Stability of Odex-HbMP

The stability of Odex-HbMP was characterized by their size, the Hb content and the fraction of functional Hb as shown in Figure 7. It is demonstrated that there was no obvious change in size and in the amount of functional Hb in saline solution at 4 °C during the period of 90 days.

### Discussion

Our new one-pot fabrication technique for protein microparticles is based on the CCD procedure, which exploits the ability of insoluble carbonates template to capture proteins and other macromolecules that are present in the aqueous solution during precipitation [30].

The proteins are precipitated and cross-linked in “one step” because the macromolecular cross-linker (Odex)

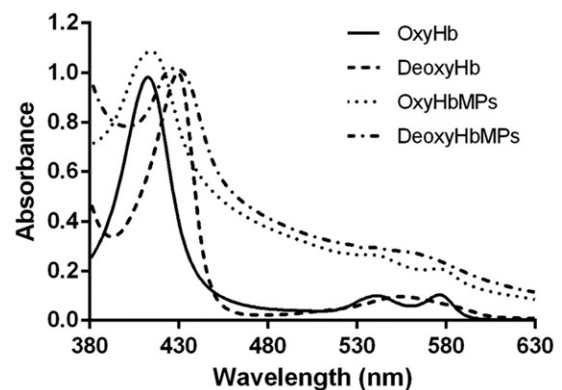


**Figure 6.** Absorption spectra of oxygenated Hb (OxyHb), deoxygenated Hb (DeoxyHb), oxygenated HbMP (OxyHbMP) and deoxygenated HbMP (DeoxyHbMP). A shift towards higher absorption of HbMP is a result of light scattering.

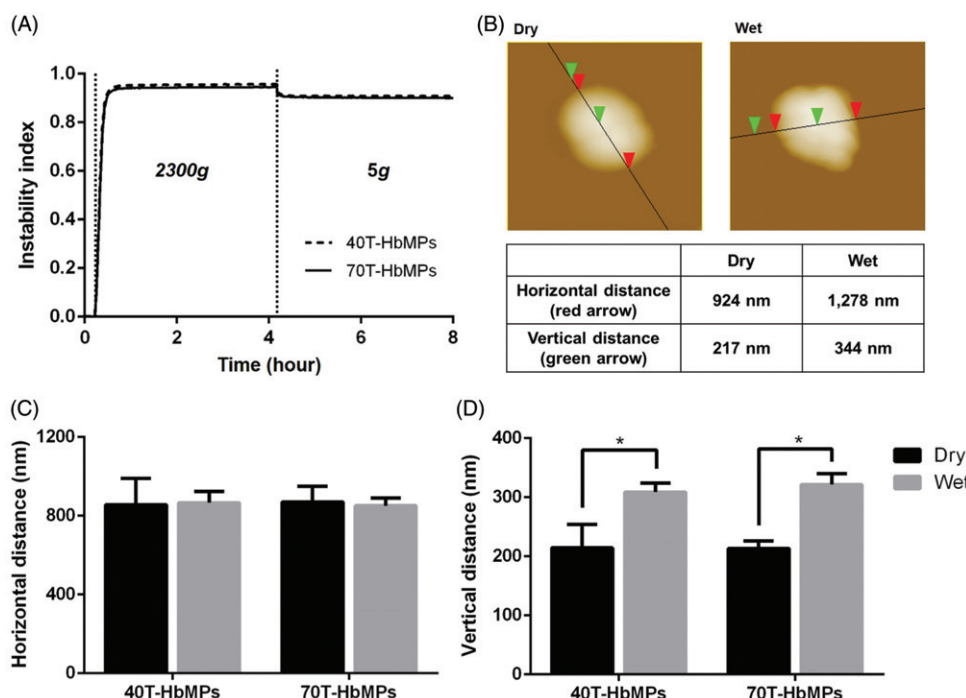


**Figure 5.** Deformability of Odex-cross-linked particles. (A) Compression and dilation behaviour of particles, the profile from the analytical centrifuge. (B) AFM images of 40T-HbMP in dry as well as wet state. (C) The width of the particles is defined as the horizontal distance and (D) the thickness of the particles is given as the vertical distance between the mica support and the top of the particle. Dried HbMP swelled after water was added. Data are presented as mean  $\pm$  SD ( $n = 5$ ),  $p < .05$ .

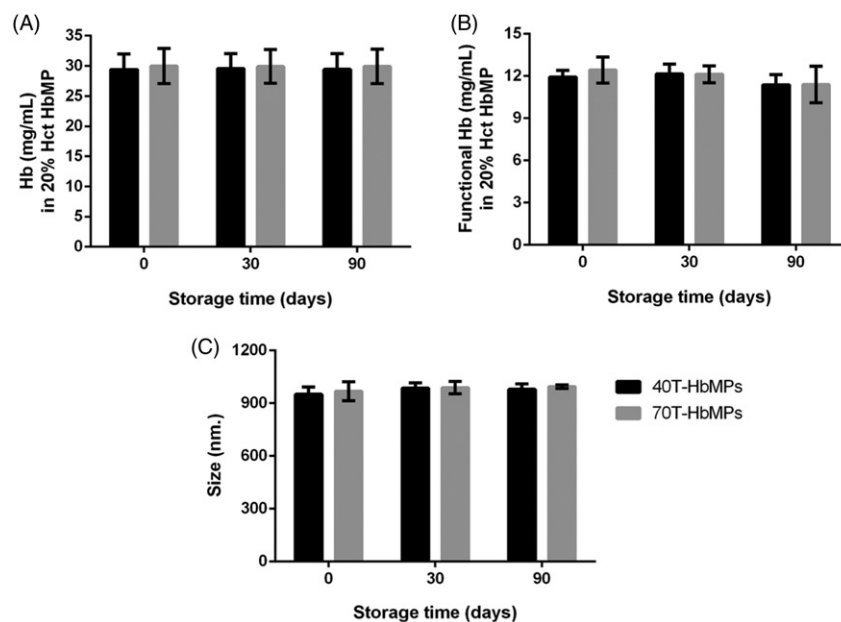


**Figure 7.** Stability of HbMP over 90 days. (A) Hb content of HbMP, (B) concentration of functional Hb (B) and (C) size stability by DLS analysis. Data are presented as mean  $\pm$  SD ( $n = 3$ ).

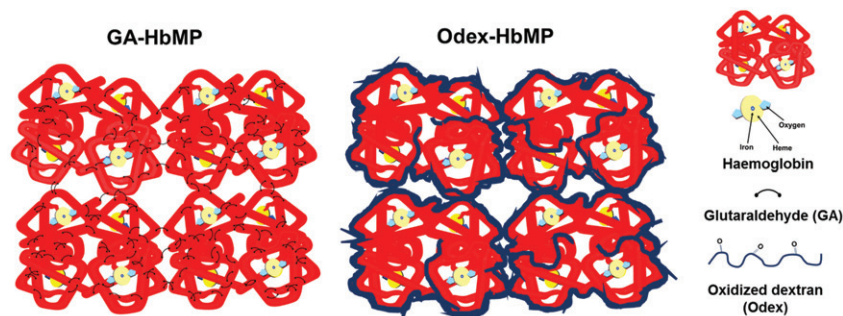


**Figure 8.** Schematic presentation of Hb cross-linking by Odex versus cross-linking by GA.

precipitates and is entrapped in the particles together with the proteins (Figure 1). Odex is promising as a highly effective macromolecular cross-linker because the carbonyl groups of the sugar open chains are capable of reacting with the free  $-NH_2$  groups on the protein; the relatively fast formation of Schiff base results in creating a cross-linked network [24,27,35,36].

In such a way, one preparation step and several respective washing steps are omitted, which significantly reduces the preparation time.  $MnCO_3$  and bovine Hb were selected as a model to demonstrate this novel fabrication procedure. Haemoglobin content in Odex-HbMP was estimated through photometric and quantitative measurement by a photometric method using the modified pronase-AHD method. The method is the combination of pronase enzyme and AHD-575 together. In comparison with HbMP-700 [6,29] prepared by CCD technique using GA as a cross-linker, Odex-HbMP contain a comparable amount of Hb. The entrapped Hb amount could not be enhanced by increasing the initial concentration of the protein. Additionally, the entrapped protein by  $MnCO_3$  using a one-pot procedure had no significant difference in the entrapment efficiency of the CCD procedure as earlier reported by Xiong et al. [7,29]. In comparison with other fabrication methods, the new one-pot procedure provides easily prepared

particles with high protein content under ambient condition and no organic solvents or catalysts are needed. The reagents are neither toxic and nor expensive. Henceforward, our new technique is fast, simple, efficient and cost-effective.

The Odex-protein cross-linking process occurs simultaneously during the precipitation. This is achieved by the large molecular size of Odex and its substantial excess in the reaction. Odex can rapidly cover the protein surface avoiding protein-protein interaction (Figure 8) [37]. The Odex concentration during coprecipitation influences the stability of Hb. At the Odex concentration of 2%, HbMP exhibits a higher amount of functional Hb. The reason could be that the dextran moiety hinders the steric expansion of Hb that would inhibit the denaturation rate of Hb. Additionally, Zhang et al. reported earlier that dextran was able to decrease the autoxidation rate of Hb and could structurally stabilize Hb to avoid the oxidation process of the haem-containing protein and its denaturation [38,39]. Cross-linking of Hb by GA has many drawbacks such as reduction of redox potential as well as increase of its autoxidation rate [40]. This could be the reason for the different amount of functional Hb in GA-HbMP and Odex-HbMP (40% in Odex-HbMP and 30% in GA-HbMP). This value was stable during storage for Odex-HbMP but not for GA-HbMP where the functional Hb decreased rapidly with

the storage time. We measured the amount of released oxygen and calculated from these numbers the amount of functional Hb. Therefore, we cannot directly conclude that the remaining 60% of the measured total Hb is MetHb. It could also be possible that the oxygen release from the particles is partly hindered and the amount of MetHb is lower than 60%. Direct measurements of the MetHb content in the particles are in progress and will give a better insight.

Particle size is a significant feature in determining the performance of particles in biological applications because it influences the biological properties, such as cellular uptake, circulating half-life and biodistribution. Particles fabricated by our new “one-pot” procedure fit to the criteria for the biomedical usages [41]. This procedure provided the uniform morphology, monodisperse, size range between 800 and 1000 nm. The Odex particles have negative zeta-potential, suggestive that the particles have a tendency to repel each other, rendering the colloid stable.

The results of analytical centrifugation clearly showed the deformability of Odex-cross-linked particles, and they were compressed when applied high centrifugal force. However, they were dilated when the force was reduced. The deformability of particles was also confirmed by scanning several Odex-HbMP by AFM in dry and wet states. An increase in thickness gives some evidence for a sponge-like structure of the particles with a high water content. Upon drying, the particles shrink but recover their thickness quickly when water is added. The deformability of particles is very important for the intravenous administration because they need to circulate through the bloodstream and pass through microvessels.

In terms of protein functionality, the UV-VIS spectrophotometric analysis in Figure 6 exhibited the ability of Odex-HbMP to bind and release oxygen in comparison with stroma-free Hb. Oxygenated Odex-HbMP demonstrated three absorption peaks at 414, 542 and 576 nm, which correspond to the oxygenated Hb (OxyHb). After deoxygenation of the Odex-HbMP using 1 mg/mL sodium dithionite (SDT), a red shift of the 414 nm peak (the Soret peak) to 432 nm was observed. A peak at 556 nm was detected instead while the peaks at 542 and 576 nm disappeared. The absorption spectra of Odex-HbMP showed the characteristic shape of oxygenated/deoxygenated Hb and confirmed the functionality of Odex-HbMP. The shift to higher absorption values of Odex-HbMP spectra compared to the Hb solution is due to the scattering of Odex-HbMP.

The stability of particles is one of the most important factors influencing their medical and pharmaceutical applications. We could show that there was no significant change of the particle size, size distribution as well as of the total Hb content and the fraction of functional Hb of the Odex-HbMP during at least 3 months storage. This information indicated the long shelf life of our new particles which is a huge benefit.

## Conclusion

We have successfully established a novel, simple, efficient and cost-effective method for biopolymer microparticle fabrication modified from CCD technique using Odex as a

biocompatible cross-linker. Monodisperse HbMP could be prepared by coprecipitation of Hb with the MnCO<sub>3</sub> template and cross-linking with Odex in one step. After removing MnCO<sub>3</sub> template with EDTA, the resulting Odex-HbMP showed homogeneous morphology with a size of about 850–1000 nm, negative zeta-potential, high deformability, high entrapment efficiency of Hb and a high fraction of functional Hb. The Odex-HbMP maintained their ability to be oxygenated/deoxygenated and they are stable at least for 90 days. The results suggest that Odex has a potential to be used as a promising alternative cross-linker for the preparation of submicron particles. We eagerly anticipate a potential of our new technique for a wide range of biomedical applications soon.

## Disclosure statement

No potential conflict of interest was reported by the authors.

## Funding

C.K. and N.S. hold an academic development scholarship from the University of Phayao, A.P. from Naresuan University, and S.C. and W.K. from Payap University.

## ORCID

Hans Bäumlér  <http://orcid.org/0000-0002-2573-2289>

## References

- [1] Zhang Y, Chan HF, Leong KW. Advanced materials and processing for drug delivery: the past and the future. *Adv Drug Deliv Rev.* 2013;65:104–120.
- [2] Teekamp N, Duque LF, Frijlink HW, et al. Production methods and stabilization strategies for polymer-based nanoparticles and microparticles for parenteral delivery of peptides and proteins. *Expert Opin Drug Deliv.* 2015;12:1311–1331.
- [3] Keshani S, Daud WRW, Nourouzi MM, et al. Spray drying: an overview on wall deposition, process and modeling. *J Food Eng.* 2015; 146:152–162.
- [4] Vehring R. Pharmaceutical particle engineering via spray drying. *Pharm Res.* 2008;25:999–1022.
- [5] Gao X, Zhang X, Wu Z, et al. Synthesis and physicochemical characterization of a novel amphiphilic polylactic acid-hyperbranched polyglycerol conjugate for protein delivery. *J Control Release.* 2009;140:141–147.
- [6] Bäumlér H, Xiong Y, Liu ZZ, et al. Novel hemoglobin particles-promising new-generation hemoglobin-based oxygen carriers. *Artif Organs.* 2014;38:708–714.
- [7] Xiong Y, Steffen A, Andreas K, et al. Hemoglobin-based oxygen carrier microparticles: synthesis, properties, and *in vitro* and *in vivo* investigations. *Biomacromolecules.* 2012;13:3292–3300.
- [8] Bäumlér H, Georgieva R. Coupled enzyme reactions in multicompartiment microparticles. *Biomacromolecules.* 2010;11:1480–1487.
- [9] Habeeb AFSA, Hiramoto R. Reaction of proteins with glutaraldehyde. *Arch Biochem Biophys.* 1968;126:16–26.
- [10] Lai J-Y. Interrelationship between cross-linking structure, molecular stability, and cytocompatibility of amniotic membranes cross-linked with glutaraldehyde of varying concentrations. *RSC Adv.* 2014;4:18871–18880.
- [11] Reddy N, Reddy R, Jiang Q. Crosslinking biopolymers for biomedical applications. *Trends Biotechnol.* 2015;33:362–369.

- [12] Sommermeyer K, Eichner W, inventor. Haemoglobin-hydroxyethyl starch conjugates as oxygen carriers. United States patent US 6,083,909, Assignee: Fresenius AG, Oberusel, Germany; 2000
- [13] Eike JH, Palmer AF. Oxidized mono-, di-, tri-, and polysaccharides as potential hemoglobin cross-linking reagents for the synthesis of high oxygen affinity artificial blood substitutes. *Biotechnol Prog.* 2004;20:953–962.
- [14] Scatena R, Giardina B. O-raffinose-polymerised haemoglobin. A biochemical and pharmacological profile of an oxygen carrier. *Expert Opin Biol Ther.* 2001;1:121–127.
- [15] Boykins RA, Buehler PW, Jia Y, et al. O-raffinose crosslinked hemoglobin lacks site-specific chemistry in the central cavity: structural and functional consequences of beta93Cys modification. *Proteins Struct Funct Genet.* 2005;59:840–855.
- [16] Bonneaux F, Labrude P, Dellacherie E. Preparation and oxygen binding properties of soluble covalent hemoglobin-dextran conjugates. *Experientia.* 1981;37(8):884–886.
- [17] Bonneaux F, Dellacherie E, Labrude P, et al. Hemoglobin-dialdehyde dextran conjugates: improvement of their oxygen-binding properties with anionic groups [Internet]. *J Protein Chem.* 1996; 15:461.
- [18] McCahon R, Hardman J. Pharmacology of plasma expanders [Internet]. In: Nick P, Mick S, editors. *Anaesthesia and intensive care medicine.* Vol. 18. Netherlands: Elsevier Amsterdam; 2017. p. 418–420.
- [19] Mehvar R. Dextran for targeted and sustained delivery of therapeutic and imaging agents. *J Control Release.* 2000;69:1–25.
- [20] Maia J, Evangelista MB, Gil H, et al. Dextran-based materials for biomedical applications. *Carbohydr Appl Med.* 2014;661:31–53.
- [21] Maia J, Carvalho RA, Coelho JFJ, et al. Insight on the periodate oxidation of dextran and its structural vicissitudes. *Polymer (Guildf).* 2011;52:258–265.
- [22] Wasiak I, Kulikowska A, Janczewska M, et al. Dextran nanoparticle synthesis and properties. *PLoS One* 2016. 11(1): e0146237. doi: [10.1371/journal.pone.0146237](https://doi.org/10.1371/journal.pone.0146237)
- [23] Lisman A, Butruk B, Wasiak I, et al. Dextran/albumin hydrogel sealant for Dacron(R) vascular prosthesis. *J Biomater Appl.* 2014; 28:1386–1396.
- [24] Cortesi R, Esposito E, Osti M, et al. Dextran cross-linked gelatin microspheres as a drug delivery system. *Eur J Pharm Biopharm.* 1999;47:153–160.
- [25] Palmer AF, Sun G, Harris DR. Tangential flow filtration of hemoglobin. *Biotechnol Prog.* 2009;25:189–199.
- [26] Haney CR, Buehler PW, Gulati A. Purification and chemical modifications of hemoglobin in developing hemoglobin based oxygen carriers. *Adv Drug Deliv Rev.* 2000;40:153–169.
- [27] Berillo D, Elowsson L, Kirsebom H. Oxidized dextran as crosslinker for chitosan cryogel scaffolds and formation of polyelectrolyte complexes between chitosan and gelatin. *Macromol Biosci.* 2012; 12:1090–1099.
- [28] Muangsiri W, Kirsch LE. The protein-binding and drug release properties of macromolecular conjugates containing daptomycin and dextran. *Int J Pharm.* 2006;315:30–43.
- [29] Xiong Y, Liu ZZ, Georgieva R, et al. Nonvasoconstrictive hemoglobin particles as oxygen carriers. *ACS Nano.* 2013;7:7454–7461.
- [30] Xiong Y, Georgieva R, Steffen A, et al. Structure and properties of hybrid biopolymer particles fabricated by co-precipitation cross-linking dissolution procedure. *J Colloid Interface Sci.* 2018;514: 156–164.
- [31] Haldane J. The ferricyanide method of determining the oxygen capacity of blood. *J Physiol (Lond).* 1900;25:295–302.
- [32] Cook SF. The action of potassium cyanide and potassium ferricyanide on certain respiratory pigments. *J Gen Physiol.* 1928;11: 339–348.
- [33] Bäumler H, Hamberger L, Zaslansky P, et al. Non-destructive mechanical testing of allograft bone-implants by analytic centrifugation. *Exp Mech.* 2016;56:1653–1660.
- [34] Kao I, Xiong Y, Steffen A, et al. Preclinical *in vitro* safety investigations of submicron sized hemoglobin based oxygen carrier HbMP-700. *Artif Organs.* 2018;42:549–559.
- [35] Gómez-Mascaraque LG, Méndez JA, Fernández-Gutiérrez M, et al. Oxidized dextrans as alternative crosslinking agents for polysaccharides: application to hydrogels of agarose–chitosan. *Acta Biomater.* 2014;10:798–811.
- [36] Ribeiro MP, Morgado PI, Miguel SP, et al. Dextran-based hydrogel containing chitosan microparticles loaded with growth factors to be used in wound healing. *Mater Sci Eng C.* 2013;33:2958–2966.
- [37] Fuentes M, Segura RL, Abian O, et al. Determination of protein-protein interactions through aldehyde-dextran intermolecular cross-linking. *Proteomics.* 2004;4:2602–2607.
- [38] Wang Y, Zhang S, Zhang J, et al. Structural, functional and physicochemical properties of dextran-bovine hemoglobin conjugate as a hemoglobin-based oxygen carrier. *Process Biochem.* 2017;60: 67–73.
- [39] Zhang J, Wang Y, You G-X, et al. Conjugation with 20 kDa dextran decreases the autoxidation rate of bovine hemoglobin. *Artif Cells Nanomed Biotechnol.* 2018;46:1436–1438.
- [40] Guillochon D, Vijayalakshmi MW, Thiam-Sow A, et al. Effect of glutaraldehyde on hemoglobin: functional aspects and Mössbauer parameters. *Biochem Cell Biol.* 1986;64:29–37.
- [41] Mayer A, Vadon M, Rinner B, et al. The role of nanoparticle size in hemocompatibility. *Toxicology.* 2009;258:139–147.

## *In-vitro* haemocompatibility of dextran-protein submicron particles

Chiraphat Kloypan<sup>a,b</sup>, Nittiya Suwannasom<sup>a,c</sup>, Saranya Chaiwaree<sup>d</sup>, Ausanai Prapan<sup>e</sup>, Kathrin Smuda<sup>a</sup>, Nuttakorn Baisaeng<sup>f</sup>, Axel Pruß<sup>a</sup>, Radostina Georgieva<sup>a,g</sup> and Hans Bäuml<sup>a</sup>

<sup>a</sup>Institute of Transfusion Medicine, Charité-Universitätsmedizin Berlin, Berlin, Germany; <sup>b</sup>Division of Clinical Immunology and Transfusion Sciences, School of Allied Health Sciences, University of Phayao, Phayao, Thailand; <sup>c</sup>Division of Biochemistry and Nutrition, School of Medical Sciences, University of Phayao, Phayao, Thailand; <sup>d</sup>Department of Radiological Technology, Faculty of Allied Health Sciences, Naresuan University, Phitsanulok, Thailand; <sup>e</sup>Department of Pharmaceutical Technology, Faculty of Pharmacy, Payap University, Chiang Mai, Thailand; <sup>f</sup>Division of Pharmaceutical Sciences, School of Pharmaceutical Sciences, University of Phayao, Phayao, Thailand; <sup>g</sup>Department of Medical Physics, Biophysics and Radiology, Faculty of Medicine, Trakia University, Stara Zagora, Bulgaria

### ABSTRACT

Blood compatibility is a key requirement to fulfil for intravenous administration of drug and oxygen carrier system. Recently, we published the fabrication of oxidised-dextran (Odex)-crosslinked protein particles by one-pot formulation. In the current study we investigate the haemocompatibility of these Odex - particles including albumin particles (Odex-APs) and haemoglobin particles (Odex-HbMPs). Odex-APs and Odex-HbMPs have a submicron size ranged 800–1000 nm with peanut-like shape and a negative surface charge. *In vitro* haemocompatibility assays included haemolysis test, indirect phagocytosis test and platelet activation test in human blood. Odex-APs and Odex-HbMPs did not provoke any undesirable effects on the blood cells. Firstly, the ratio of haemolysis after contacted with Odex-crosslinked protein particles were less than 5% and therefore the particles may be considered non-haemolytic. Secondly, the incubation of leukocyte with Odex-APs/HbMPs did not influence the phagocytosis of leukocyte. We conclude that our particles are not recognized by monocytes or granulocytes. Finally, exposure of Odex-APs/HbMPs to platelets did not cause an activation of platelets. Additionally, Odex-HbMP/AP did not enhance or attenuate agonist-induced platelet activation. We conclude that Odex-crosslinked protein particles exhibit a very good haemocompatibility and represent highly promising carriers for drugs or oxygen.

### ARTICLE HISTORY

Received 8 October 2018  
Revised 2 November 2018  
Accepted 2 November 2018

### KEYWORDS

Haemocompatibility;  
submicron particles;  
dextran; hemoglobin

## Introduction

A major part of the micro- and nanometer size particles in clinical and preclinical investigations are biomolecule-based particles fabricated from polysaccharides, polyaminoacids, polypeptides, proteins or lipids. Among them, protein-based micro- and nanoparticles have been extensively investigated [1] as a site-specific drug carrier for cancer [2–7] as well as haemoglobin-based oxygen carriers (HBOCs) [8–16].

However, questions concerning the safety of prolonged use of nano- and micro-particles have been raised since most biomedical nanoparticles, for therapeutic and/or diagnostic purposes, are typically intravenously administered and directly interact with the blood. Hence, the haemocompatibility of the nano- and micro- particles becomes important and critical. Materials are considered to be haemocompatible, if they are able to remain effectual after being exposed to blood but do not bring about any form of toxicity to the blood cells and do not cause any changes in composition and viscosity of the blood plasma [17]. For instance, the rupture of red blood cells (RBCs) and subsequent haemoglobin releasing can cause the symptoms haemoglobinuria or anuria

followed by renal failure [18]. Additionally, platelets are critical to haemostasis by virtue of their ability to adhere, aggregate and release the contents of their granules as well as their capacity to alter their surface characteristics to support blood coagulation. Therefore, thrombotic and thromboembolic complications, as well as bleeding risks associated with the disseminated intravascular coagulopathy (DIC) remain of serious concern. Besides, the phagocytic cells (e.g. granulocytes and monocytes) can proficiently engulf particles in the blood which results in serious limitation of their blood circulation time and extravasation into target tissues [19]. Therefore, to avoid these events, the use of biocompatible and biodegradable materials are crucial factors for the fabrication of particles suitable for clinical applications.

The haemocompatibility of particles is mainly affected by their physicochemical characteristics such as chemical composition, size, shape, surface charge, hydrophobicity or hydrophilicity [20–22]. The fabrication techniques and selection of biomaterials are the fundamental steps, which can drastically impact the haemocompatibility of the particles as well as the efficacy of the proteins in the particles. Recently, we described a new promising formulation of protein submicron

**CONTACT** Hans Bäuml  [hans.baeuml@charite.de](mailto:hans.baeuml@charite.de)  Institute of Transfusion Medicine, Charité-Universitätsmedizin Berlin, Berlin, Germany

© 2019 Informa UK Limited, trading as Taylor & Francis Group.

This is an Open Access article distributed under the terms of the Creative Commons Attribution License (<http://creativecommons.org/licenses/by/4.0/>), which permits unrestricted use, distribution, and reproduction in any medium, provided the original work is properly cited.

particles called “One-Pot formulation” [23]. The new procedure is based on the coprecipitation-crosslinking-dissolution (CCD) method where the biopolymer particles are obtained in three main steps exploiting the ability of insoluble inorganic salts to incorporate macromolecules during precipitation in aqueous solutions. These macromolecules are subsequently crosslinked, and the inorganic precipitate is dissolved usually by complexation of the metal ions or pH change. With the one-pot procedure, coprecipitation and crosslinking were combined in one step due to the use of a biopolymer crosslinker, oxidised-dextran (Odex), which is coprecipitated together with a protein into a manganese carbonate ( $\text{MnCO}_3$ ) template. Odex-HbMPs fabricated by one-pot demonstrated an improved oxygen storage capability. We hypothesized that dextran is able to improve not only the protein function and stability but also the haemocompatibility of the particles because of its protein-rejecting and cell repelling abilities [36,37]. In addition, the multivalent nature of dextran is advantageous for surface immobilization of biologically active molecules.

Therefore, the aim of this study is to investigate the haemocompatibility of Odex-APs and Odex-HbMPs using several methods including RBCs haemolysis, phagocytic activity of leukocytes and activation/aggregation of thrombocytes, *in vitro*.

## Materials and methods

### Materials

Dextran (M.W. 40,000 and 70,000 Da named as 40T and 70T, respectively) were purchased from AppliChem GmbH, Germany. Human serum albumin (HSA) solution for injection (200 g/L HSA, contains 16 mM sodium caprylate, 16 mM sodium N-acetyltryptophanate, 100–130 mM sodium chloride) was purchased from Baxalta Deutschland GmbH, Germany. Bovine haemoglobin solution (50 g/L in 0.9% NaCl) was obtained from Biophyll GmbH, Germany. Ethylenediaminetetraacetic acid disodium salt dihydrate ( $\text{EDTA-Na}_2$ ), glycine, manganese chloride, sodium carbonate, sodium chloride, sodium hydroxide, and sodium (meta) periodate were purchased from Sigma-Aldrich, Germany. Phosphate buffered saline pH 7.4 (PBS, solutions contains 10 mM sodium phosphate dibasic, 1.9 mM potassium phosphate monobasic, 137 mM sodium chloride and 2.7 mM potassium chloride) was purchased from Fisher Scientific, USA. PHAGOTEST™ and PHAGOBURST™ kits were purchased from Glycotope Biotechnology GmbH, Germany.

### Odex-crosslinked protein particles

50 mL of 10% dextran solutions (40T and 70T, 30.9 mmol/L glucose subunits) were oxidised by sodium periodate (6.6 g, 30.9 mmol/L) for 1 h at room temperature [24]. Then, the resulting oxidised dextran (Odex) was transferred to a cellulose dialysis tube (MWCO of 12,000: Carl Roth GmbH, Germany) and dialysed against water. The amount of aldehyde in Odex was quantified by hydroxylamine hydrochloride titration method with unmodified dextran as a reference [25].

Albumin particles (APs) and haemoglobin (HbMPs) were prepared by the one-pot procedure using 40T- and 70T-Odex as crosslinking as described earlier [23]. Briefly, equal volumes

of solution 1 consisting of 0.25 M of  $\text{MnCl}_2$  and 50 mg/mL of HSA or Hb were rapidly mixed with solution 2 containing 0.25 M of  $\text{Na}_2\text{CO}_3$  and 40 mg/mL of Odex (40T or 70T, individually) in the beaker under vigorous stirring at room temperature. After 30 s, 5 mg/mL of HSA was added to the suspension and incubated for 5 min under stirring to allow the HSA to absorb into particles surface. The resulting particle suspensions were then proceeded to the dissolution of the  $\text{MnCO}_3$  template by 0.25 M EDTA/0.05 M Glycine for 30 min and the reduction by 0.4 mg/mL of  $\text{NaBH}_4$ . Finally, the obtained Odex cross-linked albumin particles (Odex-APs) or haemoglobin particles (Odex-HbMPs) were washed three times with PBS (6000 g for 5 min) and finally suspended in sterile PBS (final particle concentration  $2 \times 10^{11}$ /mL). APs and HbMPs crosslinked with 40T-Odex and 70T-Odex are named 40T-APs, 70T-APs, 40T-HbMPs and 70T-HbMPs, correspondingly.

For SEM imaging, samples were prepared by applying a drop of particles suspension onto glass slide followed by drying overnight. After sputtering with gold, measurements were conducted at an operation voltage of 3 keV using Gemini Leo 1550 instrument (Oberkochen, Germany) and ImageJ 1.44p software (Wayne Rasband, National Institute of Mental Health, Bethesda, MD, USA).

The hydrodynamic diameter and the zeta-potential of the Odex-APs and Odex-HbMPs were measured by dynamic light scattering using a Zetasizer Nano ZS instrument (Malvern Instruments Ltd., Malvern, UK) in PBS solution. Additionally, Odex-crosslinked particles were dispersed in PBS and analysed for autofluorescence using flow cytometry (BD FACSCanto II), FITC and PE channel were gated. BD FACSDIVA software (BD Biosciences, USA) was employed for data analysis.

### Blood collection

Venous blood anticoagulated by lithium heparin or sodium citrate was collected from healthy volunteers. Informed consent was obtained from all donors in written form. The blood samples were withdrawn in accordance with the transfusion law of Germany. The use of donor blood samples for scientific purposes was approved by the ethics committee of the Charité – Universitätsmedizin Berlin (# EA1/137/14). Immediately after blood collection, tubes were slowly agitated to ensure an appropriate mixing of anticoagulant and blood and discarded if there was any evidence of clotting. The assays were performed within 2 h after blood collection.

### Haemolysis test

The haemolytic test is based on the release of haemoglobin from damaged erythrocytes *in vitro*. Human heparinized erythrocytes were washed (3000 g, 5 min) in PBS until the supernatant was clear and colourless. RBCs were then to obtain a cell suspension with a volume concentration of 2% in PBS. 0.5 mL of 2% Odex-crosslinked particles suspension was mixed with 0.5 mL of the 2% washed human erythrocyte suspension. This ratio of particles to RBC corresponds to an exchange of 50% blood with particle suspension. 0.5 mL of

double distilled water and PBS were employed as the positive (PC) and negative (NC) control, respectively. After incubation at 37 °C for 3 h, the erythrocyte suspensions were centrifuged at 3000 g for 5 min, the supernatants were collected and pipetted into a 96-well plate. The haemolytic ratio was determined by measuring the absorbance of the supernatants at 545 nm using a microplate reader (Cytation™ 3 Cell Imaging Multi-Mode Reader, BioTek) and calculated according to the following equation:

$$\% \text{Haemolytic ratio} = \frac{(\text{OD}_{\text{test}} - \text{OD}_{\text{NC}})}{(\text{OD}_{\text{PC}} - \text{OD}_{\text{NC}})} \times 100 \quad (1)$$

All results were estimated from the data of three individual experiments, and all data were expressed as the mean  $\pm$  SD [26]. The value of the positive control (water) was set to 100% haemolysis.

### Phagocytosis test

The activation of phagocytosis performance of granulocytes and monocytes in whole blood was investigated using an indirect method based on a modified PHAGOTEST. The method is suitable for non-fluorescing particles. The different particles (10  $\mu$ L of  $2 \times 10^{11}$  per mL) were added to 50  $\mu$ L of heparinized-whole blood and incubated at 37 °C for 0, 10, 30, 60, 120 min to allow uptake by the leucocytes. Samples with non-fluorescent *Escherichia coli* ( $2 \times 10^9$  bacteria per mL from PHAGOBURST kit) and PBS were used as a positive and negative control, respectively. After reaching the corresponding incubation time, the standard test for phagocytosis activity (PHAGOTEST) was performed with all samples. Briefly, 10  $\mu$ L of fluorescein isothiocyanate labelled *E. coli* (FITC-*E. coli*,  $2 \times 10^9$  bacteria per mL from Phagotest kit) were added to each sample and incubated at 37 °C for further 10 min. Afterwards, the fluorescence of non-phagocytosed *E. coli* was quenched, the RBCs were lysed and the leucocytes were fixed and DNA-stained by propidium iodide. Washing steps with PBS were performed between each preparation step. Finally, the leukocyte populations were analysed by flow cytometry (BD FACSCanto II) to obtain the percentage of granulocytes and monocytes which have phagocytosed FITC-*E. coli*. Leukocytes previously saturated with non-fluorescent bacteria or particles are not able to uptake the FITC-*E. coli*, and therefore decreased phagocytic activity to FITC-*E. coli* indicates phagocytic activity to the non-fluorescent bacteria or particles.

### Platelet activation test

The influence of Odex-AP and Odex-HbMP on human platelets was investigated in platelet-rich plasma (PRP) samples. Citrated human whole blood was centrifuged at 150 g for 15 min at 20–25 °C, and the PRP fraction was collected. The platelet amount was detected before the test using a haematology analyser ABX Micros 60 (HORIBA Europe GmbH, Germany). 45  $\mu$ L of PRP was gently mixed with 5  $\mu$ L of particle suspensions (to a ratio of 10 = particles per 1 platelet). Platelets incubated with PBS were used as a control. The samples were incubated at 37 °C for 30 min with gently shaking. Then, the pre-incubated human platelets were activated with platelet agonists (0.5 mg/mL arachidonic acid (AA), 0.2 mg/mL collagen and 0.01 mM epinephrine (Epi): möLab GmbH, Germany) to induce platelet activation and aggregation. The mixtures were incubated at 37 °C for further 30 min with shaking and the samples were then fixed by 0.5% formaldehyde in PBS. Finally, the platelets were stained by APC anti-human CD42b (GPIb $\alpha$ ) antibody and Alexa Fluor® 488 anti-human CD62P (P-Selectin) antibody (BioLegend, San Diego, USA) and analysed by flow cytometry (BD FACSCanto II). Double-stained events were counted as activated platelets [27,28].

### Statistical analysis

Data were presented as means  $\pm$  standard deviation (SD), and statistical differences between groups were compared using ANOVA-like test. GraphPad Prism 6 software (GraphPad, La Jolla, CA, USA) was employed for graphs and statistical analyses. *p* Values  $< .05$  was considered statistically significant.

## Results

### Particle characterisation

Odex-APs and Odex-HbMPs were successfully fabricated by the One-pot procedure. Like the CCD-technique using MnCO<sub>3</sub> as inorganic template, the morphology and the size of the obtained haemoglobin and albumin particles by the One-pot procedure were not significantly different as observed by SEM (Figure 1). The dynamic light scattering analysis of the particles is represented in Figure 2. The size of Odex-APs and Odex-HbMPs was about 800–1000 nm and the zeta-potential was approximately  $-13$  mV and  $-9$  mV as measured in PBS (conductivity 18–20 mS/cm) for Odex-APs and Odex-HbMPs,

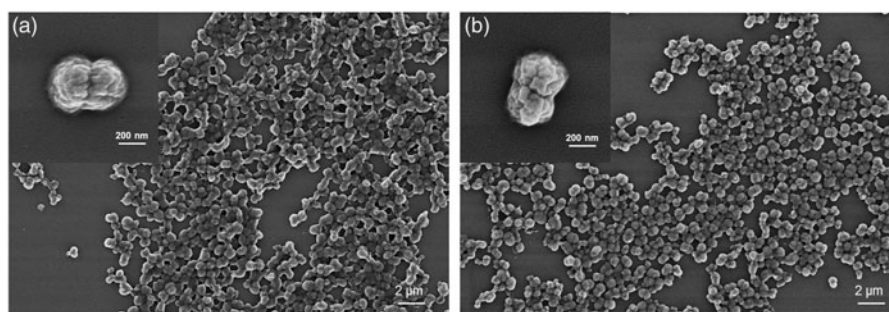
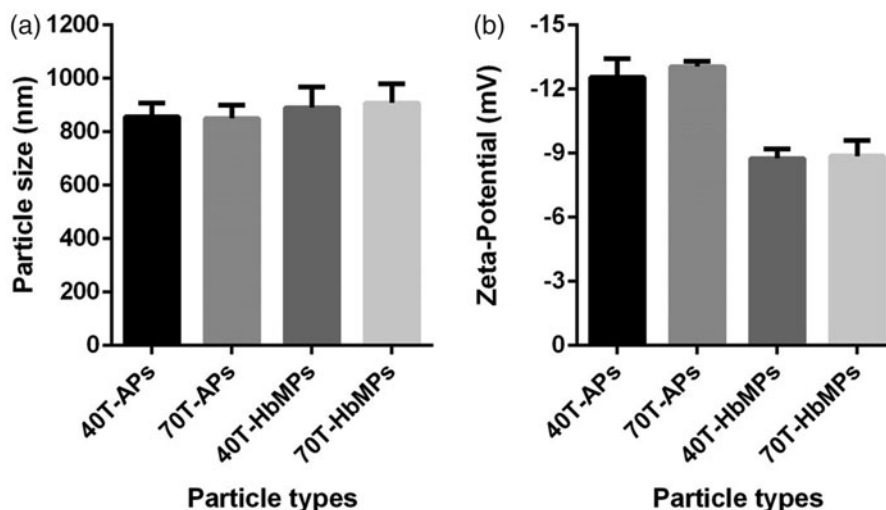
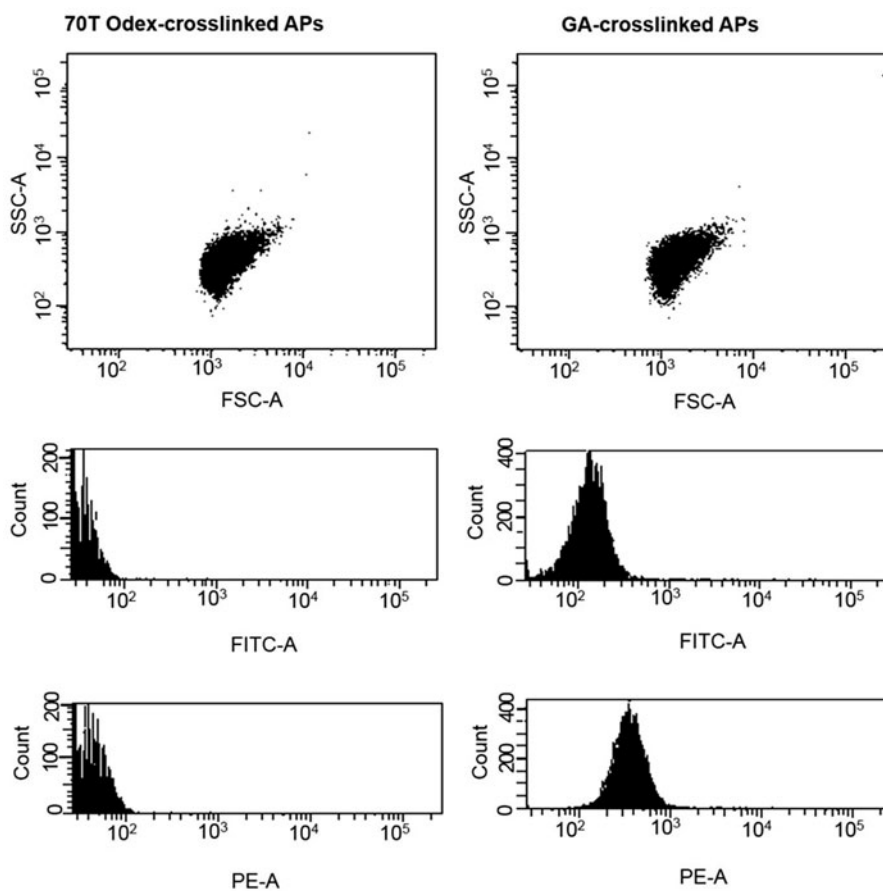


Figure 1. SEM images of Odex-AP (a) and Odex-HbMP (b) fabricated by One-pot formulation. The insets show peanut-like single particles.



**Figure 2.** Characteristics of Odex-crosslinked protein particles. (a) Size and (b) Zeta-potential measured in 10 mM PBS (conductivity 18–20 mS/cm) at room temperature by Dynamic Light Scattering analysis. Data are presented as mean  $\pm$  SD ( $n=5$ ).



**Figure 3.** The side vs forward scatter dot plot of 70T-APs and GA-crosslinked APs (GA-APs). The stronger fluorescence intensity of GA-APs was observed compared to Odex-crosslinked particles. (APs and HbMPs crosslinked with both 40T and 70T Odex have the same phenomenon, figures were not shown).

respectively. No significant differences in size and zeta-potential could be detected for the particles prepared with 40T- and 70T-Odex.

The results of flow cytometry analysis in Figure 3 also demonstrated that Odex-particles had no auto-fluorescence in contrast to the protein particles prepared using the CCD technique and crosslinked by glutaraldehyde [8–10,29,30].

### Haemolysis test

Haemolysis refers to the release of haemoglobin from RBCs due to damage of RBCs membrane, which is extensively applied to evaluate the biosafety of particles. A haemolytic ratio higher than 5% is considered as a significant damage of RBCs. The haemolytic ratio of the RBCs incubated with different Odex-crosslinked particles for 3 h at 37 °C is

demonstrated in Table 1. It can be seen clearly that the haemolysis ratio for the samples with Odex-APs and Odex-HbMPs was between 1% and 2% and so far, they obviously did not deteriorate significantly the RBCs.

### Phagocytosis test

The commercial phagotest kit allows determinations of the percentage of phagocytes (in whole blood samples) which ingest FITC-labelled opsonized *E. coli* bacteria and is used as a diagnostic tool for functional testing of leukocytes. The test can be directly used to determine the phagocytosis of fluorescent particles by the phagocytes in the blood (mainly granulocytes and monocytes). However, in the case of the non-fluorescent particles, an additional fluorescent staining is needed which may alter their surface properties and influence the phagocytosis. Therefore, we employed an indirect method as described in the part Materials and Methods. Non-fluorescent *E. coli*, Odex-APs and Odex-HbMPs were

**Table 1.** Haemolytic ratio of odex-crosslinked particles.

Test sample	Haemolysis ratio (%)
40T-APs	1.14 ± 0.36
70T-APs	1.03 ± 0.16
40T-HbMPs	1.67 ± 0.58
70T-HbMPs	1.77 ± 0.52
PBS	0 ± 0.00
Water	100 ± 0.00

Data are presented as mean ± SD ( $n = 3$ ).

added to the whole blood sample and incubated at 37 °C for 10–120 min in order to reach a saturated phagocytosis by the granulocytes and monocytes. Then, the standard test with FITC-labelled *E. coli* at 37 °C was performed with all samples. Results of the flow cytometry analysis of samples pre-incubated with non-stained *E. coli*, PBS, Odex-APs and Odex-HbMPs for 120 min is presented in Figure 4 as dot plots of granulocyte and monocyte populations detectable in the FITC channel. It can be seen that the distribution of the FITC-labelled cells is similar for the samples pre-incubated with PBS, 40T-APs and 40T-HbMPs. Only the positive control (pre-incubated with non-fluorescent *E. coli*) shows different behavior with an increased number of non-fluorescent cells.

The summarized results in dependency on the pre-incubation time are shown in Figure 5. The number of granulocytes and monocytes phagocytosing FITC-*E. coli* was not significantly different for Odex-crosslinked particles and PBS (negative control) over all pre-incubation times. In contrast, the positive control, *E. coli*, demonstrated a decrease in the percentage of the cells engulfing FITC-*E. coli* in a time-dependent manner, due to the phagocytosis of non-fluorescing *E. coli*.

### Platelet activation test

To evaluate whether our Odex-APs and Odex-HbMPs alter the haemostasis system, their influence on the activation of

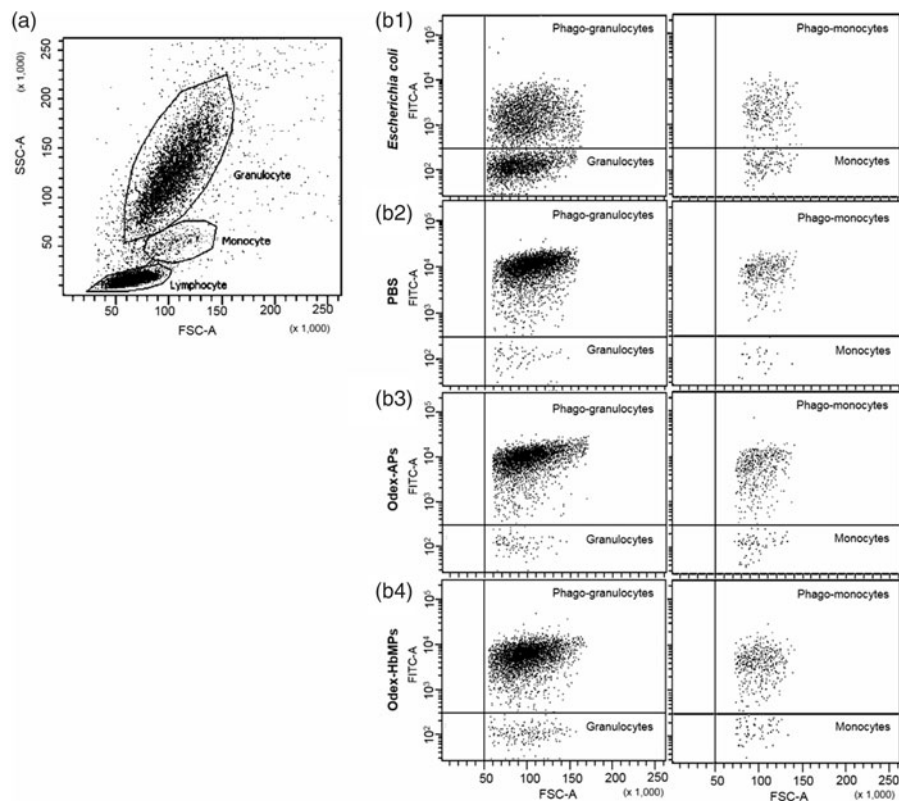


**Figure 4.** Flow cytometric dot plot of human peripheral blood leukocytes. (a) Sub-populations of leukocytes can be distinguished based on forward scatter (relative size) and side scatter (relative complexity). Granulocyte are large and complex; monocytes are slightly larger than lymphocytes and less complex than granulocyte, while lymphocytes are smaller and less complex. (b) Dot plots FITC/FSC demonstrate the phagocytic activity of granulocytes (left panel) and monocytes (right panel) detected with FITC-labelled *E. coli*. Preincubation with different particles was performed for 120 min. (b1) Preincubation of leukocytes with non-stained *E. coli* (positive control), (b2) Preincubation of leukocytes with PBS (negative control), (b3) Preincubation of leukocytes with Odex-APs, (b4) Preincubation of leukocytes with Odex-HbMPs.

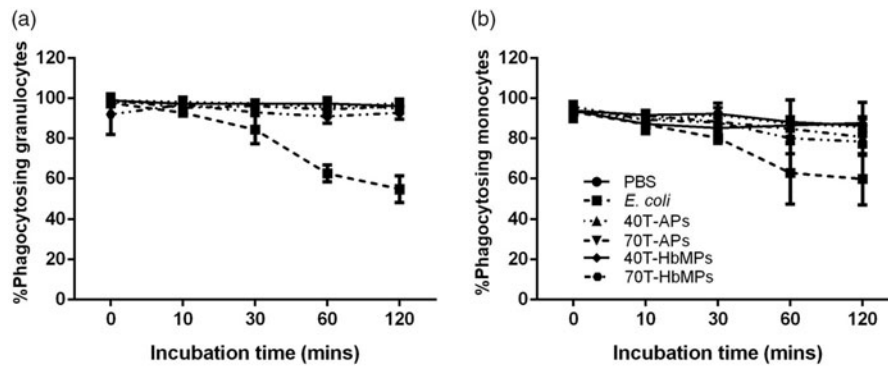


**Figure 5.** Percentage of phagocytic activity of (a) granulocyte and (b) monocyte on Odex-APs and Odex-HbMPs compared with PBS (negative control) and *E. coli* (positive control). On one hand, the fluorescence signal of detective FITC-*E. coli* decreased grammatically across incubation periods in positive control. On the other hand, leukocyte preincubated with PBS as well as Odex-APs and Odex-HbMPs showed a strong detective FITC-*E. coli* and there was no change over the incubation times. Data are presented as mean  $\pm$  SD ( $n = 3$ ).

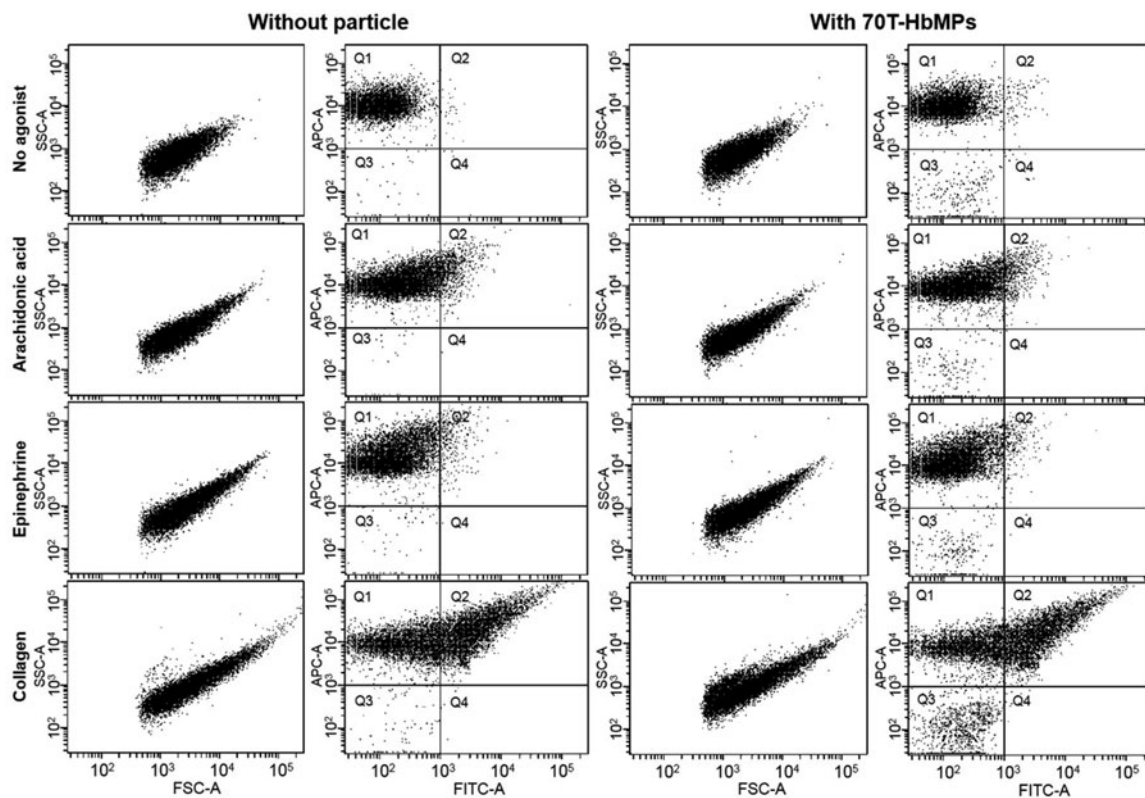


**Figure 6.** Flow cytometric analysis of the activation of platelets. Example of 70T-HbMPs compared to negative control. The events of the forward and side scatter as well as APC and FITC fluorescence channel are shown as dot plot. Platelets stained with APC-Antihuman CD42b (GPIIb $\alpha$ ) are enclosed in quadrant Q1. Double-stained with APC Anti-CD42ba and AlexaFlour 488 Antihuman-CD62P (P-selectin) events in quadrant Q2 represent activated-platelets. Non-stained particles were presented in Q3.

platelets was investigated. **Figure 6** shows results of the flow cytometry analysis of platelets using the platelet-specific membrane receptor CD42b (GPIIb $\alpha$ ), and then distinguished those platelets that were activated using the activation marker CD62P. The results showed that the platelet activation assay was able to distinguish between platelets that are resting with high fluorescence level for CD42b and lower fluorescence levels for activation markers, CD62P, and those that have been activated by agonists with higher fluorescence levels for the two activation markers, CD42b and CD62P. Simultaneously, upon the stimulation of platelets by agonists, the aggregation of platelets was also observed as the shift of

forward scatter/side scatter positioning compared with the control.

**Figure 7** summarizes the results of the flow cytometry analysis. Obviously, the Odex-APs or Odex-HbMPs did not cause activation of the platelets as compared to the control sample which was incubated with PBS. Additionally, platelet activation induced by agonists including arachidonic acid, collagen and epinephrine of pre-incubated PRP with particles was comparable to the control samples.

It can be concluded that Odex-APs or Odex-HbMPs do not influence the function of platelets and therefore no negative side effects on the haemostasis are expected.

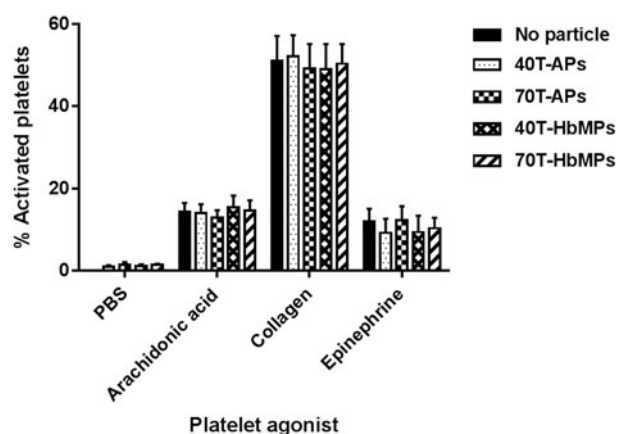


**Figure 7.** Platelet activation (as determined by %CD62P expression) is not influenced by Odex-APs and Odex-HbMPs. Fresh citrated PRP was treated with the different particles or PBS as a control. The presence of particles did not influence on arachidonic acid-, collagen- and epinephrine-induced platelet activation. Non-stimulated labelled platelets are shown as a baseline for spontaneous activation. Data are presented as mean  $\pm$  SD ( $n = 3$ ).

## Discussion

Prior to all intravenous administration applications, the influence of particles on the blood cells needs to be evaluated. The haemocompatibility of particles is affected by their physical attributes, including size, shape, and flexibility, as well as their chemical composition, for instance, the incorporation of toxic compounds or active ligands for recognition and triggering of biological receptors. It has been well described that small particle size and positive charge caused thrombocyte and granulocyte activation, and haemolysis. Negatively charged particles larger than 60 nm hydrodynamic diameter appear to be considerably less haemotoxic than smaller ones [21]. Our new particles fit to these criteria. Additionally, a successful perfusion of isolated mouse glomeruli with concentrated HbMP suspensions of the same size *in vitro* without vasoconstriction of the afferent arterioles could be shown [10]. As the size of a particle decreases, its surface area per unit volume (or mass) increases and also allows a greater proportion of its atoms or molecules to be displayed on the surface rather than the interior of the material [31,32]. Therefore, it is very important to utilize procedures that allow preparation of particles with high degrees of uniformity, and with control over their physical and chemical characterisations.

Odex-APs and Odex-HbMPs fabricated by One-pot formulation have a size in the submicron range, uniform morphology and negative surface charge. The coating of the particles with human serum albumin improves significantly their blood compatibility by reducing the adsorption of other proteins as well the interaction with platelets and leukocytes [33]. Due to the covalent binding of albumin to haemoglobin the stability of the coating is sufficient to protect the particles during their circulation in the blood stream against non-specific adsorption of other plasma proteins.

Currently described *in vitro* assays for haemocompatibility testing of particulate materials are not standardized. We evaluated the haemocompatibility of the Odex-crosslinked particles by testing haemolysis (destruction of RBCs),

phagocytosis by leucocytes and platelet activation in order to explore possible adverse effects of Odex-crosslinked protein particles to blood cells

RBCs are the most abundant compartment in the bloodstream and are an important component determining the haemocompatibility. Once they are lysed, they release not only haemoglobin but also procoagulant factors which can cause serious adverse effects [34]. According to the ISO 10993-4:2017, the haemolysis assays of Odex-AP and Odex-HbMP were considered to be non-haemolytic because these particles induced less than 5% haemolysis. Particle-induced haemolysis can be caused by the release of toxic substances from a biomaterial surface or from the interaction between particles and RBCs which result in the disruption and integrity of the RBC membrane and release of haemoglobin into the plasma. Additionally, it is generally agreed that surface properties (especially surface charge) are important, and there are several studies which have demonstrated this. For example, among a set of similar-sized fullerenes (C60-derivatives) bearing different numbers of anionic and cationic surface moieties, those with negative surface charge were not haemolytic, and haemolytic tendency increased in proportion to the number of attached cationic surface groups (positive surface charge) [18].

The charge of particles stemming from distinct surface chemistries influences opsonisation, circulation times and interaction with resident macrophages of organs comprising the phagocytic system. On the one hand, positively charged particles more prone to sequestration by macrophages in the lungs, liver and spleen. On the other hand, neutral and slightly negatively charged nanoparticles have longer circulation lifetimes and less accumulation in the aforementioned organs [35]. Our indirect phagotest assay showed that Odex-APs and Odex-HbMPs particles were not recognized by phagocytic cells including granulocytes and monocytes. As the adsorption of plasma proteins on the nanoparticle surface can have an important influence on the interactions between cells and the particles. Therefore, diminishing the susceptibility of particles to recognition by the phagocytes through coverage of their surface with hydrophilic polymers such as polyethylene glycol, dextrans or mimic the surface using human serum albumin is another strategy to prolong the residence time of particles in the circular system [22].

Activation of platelet plays a crucial role in the coagulation cascade. They are very sensitive to the presence of foreign materials that can enhance or attenuate the activity of platelets and further affect the blood coagulation.

It should also be considered that on the one dextran used as plasma expander influences the function of platelets due to its adsorption on platelets surface [36]. On the other hand, dextran forms not only a depletion layer around the blood cells and reduces the adsorption of proteins but can also be adsorbed to the cell surface. The dextran in the Odex-HbMP is covalently bound to haemoglobin and not free available for adsorption. But the moieties of dextran partially presented on the particle surface contribute to a repulsive force against other macromolecules [37].

Therefore, the interaction between platelets and particle is an important evaluation of biomaterials for blood

compatibility. In this study, the presence of Odex-APs and Odex-HbMPs influenced neither the platelet activation/aggregation nor the agonist induced-platelet activation. The mechanisms through which particles induce platelet aggregation are largely unknown. Nevertheless, trends observed in studies of polymer-based nanoparticles are similar in their charge-dependence to those described above for haemolysis [18]. We assume that the negative surface charge as well as the albumin coating of Odex-APs and Odex-HbMPs prevent interaction between the particles and the platelets and therefore we do not expect negative effects on haemostasis.

## Conclusions

In the current study, we demonstrated the *in vitro* evaluation of the compatibility of Odex-APs and Odex-HbMPs fabricated by “One-pot formulation” with human blood. The results of the haemolysis test, the direct phagocytosis test and of the platelet activation tests reflected good haemocompatibility. No biologically relevant alterations during blood contact were observed and therefore Odex-APs and Odex-HbMPs fabricated by “One-pot formulation” fulfill the requirements according to ISO 10993-4 for blood contacting materials. Therefore, their application potential is worthwhile to be further developed and explored.

## Disclosure statement

No potential conflict of interest was reported by the authors.

## Acknowledgements

C.K. and N.S. hold an academic development scholarship from the University of Phayao, A.P. from Naresuan University and S.C. from Payap University.

## References

- [1] Jao D, Xue Y, Medina J, et al. Protein-based drug-delivery materials. *Materials* (Basel) 2017;10:1–24.
- [2] Nitta SK, Numata K. Biopolymer-based nanoparticles for drug/gene delivery and tissue engineering. *Int J Mol Sci*. 2013;14:1629–1654.
- [3] Elzoghby AO, Samy WM, Elgindy NA. Protein-based nanocarriers as promising drug and gene delivery systems. *J Control Release*. 2012;161:38–49.
- [4] Elzoghby AO, Samy WM, Elgindy NA. Albumin-based nanoparticles as potential controlled release drug delivery systems. *J Control Release*. 2012;157:168–182.
- [5] Lohcharoenkal W, Wang L, Chen YC, et al. Protein nanoparticles as drug delivery carriers for cancer therapy. *Biomed Res Int*. 2014;2014:1.
- [6] Hawkins MJ, Soon-Shiong P, Desai N. Protein nanoparticles as drug carriers in clinical medicine [Internet]. *Adv Drug Deliv Rev*. 2008;60:876–885.
- [7] Kudarha RR, Sawant KK. Albumin based versatile multifunctional nanocarriers for cancer therapy: fabrication, surface modification, multimodal therapeutics and imaging approaches. *Mater Sci Eng C*. 2017;81:607–626.
- [8] Xiong Y, Steffen A, Andreas K, et al. Hemoglobin-based oxygen carrier microparticles: synthesis, properties, and *in vitro* and *in vivo* investigations. *Biomacromolecules*. 2012;13:3292–3300.
- [9] Bäumler H, Xiong Y, Liu ZZ, et al. Novel hemoglobin particles-promising new-generation hemoglobin-based oxygen carriers. *Artif Organs*. 2014;38:708–714.
- [10] Xiong Y, Liu ZZ, Georgieva R, et al. Nonvasoconstrictive hemoglobin particles as oxygen carriers. *ACS Nano*. 2013;7:7454–7461.
- [11] Jia Y, Duan L, Li J. Hemoglobin-based nanoarchitectonic assemblies as oxygen carriers. *Adv Mater*. 2016;28:1312–1318.
- [12] Tao Z, Peter Ghoroghchian P. Microparticle, nanoparticle, and stem cell-based oxygen carriers as advanced blood substitutes. *Trends Biotechnol*. 2014;32:466–473.
- [13] De Frates K, Markiewicz T, Gallo P, et al. Protein polymer-based nanoparticles: fabrication and medical applications. *Int J Mol Sci*. 2018;19:1–20.
- [14] Duan L, Yan X, Wang A, et al. Highly loaded hemoglobin spheres as promising artificial oxygen carriers. *ACS Nano*. 2012;6:6897–6904.
- [15] Tsuchida E, Sou K, Nakagawa A, et al. Artificial oxygen carriers, hemoglobin vesicles and albumin-hemes, based on bioconjugate chemistry. *Bioconjugate Chem*. 2009;20:1419–1440.
- [16] Piras AM, Dessy A, Chiellini F, et al. Polymeric nanoparticles for hemoglobin-based oxygen carriers. *Biochim Biophys Acta - Proteins Proteomics*. 2008;1784:1454–1461.
- [17] Naeye B, Deschout H, Röding M, et al. Hemocompatibility of siRNA loaded dextran nanogels. *Biomaterials*. 2011;32:9120–9127.
- [18] Dobrovolskaia MA, Aggarwal P, Hall JB, et al. Preclinical studies to understand nanoparticle interaction with the immune system and its potential effects on nanoparticle biodistribution. *Mol Pharm*. 2008;5:487–495.
- [19] Owens DE, Peppas NA. Opsonization, biodistribution, and pharmacokinetics of polymeric nanoparticles [Internet]. *Int J Pharm*. 2006;307:93–102.
- [20] Albanese A, Tang PS, Chan WCW. The effect of nanoparticle size, shape, and surface chemistry on biological systems. *Annu Rev Biomed Eng*. 2012;14:1–16.
- [21] Mayer A, Vadon M, Rinner B, et al. The role of nanoparticle size in hemocompatibility. *Toxicology*. 2009;258:139–147.
- [22] Lundqvist M, Stigler J, Elia G, et al. Nanoparticle size and surface properties determine the protein corona with possible implications for biological impacts. *Appl Phys Sci*. 2008;105:14265–14270.
- [23] Kloypan C, Prapan A, Suwannasom N, et al. Improved oxygen storage capacity of haemoglobin submicron particles by one-pot formulation. *Artif Cells, Blood Substit Biotechnol*. 2018; doi: [10.1080/21691401.2018.1521819](https://doi.org/10.1080/21691401.2018.1521819)
- [24] Berillo D, Elowsson L, Kirsebom H. Oxidized dextran as crosslinker for chitosan cryogel scaffolds and formation of polyelectrolyte complexes between chitosan and gelatin. *Macromol Biosci*. 2012;12:1090–1099.
- [25] Lisman A, Butruk B, Wasiak I, et al. Dextran/albumin hydrogel sealant for Dacron(R) vascular prosthesis. *J Biomater Appl*. 2014;28:1386–1396.
- [26] Lu M, Zhao C, Wang Q, et al. Preparation, characterization and *in vivo* investigation of blood-compatible hemoglobin-loaded nanoparticles as oxygen carriers. *Colloids Surf B Biointerfaces*. 2016 ;1:171–179.
- [27] Braune S, Walter M, Schulze F, et al. Changes in platelet morphology and function during 24 hours of storage. *Clin Hemorheol Microcirc*. 2014;58:159–170.
- [28] Cuyper IMD, Meinders M, Vijver EVD, et al. A novel flow cytometry – based platelet aggregation assay. *Blood*. 2013;121:70–80.
- [29] Bäumler H, Georgieva R. Coupled enzyme reactions in multicompartment microparticles. *Biomacromolecules*. 2010;11:1480–1487.
- [30] Xiong Y, Georgieva R, Steffen A, et al. Structure and properties of hybrid biopolymer particles fabricated by co-precipitation cross-linking dissolution procedure. *J Colloid Interface Sci*. 2018;15:156–164.
- [31] Nel A, Xia T, Mädler L, et al. Toxic potential of materials at the nanolevel [Internet]. *Science*. 2006;311:622–627.
- [32] Blanco E, Shen H, Ferrari M. Principles of nanoparticle design for overcoming biological barriers to drug delivery. *Nat Biotechnol*. 2015;33:941–951.
- [33] Tanzi MC. Bioactive technologies for hemocompatibility. *Expert Rev Med Devices*. 2005;2:473–492.

- [34] Helms CC, Marvel M, Zhao W, et al. Mechanisms of hemolysis-associated platelet activation. *J Thromb Haemost.* 2013;11:2148–2154.
- [35] Elci SG, Jiang Y, Yan B, et al. Surface charge controls the suborgan biodistributions of gold nanoparticles. *ACS Nano.* 2016;10:5536–5542.
- [36] Bäuml H, Donath E, Krabi A, et al. Electrophoresis of human red blood cells and platelets. Evidence for depletion of dextran. *Biorheology.* 1996; 33:333–351.
- [37] Bäuml H, Neu B, Donath E, et al. Basic phenomena of red blood cell rouleaux formation. *Biorheology.* 1999; 36:439–442.

## **Curriculum vitae**

"Mein Lebenslauf ist in der elektronischen Version der Dissertation aus datenschutzrechtlichen Gründen nicht enthalten."



## Complete list of publications

Suwannasom N, Smuda K, Kloypan C, Kaewprayoon W, Baisaeng N, Prapan A, Chaiwaree S, Georgieva R, Bäuml H. Albumin submicron particles with entrapped riboflavin – fabrication and characterization. *Nanomaterials*. (2019);9(3):482. IF: 3.504 (2017/2018).

Kloypan C, Suwannasom N, Chaiwaree S, Prapan A, Smuda K, Baisaeng N, Pruß A, Georgieva R, Bäuml H. *In-vitro* haemocompatibility of dextran-protein submicron particles. *Artif Cells, Nanomedicine, Biotechnol*. (2019);47(1):241-249. IF: 3.026 (2017/2018).

Kloypan C, Prapan A, Suwannasom N, Kaewprayoon W, Steffen A, Xiong Y, Baisaeng N, Georgieva R, Bäuml H. Improved Oxygen Storage Capacity of Haemoglobin Submicron Particles by One-Pot Formulation. *Artif Cells, Blood Substitutes, Biotechnol*. 2018; 46(sup3):S964-S972. IF: 3.026 (2017/2018).

## **Acknowledgments**

My years as a PhD student, it has been a period of powerful learning for me, both on scientific area and personal level. Completion of this dissertation was possible with great assistance and extraordinary support of several people.

First and foremost, I would like to express my deepest gratitude to my supervisor PD Dr. Hans Bäumler for the patient guidance, encouragement, and insightful discussions and suggestion he has provided throughout the project. I have been lucky to have a supervisor who responded to my questions and queries so promptly, and who opened to discuss new ideas for allowing me to grow as a research scholar without him this work would have never seen the light as it is today.

Also, I would like to express my deepest heartfelt appreciation to my co-supervisor, Dr. Radostina Georgieva, for her unreserved help, useful advices, and guidance throughout this work. Her valuable suggestions, comments and guidance encourage me to learn more day by day.

I am also grateful for the continues interest and support of Prof. Dr. Axel Pruß in the progress of my work in the institute of transfusion medicine.

I am grateful to all current and past members of the AG-Bäumler for their friendship and professional support. I would like to specifically thank Kathrine Smuda for reading my manuscript and helpful suggestions. I am grateful to Waraporn Kaewprayoon, Chiraphat Kloypan, Ausanai Prapan, Saranya Chaiwaree, and Wanit Chaisorn for their friendship and providing a stimulating atmosphere in which it was a pleasure to work in the lab.

I would also like to take this opportunity to thank the excellent technical assistance and advice of Dr. Yu Xiong, Josephine Waade, Stefanie Dolling, Axel Steffen, Anja Schnabel. Your generosity has been one of the valuable contributions for this thesis.

I am also thankful an academic development scholarship from the University of Phayao who not granted me the financial support and the security of four-year scholarship, but also provided me incredible opportunity to study abroad, where I had a great chance to gain my knowledge as well as fulfill my life with amazing both in my professional and personal experiences.

I would like to thank Dr. Nuttakorn Baisaeng who recommended me to pursue my study in Berlin, Germany without her I would not have been where I am today.

I am also indebted to my friends Pranee Lertkaew, Chutamas Thepmalee for all her help and useful suggestions but also for being there to listen when I needed an ear.

I would like say special thanks to my boyfriend Jörg Schellbach for his continued support and encouragement throughout these years through the process of researching and writing this thesis.

I also thank all the departmental staffs for helping me during these years of my study both academically and officially.

Finally, my heartfelt thanks to my supportive wonderful, loving parents Sompong and Somjit Suwannasom, my sisters Saowanee and my brother Teerawat Suwannasom, and the entire family including my grandmother Klin Kudwongsa who passed away during my studies for being as my mentally support throughout my studies. Your prayer for me was what sustained me thus far.